UNIVERSITÀ
DEGLI STUDI
DI PADOVA

Dipartimento di Ingegneria Industriale

Corso di Laurea Magistrale in Ingegneria dell'Energia Elettrica

TESI DI LAUREA MAGISTRALE IN
INGEGNERIA DELL'ENERGIA ELETTRICA

NUMERICAL SIMULATIONS AND ANALYSIS FOR DEMO TOROIDAL CIRCUIT TOPOLOGY DEFINITION, FUSION ENERGY PRODUCTION DEMONSTRATIVE REACTOR

RELATORE: Prof. Piergiorgio Sonato

CORRELATORE: Dott. Ing. Alberto Maistrello
Dott. Ing. Elena Gaio

LAUREANDO: Giovanni Ferronato

ANNO ACCADEMICO 2016-17

UNIVERSITÀ DEGLI STUDI DI PADOVA

DIPARTIMENTO DI INGEGNERIA INDUSTRIALE

CORSO DI LAUREA MAGISTRALE IN INGEGNERIA DELL'ENERGIA ELETTRICA

Tesi di laurea magistrale in Ingegneria dell'Energia Elettrica

NUMERICAL SIMULATIONS AND ANALYSIS FOR DEMO TOROIDAL CIRCUIT TOPOLOGY DEFINITION, FUSION ENERGY PRODUCTION DEMONSTRATIVE REACTOR

Relatore: Prof. Piergiorgio Sonato

Correlatore: Dott. Ing. Alberto Maistrello

Dott. Ing. Elena Gaio

Laureando: Giovanni Ferronato

ANNO ACCADEMICO: 2016/2017

Abstract

The energy production from fusion is a very difficult target, for which today exists an active international cooperation with many parallel lines like ITER (International Thermonuclear Experimental Reactor - Cadarache, FRA) which is a demonstrative reactor; these lines are supported by many conceptual studies for a subsequent commercial reactor that can be able to produce electricity, and this is the case of DEMO (DEMOnstrating fusion power reactor). There is an active parallel research chain for the technological development signed with the Broader Approach Agreement between Europe and Japan, which led to the realisation of JT-60SA experiment and the International Fusion Materials Irradiation Facility (IFMIF). There are in addition many other laboratories which are working to experiments aimed at studying for specific issues with the same common target, like Consorzio RFX in Padua.

The realisation of nuclear fusion, in accordance with the magnetic confinement approach, requires the maintenance of an extremely high temperature plasma confined by a suitable magnetic field inside a chamber. One of the most used magnetic configuration is the so called “Tokamak”, in which the desired magnetic configuration is produced by two circuits called “toroidal” and “poloidal”, placed around the chamber; this configuration is the one adopted both in DEMO, ITER and JT-60SA. These experiments are characterised by steady state currents of several tens of kiloamps inside the coils, and in order to work with them it is necessary to adopt the superconductors technology, which are special conductors that do not dissipate if their temperature is close to the absolute zero. However in order to preserve this property there are precise temperature, magnetic field and current density values that must not be exceeded, otherwise these material can locally lose their superconductivity and start dissipating with a phenomenon called “Quench”; then it is necessary to quickly discharge the stored energy of the circuit with proper protection systems called “Quench Protection Circuits” (QPC). IN DEMO the toroidal circuit structure consists of a superconductive magnet composed by 18 superconductive coils in series, a two quadrants AC/DC converter for the slow charging and discharging processes of the circuit and the already quoted protection system (QPC).

This thesis focuses on the study of DEMO toroidal circuit, which generates the main magnetic field to confine the plasma inside the tokamak; during the work I studied the circuit dealing first with its preliminary analysis, highlighting the orders of magnitude of the power supply rating. Next I analysed many different topologies for the circuit in order to identify the best solutions to reduce the overvoltages during anomalous operating conditions. In normal functioning the voltage applied to the coils is low due to the superconductivity; vice versa the voltage becomes higher during the protections intervention, which occurs with the operative current interruption and its transfer over proper resistors, in order to discharge the stored energy. This is a very delicate phase, that must occur in respect of many constraints: a discharge time constant is defined in order to observe a certain i^2t value, which is an important energetic parameter of the circuit. Another important design constraint is the maximum voltage that can be applied to the coils, according to their insulation features.

The objective of the study is to analyse different possible topologies for the toroidal circuit of DEMO in order to identify the best compromise to satisfy all the design constraints. Besides the protection system intervention in case of quench or due to the necessity of discharging the coils, there are also other anomalous conditions that can occur, which could lead to a voltage displacement inside the circuit. Then it makes sense to study the structure, the way of grouping and the earthing topology, in order to identify the best compromise to reduce the stress on the circuit.

The analysis has been done developing a program with a software that could reproduce the voltages in various points of the circuits as well as to calculate the i^2t associated to the different operative

conditions, in order to make a comparative analysis of the various given waveforms from the numerical and graphical points of view.
In Chapter 1 the fusion physics are presented, including a quick overview on nuclear fusion technology and superconductivity and a short explanation about DEMO and its state of art. In Chapter 2 the DEMO design is described, relying to the data of "PROCESS" code. In chapter 3 the power supply sizing is outlined, taking into account typical parameters for the components, focusing in particular on the losses inside the system. In chapter 4 the different circuit configurations and components of the toroidal field circuit are presented, and then analysed through numerical simulations during different operating conditions, and finally discussed and compared.

Index

1 Introduction

During the last years energetic and environmental problems have become one of the most severe challenges for all the mankind, since the world population shows a continuous and exponential growth requiring at the same time an increasing pro-capita energy demand in order to improve the living conditions. For these reasons the primary energy demand is inexorably growing, and in order to satisfy this request it is necessary to find out new technological solutions: in particular fossil fuels are not limitless, though the stocks seem to be bigger than what was expected in the past due to the technological development: however this continuous and heavy use of fossils is absolutely unsustainable from the environmental point of view. The most evident effect of this issue is the undeniable climate change that is afflicting the entire world due to the growing concentration of greenhouse gases; it was confirmed in 2016 that the average CO_2 concentration in the atmosphere exceeded 400 ppm, a value never reached in the last millions of years in the earth and well correlated with the dynamic of increase of earth temperature. [1]

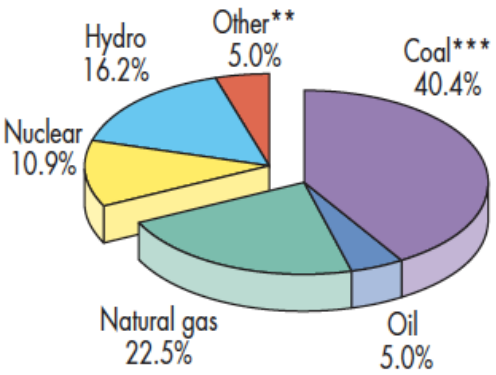

Figure 1 - Global energy production

Another non-negligible issue derived from the fossil fuels combustion is the exasperation of the air quality in certain zones, bringing severe health problems to the populations.
It is necessary to aim at a sustainable development, which would be able to meet current needs without compromising the possibility of future generations to meet their own needs. [2]

Alternative energy sources for electrical energy production have to be investigated and analysed; in particular controlled thermonuclear fusion can be a good candidate to meet these needs for several reasons like the abundance of fuel reserves, low environmental impact and safety.

In this chapter the main physical principles of nuclear fusion reactions will be briefly presented as well as the way to exploit it to produce electrical energy; then there will be explained what DEMO is expecting to demonstrate, and which are its main operative limits. Finally there will be illustrated the different toroidal circuit topologies.

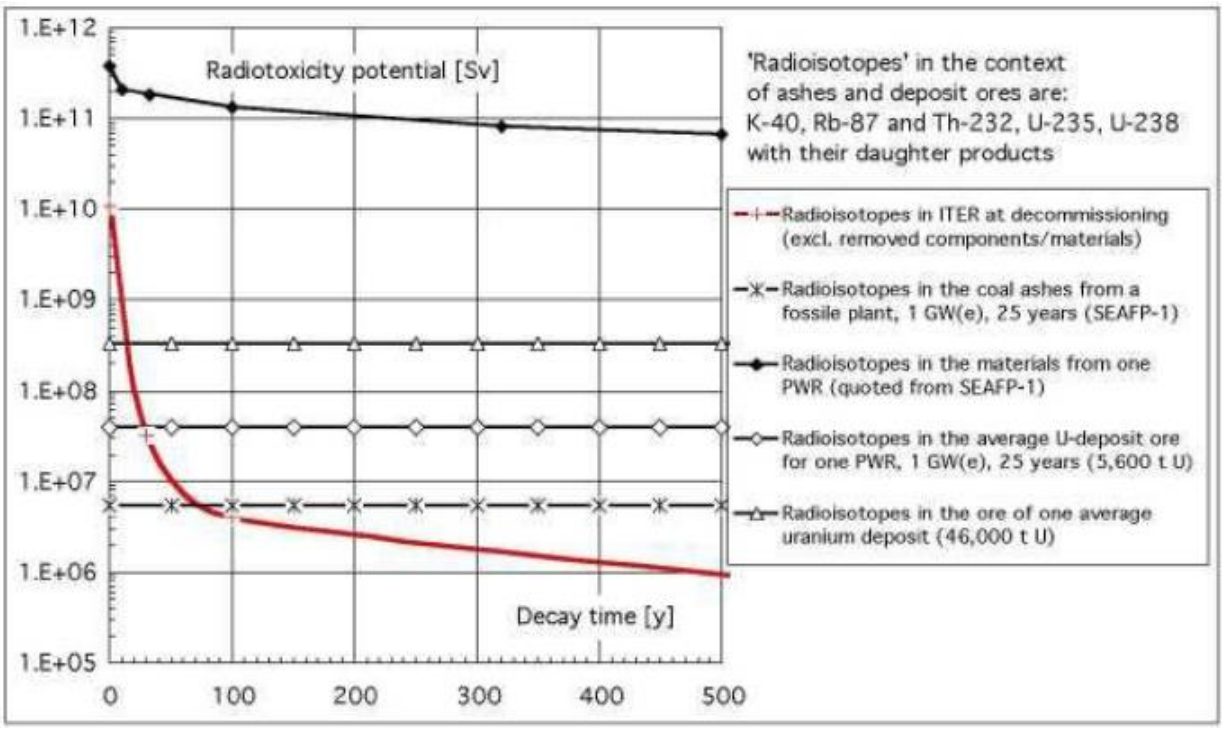

Figure 2 - ITER waste radiotoxicity compared to many traditional power plants

1.1 Nuclear fusion

While in the nuclear fission heavy nuclei like Uranium are fragmented in lighter ones releasing energy, the fusion instead consists of the fusion of light nuclei to form heavier elements and releasing much more energy than in the fission reaction. The energy comes out in the form of kinetic energy of the products, which interact with appropriate components in order to take advantage of this energy.

For both fission and fusion the principle to energy conversion is the same: products have less mass than reactants and this difference is the so called mass defect **Δm**; the energy produced **E** is proportional to the mass defect and it can be evaluated from the Einstein equation where **c** is the speed of light:

$$E = \Delta m c^2$$

In order to obtain a fusion reaction, two nuclei require to win their repulsion force, which is given by:

$$F = k\frac{Q_1 Q_2}{d^2}$$

where Q_1 and Q_2 are the nuclei charges, d their distance and k is equal to:

$$\frac{1}{4\pi\varepsilon_0}$$

When d is lower than the radius of a proton (1 Fermi), the Strong Forces win the Repulsion Force; more in detail, the Coulomb Barrier is overcome by the nuclei force. In the case of Deuterium and Tritium the necessary energy to overcome the barrier is approximately 280 [keV], which is not practically obtainable artificially, however the fusion reaction is possible also with a lower energy due to the

Tunnel Effect and the high energetic queue of the energy particle distribution function. The fusion reaction probability is given by the following:

$$p = e^{-\frac{\pi z_1 z_2 e^2}{2\varepsilon_0 d}(2\frac{m_r}{E})^{\frac{1}{2}}}$$

In order to sustain this reaction, it is necessary to apply very high temperatures (about $100*10^6$ K) since the gravity is too low to sustain this reaction, differently to what happens in the stars like the Sun in which the temperature is about $16*10^6$ K but the gravity force is enormously bigger than on earth. [3]

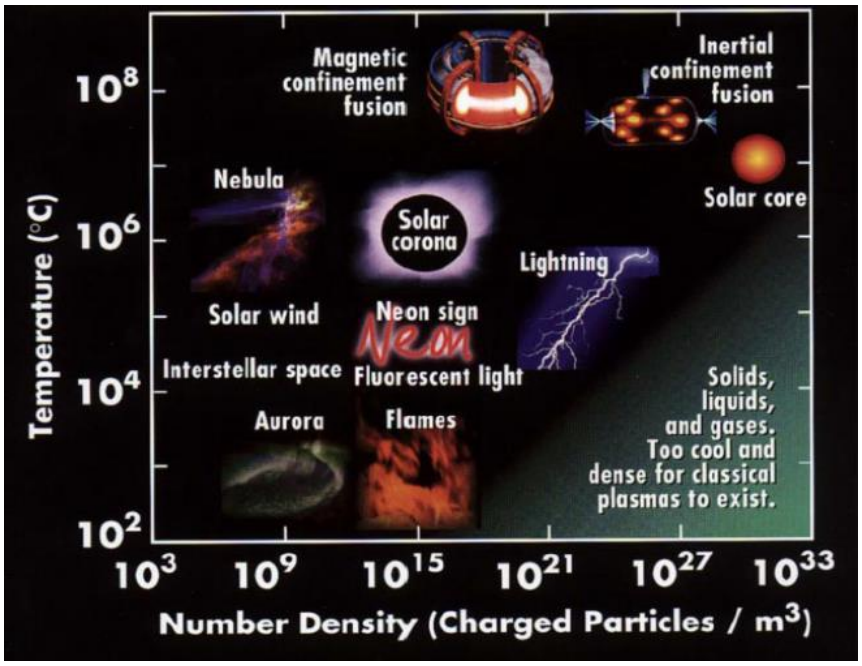

Figure 3 - Different plasma conditions

Several possible fusion reactions are known; on the Sun and most of the other stars in the Universe the reaction is:

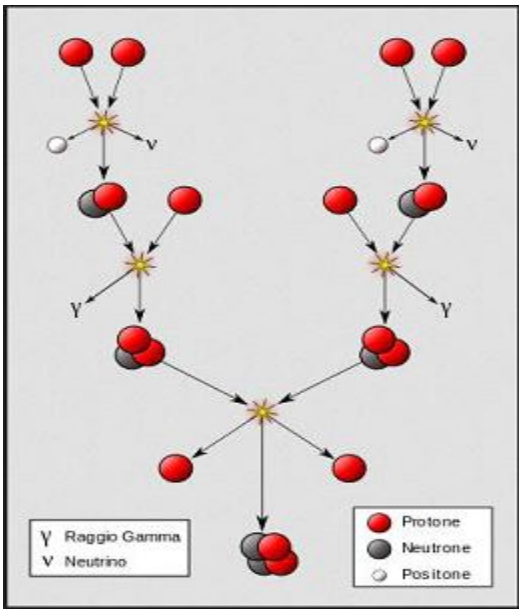

Figure 4 - Proton-proton chain reaction

$$p + p \rightarrow D + e^{+} + \nu_e + \text{energy}$$
$$D + p \rightarrow {}^{3}He + \gamma + \text{energy}$$
$${}^{3}He + {}^{3}He \rightarrow {}^{4}He + p + p + \text{energy}$$

This reaction releases 26.22 [MeV], but it is not obtainable on Earth because the first passage requires a proton-to-neutron decay, which requires 10^9 years.

Other possible reactions are the following:

- **Deuterium – Tritium**
  $D + T \rightarrow {}^{4}He$ (3.52 MeV) + n (14.1 MeV)
- **Deuterium → Deuterium**
  $D + D \rightarrow {}^{3}He$ (0.82 MeV) + n (2.45 MeV)
  $D + D \rightarrow T$ (1.01 MeV) + p (3.02 MeV)
- **Deuterium – ^{3}He**
  $D + {}^{3}He \rightarrow H$ (14.7 MeV) + ^{4}He (3.7 MeV)

The first one has the larger cross section at the lowest temperature, which is proportional to the reaction probability. The products of this reaction behave differently: ^{4}He is positively charged, so if we are talking of magnetic confinement it will contribute to heat up the plasma inside the reactor thanks to its energy (3.52 [MeV]); instead the neutron is not influenced by the confinement, and collides against the reactor, releasing a big amount of thermal energy.

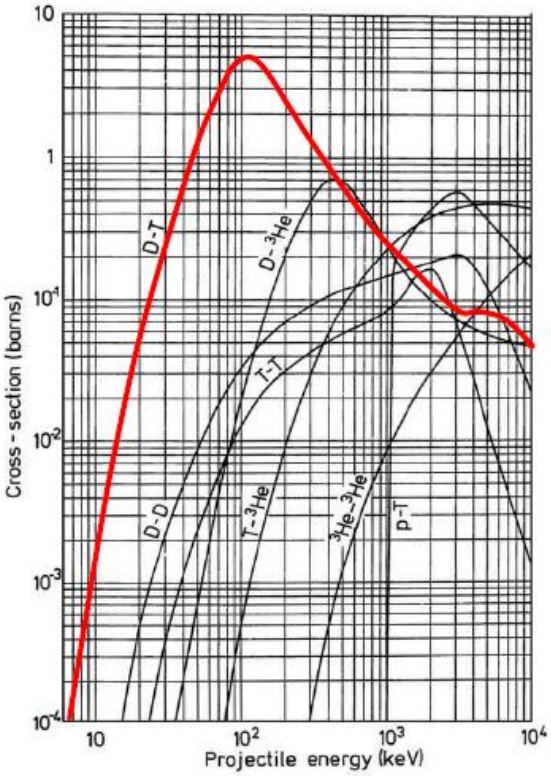

Figure 5 - Cross sections of the different reactions

1.1.1 Fusion reactants

Deuterium can be found in the water with a concentration of 1/7000; due to its heavier mass it is easy to be extracted and relatively cheap. Tritium is a radioactive isotope, and for this reason it decays; its half-life is equal to 12 years, so it is impossible to find it concentrated in nature; it can be produced in the high layers of the atmosphere from the interaction between γ-rays and nitrogen, or in the CANDU fission reactors, but in the future it will be provided by the fusion reactors chain starting from the Lithium in the breeding blanket:

$$^{6}Li + n \rightarrow T + {}^{4}He + 4.78\ [MeV]$$

$$^{7}Li + n \rightarrow T + {}^{4}He + n - 2.5\ [MeV]$$

In a fusion reactor there will be the need to have two fuel cycles: one for Helium and one for Tritium; due to the extremely low pressure, inside the reactor there are 1-to-10 [g] of Tritium and in all the plant 1 [kg] overall, so there is a very low biological risk outside the plant.

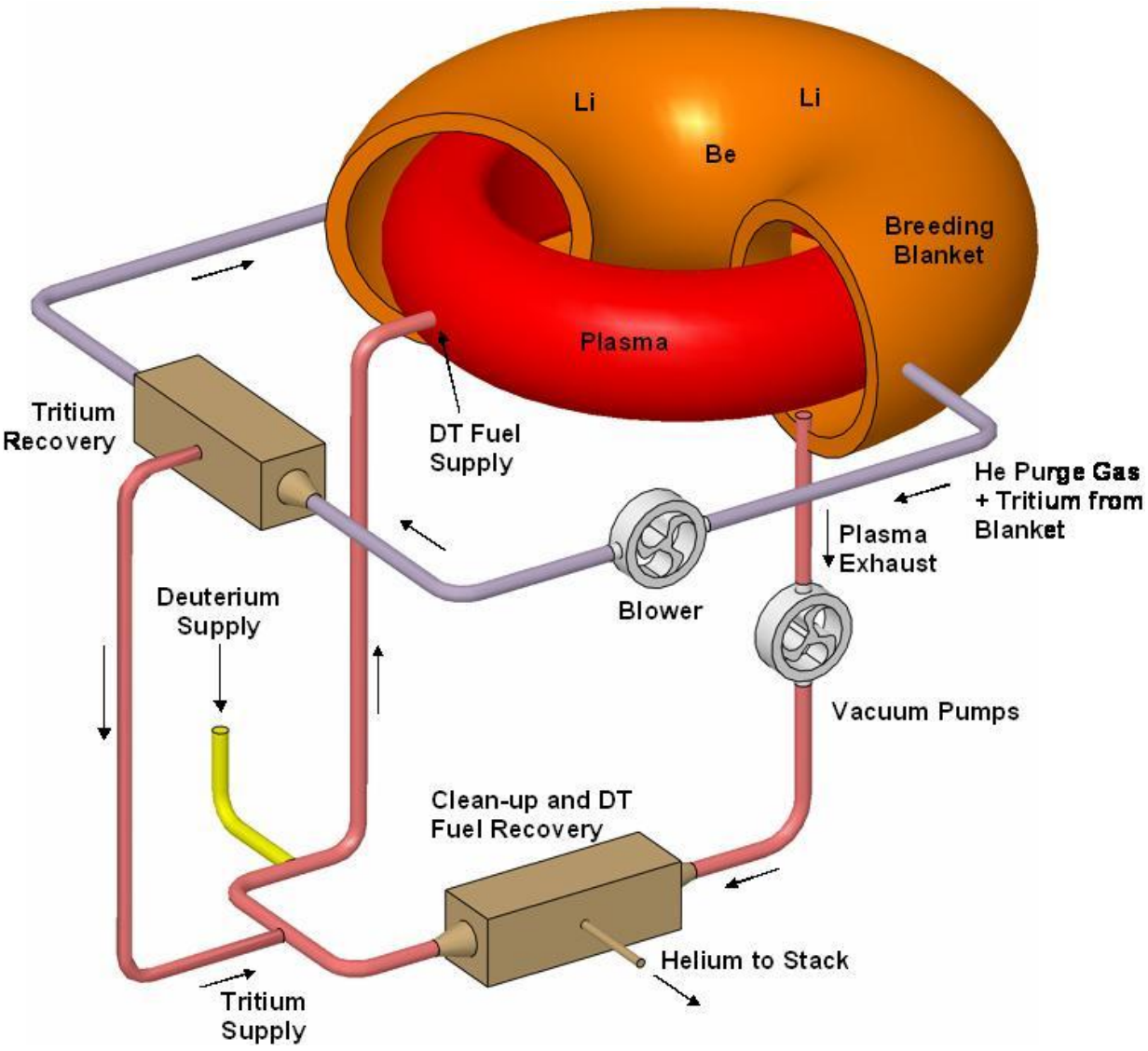

Figure 6 - Helium and Tritium cycles

With respect to the nuclear fission this technology has several big advantages in addition to fuel availability:

- The fusion reaction is inherently safe. There is no danger of runaway reactions, criticality or a meltdown. At a given instant of time the total inventory of fusion materials in the device is just enough to produce the power for a few seconds. This is a very different condition with respect to the fission, where the inventory stored at a given instant is enough to cause a major explosion.
- The radioactive pollution is still present, due to the activation of materials by high energy neutrons, but the life time of the radioactive waste is hundreds of years instead of thousands of years such as for nuclear fission.

1.1.2 Thermonuclear power balance

There are different types of losses for the plasma:

- Electromagnetic radiation losses: Bremsstrahlung, recombination, cyclotron radiation, energy shifts of non-ionized particles due to impurities
- Transport losses: conduction, convection, particles diffusion

The radiation losses are inevitable, but can be minimized and so neglected compared to the transport losses; it is possible to introduce the *Energy confinement time*:

$$\tau_E = \frac{Plasma\ stored\ energy\ per\ volume\ unit}{Transport\ losses\ per\ volume\ unit} = \frac{W}{P_{TRAN}}$$

with:

$$W = \frac{3}{2} n_e k T_e + \frac{3}{2} n_i k T_i$$

where *n* is the particle density, *k* is the Boltzmann constant, *T* is the particle temperature, the subscripts *e* and *i* stand for electrons and ions; the ½ factor stands for an equal distribution inside the plasma of ions and electrons, and the *3* factor is equal to the degrees of freedom of the system.

If $n_e = n_i = n_D + n_T = n$ and $T_e = T_i = T$, where the subscripts D and T stands for Deuterium and Tritium, then:

$$W = 3nkT$$

So we obtain:

$$P_{TRAN} = \frac{W}{\tau_E} = \frac{3nkT}{\tau_E}$$

Expressing in eV, we can elide the Boltzmann constant:

$$P_{TRAN} = \frac{3nT}{\tau_E}$$

The equilibrium condition is:

$$P_H = P_{LOSSES} - P_{He} = P_{TRAN} - P_{He}$$

where P_H is the heating power to be injected inside the reactor to maintain the reaction.

The power provided by the Helium can be obtained by simple considerations; let's assume to have two different species nuclei, having densities n_1 and n_2, and v is their relative velocity. The reactivity g is defined as the number of reactions per volume unit and time unit:

$$g = n_1 n_2 < \sigma v > \quad [\frac{1}{sm^3}]$$

where <σv> is the average, due to the fact that not all the nuclei have the same velocity.

Since Q_{th} is the thermonuclear energy produced by a reaction, then the power per volume unit is:

$$P = gQ_{th} \quad [\frac{W}{m^3}]$$

In this specific case, as reported in [1.1]:

$$Q_{th} = \xi_n + \xi_{He} = 14.1 + 3.52\ MeV = 17.6\ MeV$$

It can be noticed that the neutron energy is about four times the Helium energy: $P_n = 4P_{He}$

But only the Helium energy contribute to heat the plasma, then we can assume:

$$Q_{th} = \xi_{He}$$

If we suppose we have a 50% D - 50% T mixture, then $n_1 = n_2 = n/2$, so:

$$P = \frac{n^2}{4} < \sigma v > Q_{th}$$

In this case:

$$P_{He} = \frac{n^2}{4} < \sigma v > \xi_{He}$$

So, finally:

$$P_H = P_{TRAN} - P_{He} = \frac{3nT}{\tau_E} - \frac{n^2}{4} < \sigma v > \xi_{He}$$

If:

$$\frac{n^2}{4} < \sigma v > \xi_{He} \quad > \quad \frac{3nT}{\tau_E}$$

we are in ignition condition, because the plasma is self-sufficient, and do not requires an external heating to maintain the reaction.

An useful parameter is the *Gain* "Q":

$$Q = \frac{P_\alpha + P_n}{P_H} = \frac{5P_\alpha}{P_H}$$

Q = 1 is the "Breakeven" condition; if Q>1, the reactor is working as a power amplifier.

1.1.3 Plasma confinement

There are essentially two types of plasma confinement: inertial confinement and magnetic confinement. The gravitational confinement is obtainable only into the stars.
A high-temperature plasma naturally tends to expand; in this situation the particles velocity is about 10^6 [m/s]. Therefore it is necessary to confine it in a non-material container, avoiding cooling and sputtering contamination.

- INERTIAL CONFINEMENT
  A little sphere with a Deuterium-Tritium core, a Deuterium-Tritium cortex in cryogenic conditions and a plastic layer is hit by hundreds of synchronized high-power lasers, causing the explosion of the plastic layer which causes an implosion of the D-T core and an ignition condition; this energy is collected by the chamber walls, including not only the neutron particles but also the Helium ones, due to the non-magnetic confinement.

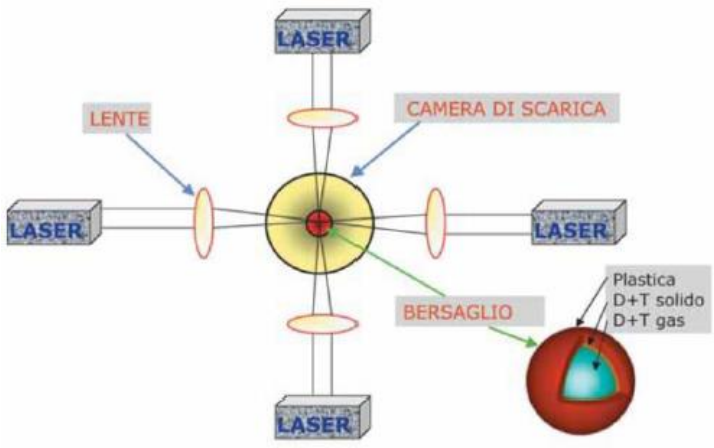

Figure 7 - Inertial confinement configuration

Another configuration is the indirect irradiation from two directions into an adsorption cavity, which internal layer emits X-rays when hit by the lasers.
Several experiments are being studied: HiPER (EU), Laser MegaJoule LMJ (FRA),FIREX (JPN), National Ignition Facility NIF (USA). LMJ and NIF are essentially military driven.

- MAGNETIC CONFINEMENT
  It is based on the fact that, under a magnetic field, charged particles move not in a chaotic way, but with a helical motion following the Lorentz law:

$$\boldsymbol{F_L} = q\boldsymbol{v} \times \boldsymbol{B}$$

For the magnetic confinement there are two possible configurations: linear configuration and toroidal configuration.
Thus far the most successful way of trapping the plasma particles along the magnetic field lines has been achieved by magnetic confinement in fusion reactors based on the Tokamak concept

[4] (see "1.2 *The magnet system of a Tokamak*"); however other magnetic configurations like Stellarator and Reversed Field Pinches (RFP) are possible.

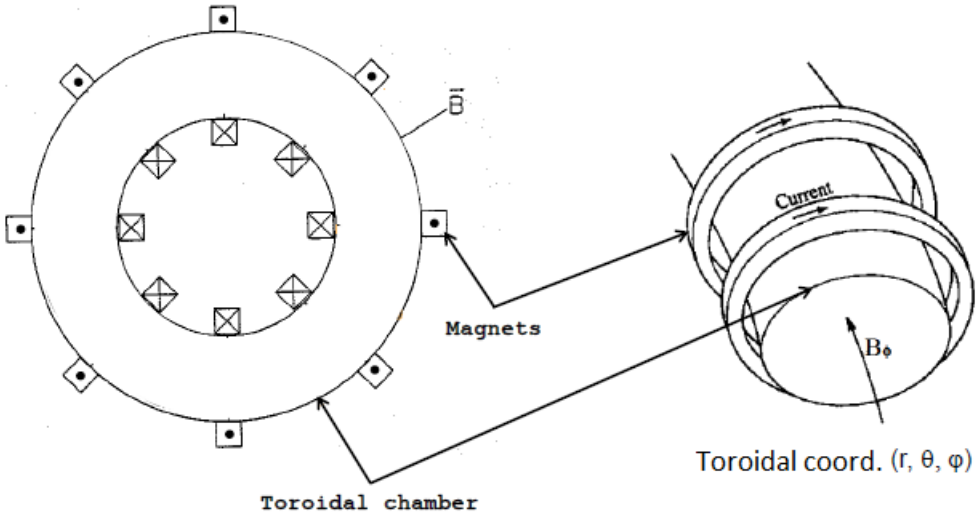

Figure 8 - Toroidal configuration

The magnetic field originated by the toroidal coils Bφ guides the particles along the chamber, but the field is stronger on the inner section of the chamber respect to the external section, so the particles are drifted; more in detail, the positive charges are driven downward and the negative charges are driven upward.

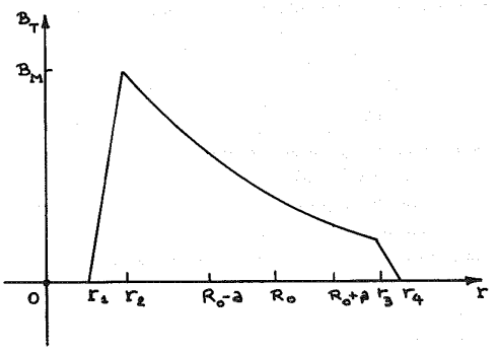

Figure 9 - B-field gradient along the radius

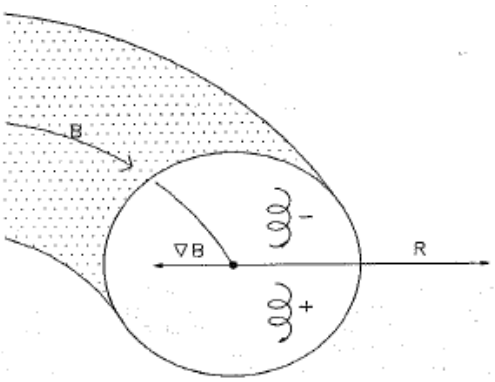

Figure 10 - Particle drift with the charge

The solution is given with the addition of a poloidal field B_Θ, created by the flowing of the plasma current along the chamber:

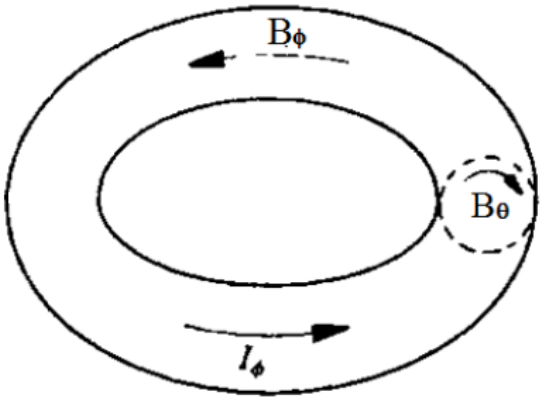

Figure 11 - Toroidal and poloidal fields

There are different magnetic configuration, depending on which current component is prevailing. In the adopted cylindrical system the z-axis coincides with the current flow, r is defined by z=0 and Θ is the polar coordinate:

- if **J** = (0 , $J_\Theta(r)$, 0) then **B** = (0 , 0 , $B_z(r)$) ⟶ Θ - Pinch Configuration

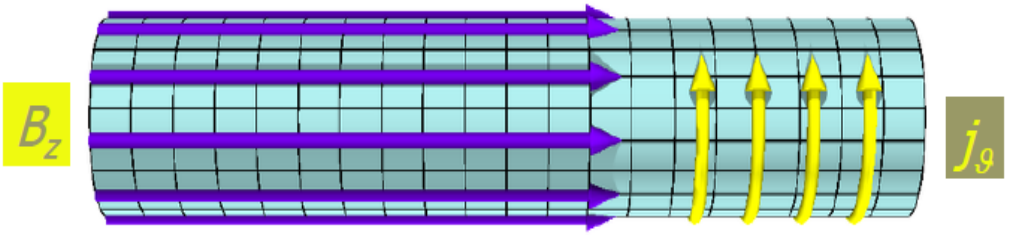

Figure 12 - Θ - Pinch Configuration

- if **J** = (0 , 0 , $J_z(r)$) then **B** = (0 , $B_\Theta(r)$, 0) ⟶ Z - Pinch Configuration

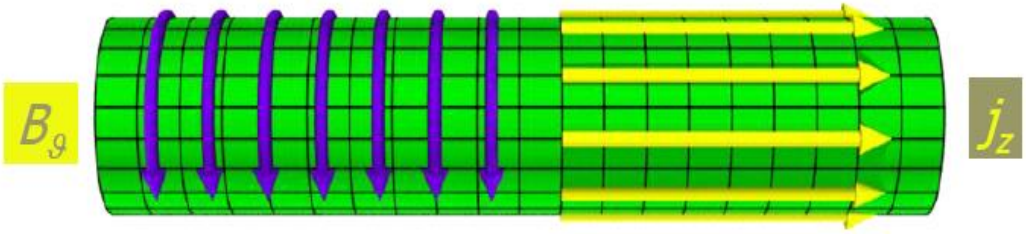

Figure 13 - Z - Pinch Configuration

An example of Z-pinch configuration is given by the Sandia Lab (USA) (Figure 14).

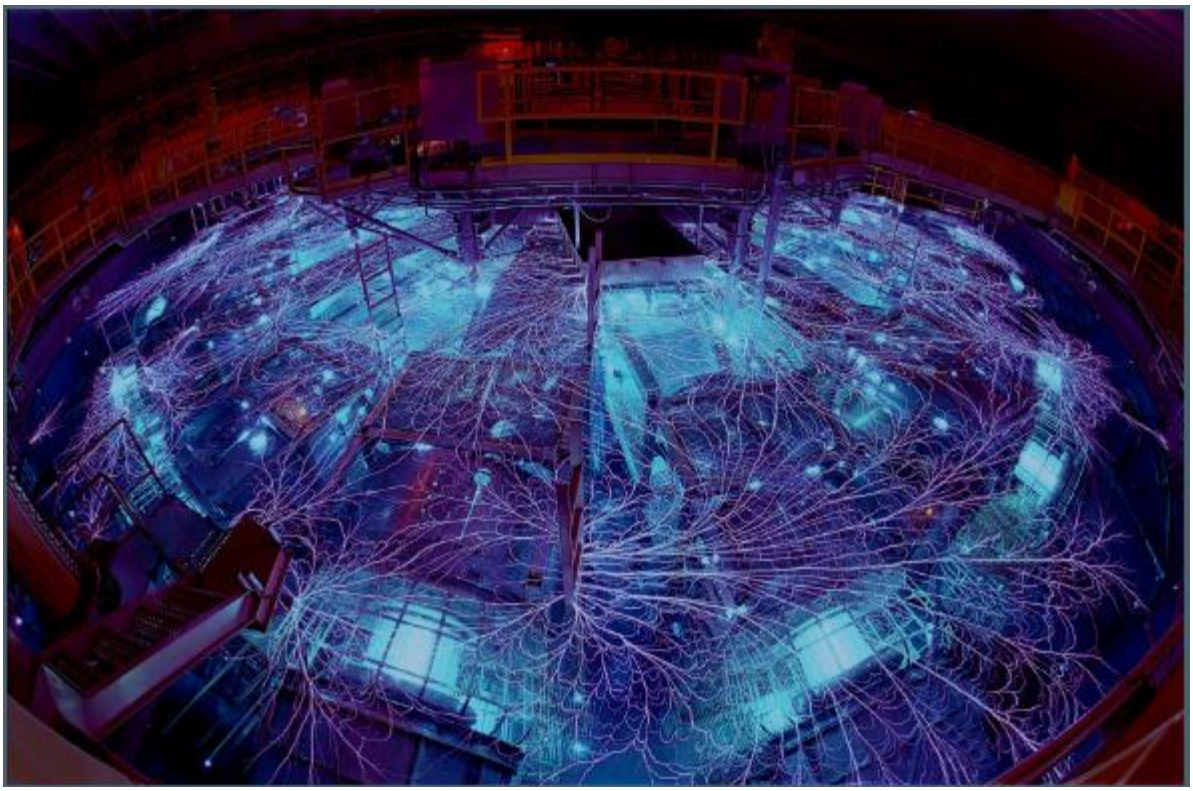

Figure 14 - Sandia Lab z-pinch

- if **B** = (0 , $B_\Theta(r)$, $B_z(r)$) ⟶ Screw - Pinch Configuration, which is the solution adopted for Tokamak, RFP and Stellarator.

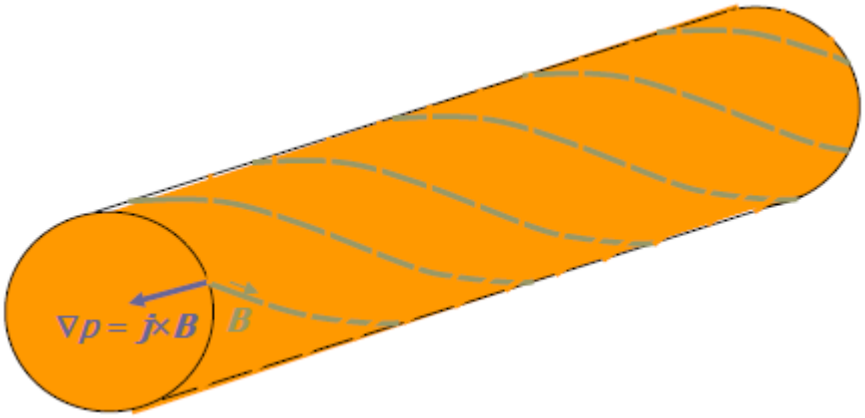

Figure 15 - Screw-Pinch configuration

A vertical magnetic field is also added to control the position and the shape of plasma, in order to balance the gas expansion.

1.2 The magnet system of a Tokamak

A tokamak (from the russian ***TO**roidal **KA**mara **MA**gnit **K**atushka*) is a device that uses a powerful magnetic field to confine plasma in the shape of a torus, and is composed by a toroidal chamber containing the plasma and a magnetic system. The magnetic system is composed by:

- The toroidal field magnets, consisting of a certain number of coils, in order to produce the toroidal field Bφ
- A central solenoid in order to induce a current inside the plasma, and an eventual iron magnetic circuit; the solenoid-plasma system is comparable to a transformer, where the plasma is its secondary
- The poloidal field magnets, consisting of a certain number of coils which are coaxial to the torus, producing a vertical magnetic field which interacts with the plasma producing a force that prevent the radial deformation of the plasma

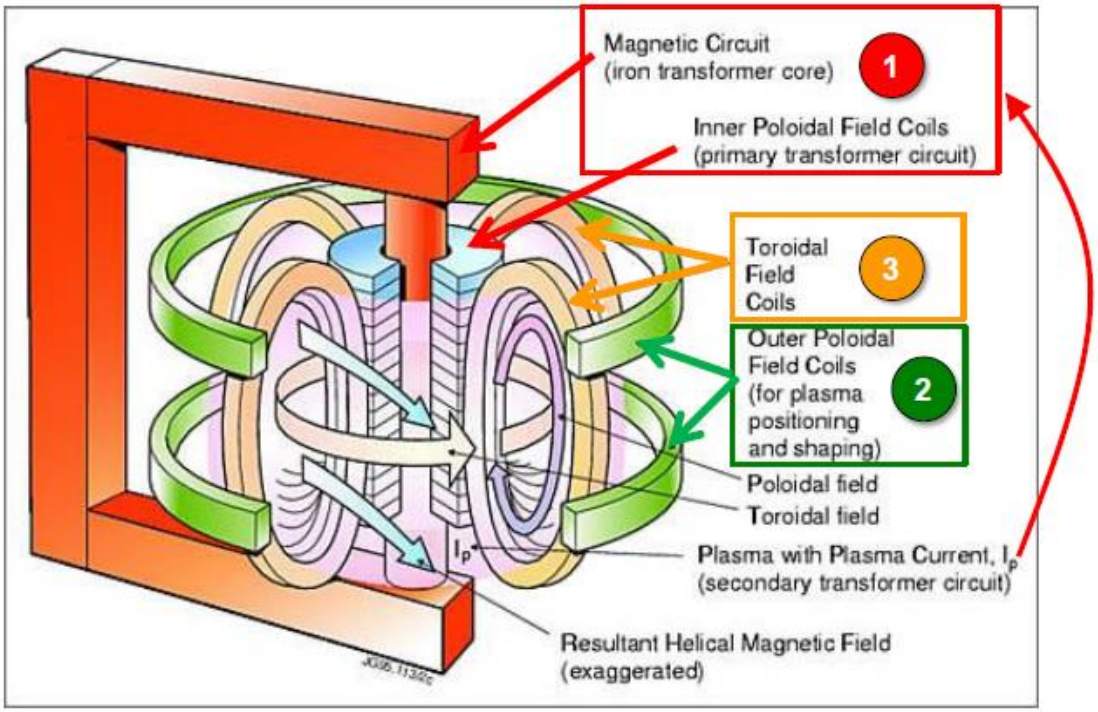

Figure 16 - Tokamak magnetic system

1.3 Superconductivity

In order to produce these magnetic fields (for example, in DEMO to produce the toroidal field Bφ there will be required current values of about 60 to 70 [kA]) it is unthinkable the use of traditional copper conductors, due to the enormous current values and the correlated ohmic losses; for this reason it is necessary the use of superconducting magnets kept in cryogenic conditions.
Superconductivity is a phenomenon of exactly zero electrical resistance and expulsion of magnetic flux fields occurring in certain materials when cooled below a characteristic critical temperature [5].

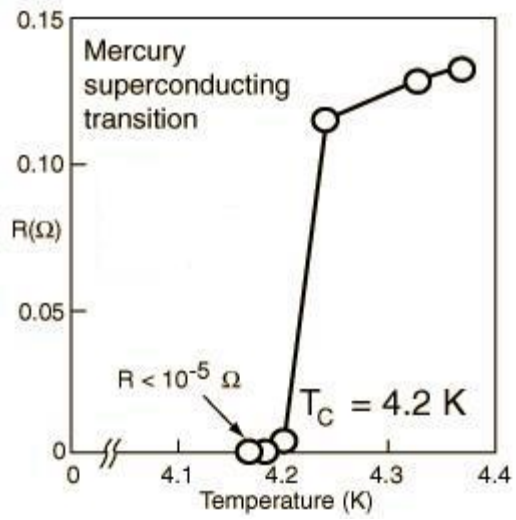

Figure 17 - Mercury superconducting transition

However if the current flowing into the superconductor exceeds the critical value Ic, the material becomes again a normal conductor.

From the physical point of view, the resistivity in metallic materials decreases with low temperatures because the ions inside the crystalline lattice reduce their vibrations. It is possible to describe the resistivity with the Matthiessen law:

$$\rho = \rho_t + \rho_r$$

where the first term is the resistivity bound to temperature and the second one is bound to the lattice imperfections. A crystal at absolute zero temperature presents only the second term.
In superconductors this rule is still valid, but only until the critical temperature Tc, below which the resistivity quickly decreases to very low values, difficultly measurable.

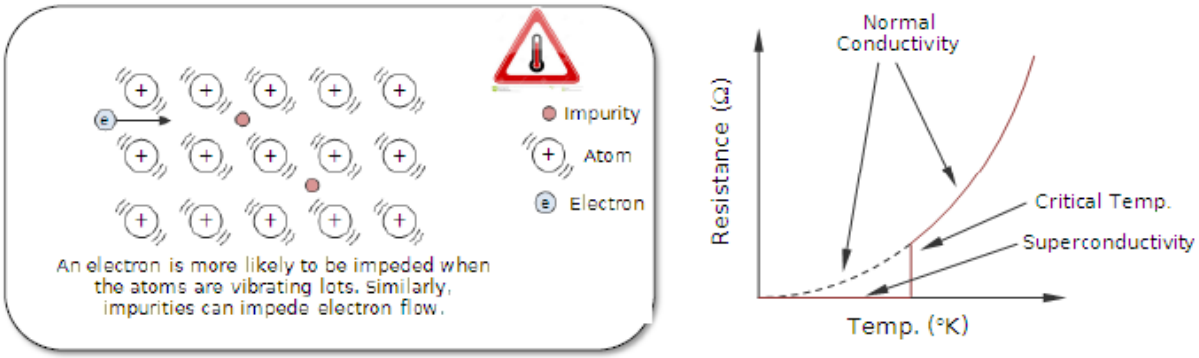

Figure 18 - Superconductivity transition

This attitude can be explained with the Bardeen, Cooper and Schrieffer theory (BCS), which bases on the *Cooper pairs theory*: the lattice ions vibrations produce energy quants called phonons; in superconducting materials these vibrations can be produced by the passage of an electron inside the lattice.

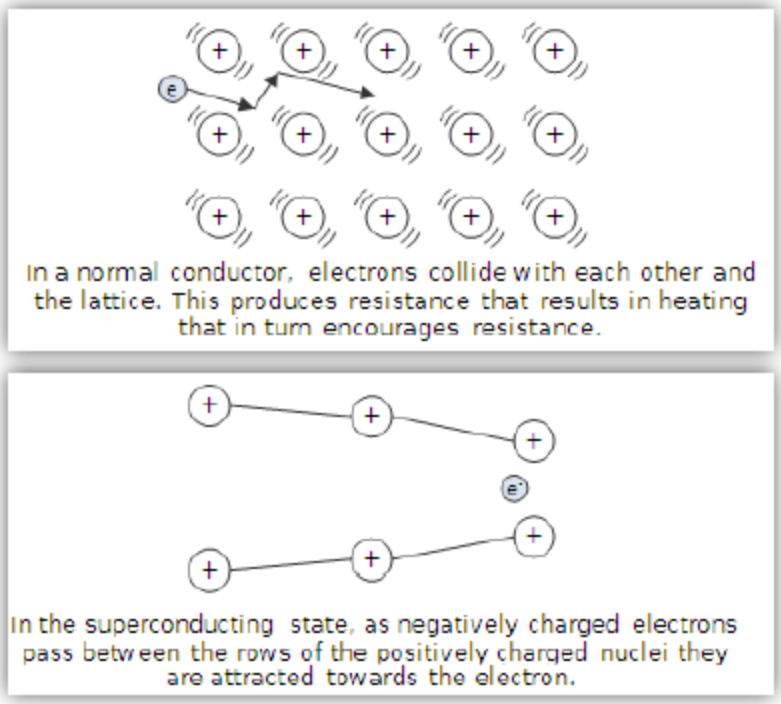

Figure 19 - BCS theory representation

The electron causes a distortion of the lattice and an accumulation of positive charge, which attract another electron; so the phonons help the Cooper pairs formations, which are able to freely move inside the crystal as an unique entity:

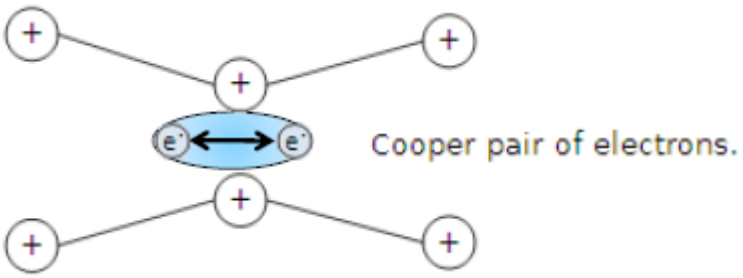

Figure 20 - Cooper pair of electrons

As said previously, another property of superconducting materials is the expulsion of magnetic flux fields below the critical temperature Tc (Meissner effect, 1933); but also in this case there is a critical value that, if exceeded, causes the loss of the superconductive properties.

Meissner effect can be explained with the surface currents, that creates inside the conductor a magnetic induction field of the same value of the external one but opposite, in order to inhibit the penetration of the external field; so the material becomes perfectly diamagnetic. The penetration depth of the currents is about 10 to 100 [nm].

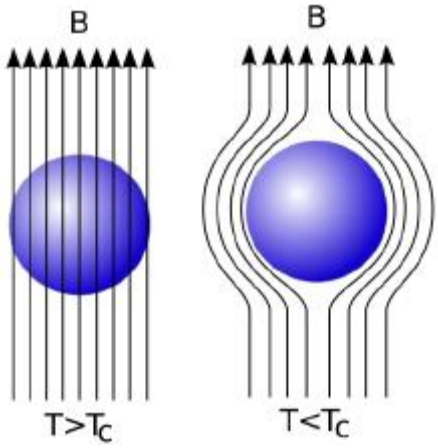

Figure 21 - Meissner effect

The properties of superconducting materials can be represented by current density, induction field and temperature surfaces:

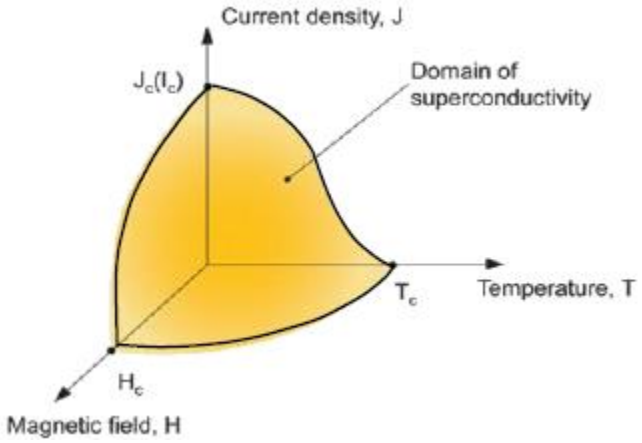

Figure 22 - J,B,T surfaces for superconductors

Superconducting materials can be distinguished in two groups: the second group, differently from the other one, provides that, after a penetration of the field, the material still remain superconductive; the passage from superconductive to non-superconductive is not net, but after a "mixed" state, where the magnetic field starts to locally penetrate inside the material (vortex theory).

Following the discovery of high-field superconductivity in the late 1950s, superconducting wires for magnet construction were produced in industry and offered for sale within a remarkably short space of time. By 1961 small magnets were being made from 1/4 [mm] diameter wires of niobium zirconium, a ductile alloy. This was quickly followed by niobium tin (Nb_3Sn), an intermetallic compound with excellent superconducting properties but so brittle that it could not be fabricated by conventional wire-drawing processes. Niobium titanium (NiTi) wires were first produced in 1965 and this ductile alloy has since become the standard "work-horse" of superconducting magnet construction, mainly because it is relatively easy to fabricate and may be co-processed with copper. [6]

1.3.1 Superconductive coils

The most used superconductive material is a NbTi alloy, but the chosen material for ITER is a Niobium-Tin alloy due to its big current density limit, equal to 10 [kA/mm^2].
For example, the common copper wiring used for domestic purpose has a current density of 1 [A/mm^2], and the copper magnets at maximum 30 [A/mm^2], which is a technical limit due to the cooling.

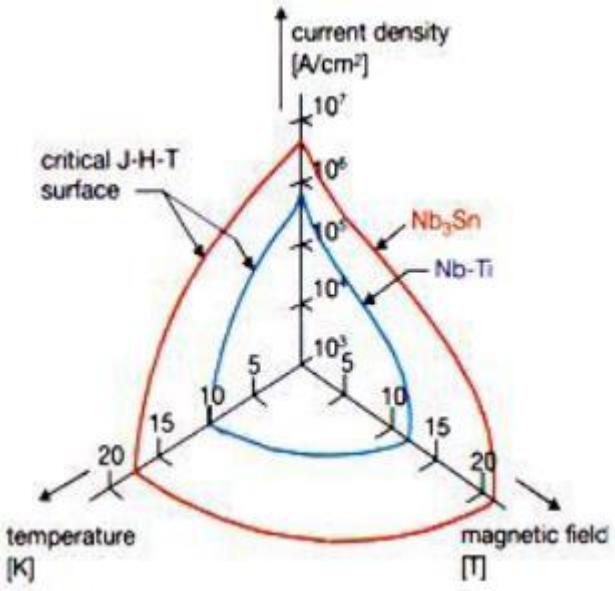

Figure 23 - Comparison between Nb-Sn and Nb-Ti alloys

There are many requirements for the magnetic system superconductors: a high current transportation in extremely high electromagnetic fields, the ability to dispose the heat produced by Joule effect, the mechanical stress resistance and, most of all, the quench protection (superconductive to non-superconductive transition) (see 1.4). The solutions adopted for each problem are a stranded wire, with an opportune channel inside the pack where cooling Helium can pass through, a high mechanical resistance is a coating or a shell (or envelope) and the adding of copper stranded wiring to bypass unexpected too high currents.

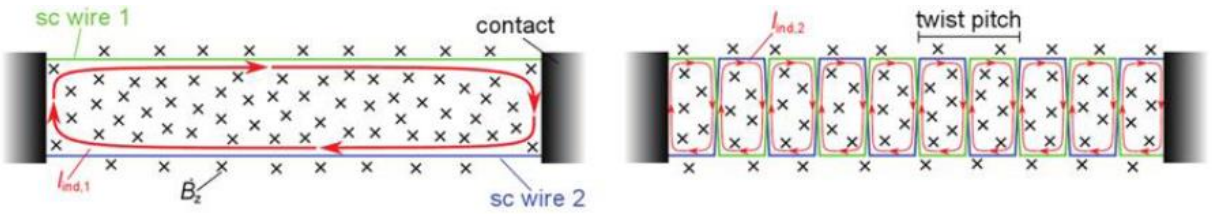

Figure 24 - Stranded winding

In high current cable-in-conduit conductors stranding is mainly used. Sometimes not all strands are stranded at once, the stranding is done in several stages. Sub-cables are formed by stranding thin wires which are then entwisted themselves. This allows low void fractions and complete transposition of all wires. In magnets the superconducting wires are exposed to varying magnetic fields. Without any transposition, the area surrounded by superconducting wires which is penetrated by the field can be very large in a magnet of fusion relevant size. Large currents, commonly referred to as coupling currents, are induced. These currents reduce the transport currents which can be carried by such a superconducting cable. This can also result in low coupling and alternating-current losses. In Figure 24 this is shown schematically for a cable consisting of two superconducting wires.

Transposition of the wires or strands is therefore essential in fusion relevant superconductor cables. To minimize the coupling currents and the AC losses, the length of the transposition, commonly referred to as the "twist pitch" of the cable should be as low as possible. However, short twist pitches increase the necessary amount of superconductor per cable length, which has to be balanced against the AC losses in finding the ideal twist pitch of the cable.

The cooling plant cost becomes much lower when working at liquid nitrogen temperature (77 K); it is possible to operate in superconducting conditions also at this temperatures with High Temperature Superconductors (HTS), as shown in Figure 25; in fact in ITER the connection between the external copper bars (ambient) and the internal superconductors (4K) (called Current Leads) have been realised using BiSrCaCuO [7], and the cryogenic plant cost has been reduced at least by 20%.

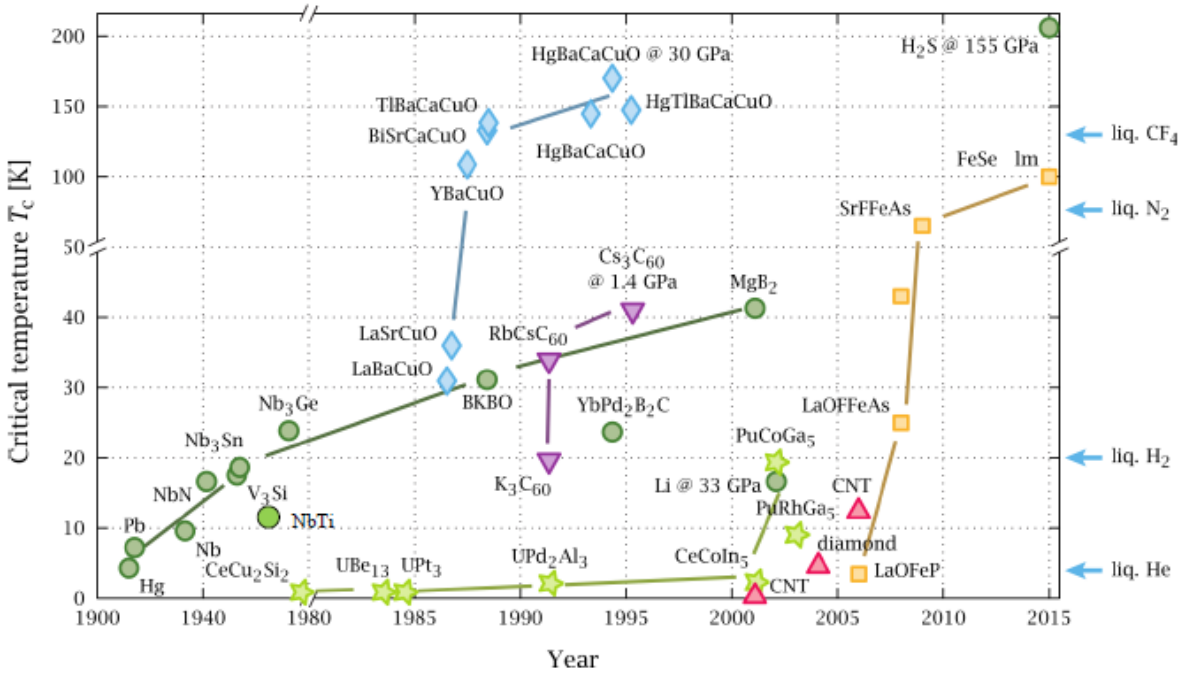

Figure 25 - Superconducting materials progress

1.4 Quench and coil protection strategies

In a superconducting coil a quench event is the local, irreversible loss of superconductivity: the critical surface (B, T, I) (see Figure 22) is exceeded in a short section of the winding and the superconductor becomes resistive. The local ohmic power generation overcomes the heat removal capability, and the temperature runaway may eventually lead to melting of the coil.

A quench event is a serious safety issue for superconducting coils. Even if a quench event should never happen according to the design, countermeasures must be planned to face a quench event. During the interval between the start of the quench and the reliable detection with related action, the power deposited at the quenched spot is in the range of few [kW] in large coils.
I^2t is a very important parameter to analyse the stored energy put in place inside an electric circuit. The temperature raises if power is deposited for a long time; if the QPC works correctly the temperature will be kept beyond the limits, because the I^2t will be equal to the project value of the coils. If the QPC does not work correctly and the resistor inserted inside the circuit is lower than the project value then the discharge is longer; consequently there will be deposited power for a longer time, causing overtemperature. In the best case there will only be thermal stress, but in the worst case it is possible to burn the coil.
The coil project value is the value that has been obtained in nominal condition, which must be not exceeded during the functioning, even during a fault condition. This value is defined as nominal i^2t for the coils.
The very first obvious action as soon as a quench is detected is to stop powering the quenched winding. However, placing the power supply in “freewheeling” (basically a short circuit), is not effective to stop the current in the winding, which is sustained by the stored energy. Even if the power supply is short circuited, the current decays very slowly, as (L/Rquench), depositing most of the stored energy at the quenched section of the winding, which expands moderately slowly. Depending on the stored energy / mass of the winding, the amount of copper in the conductor, the heat diffusion in the winding, etc, various approaches can be taken to preserve the integrity of the coil in case of quench, most of all the insertion of Quench Protection Circuits (QPC). Normally the operative current Iop flows through the crowbar (CB), which is put after the coil as shown in Figure 26; in case of quench event the QPC is opened by a command, and the opening time is called “tq”; after that the current is diverted to the DR, and the coils starts to discharge. The time trends of the process are shown in Figure 27:

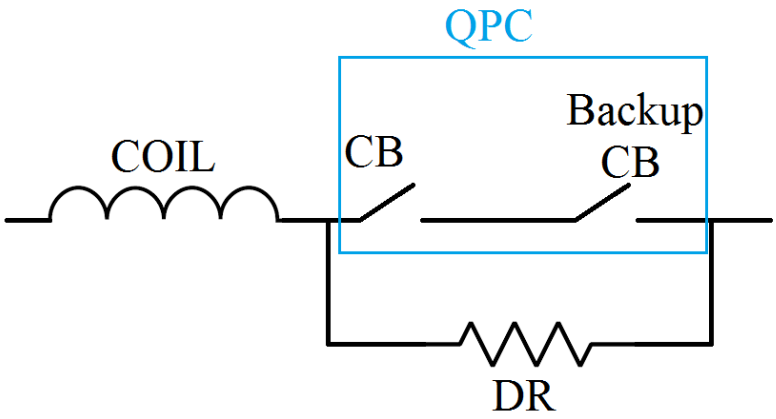

Figure 26- QPC configuration

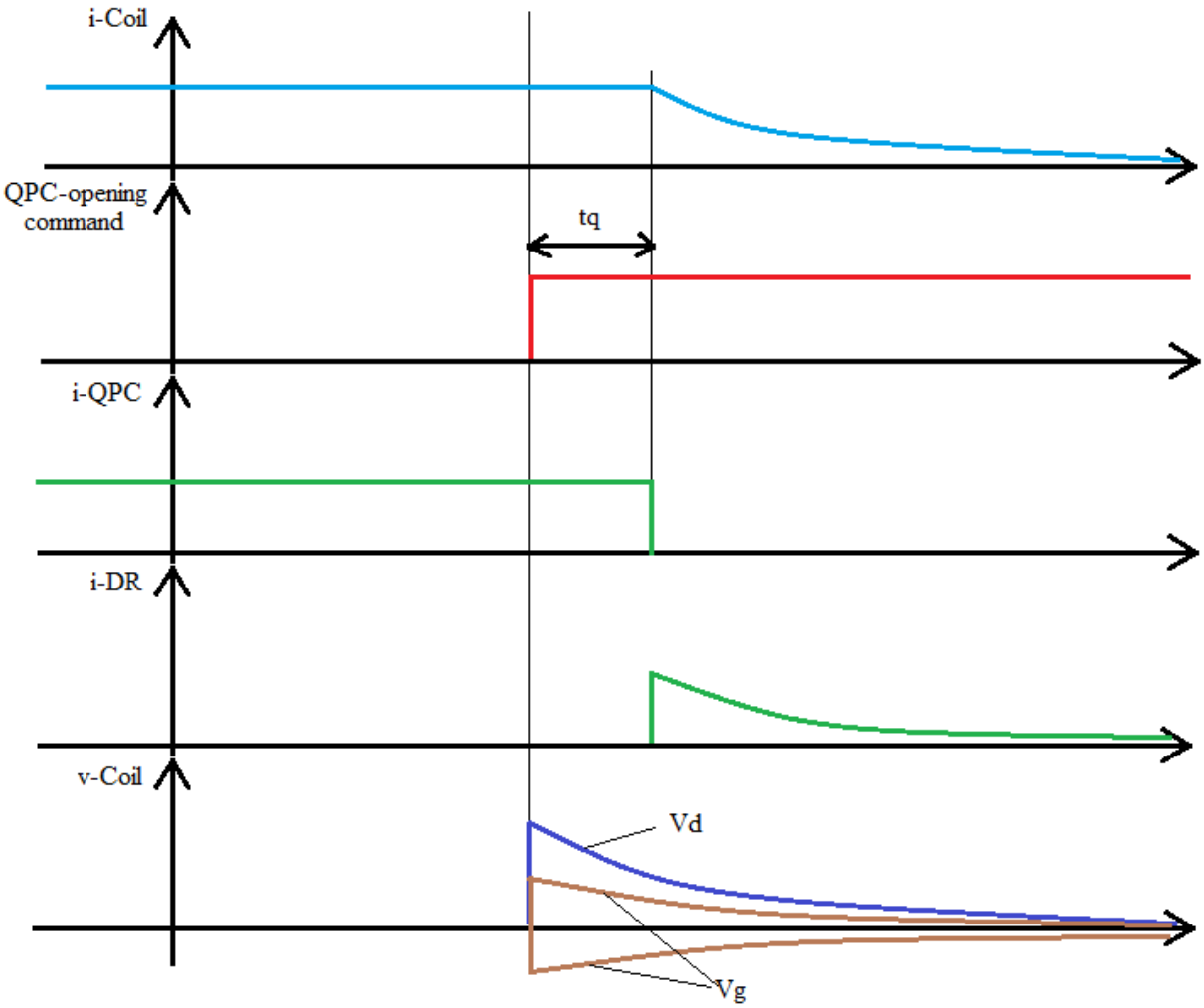

Figure 27 - Quench protection strategy

Whenever the CB does not work, it is provided a Backup CB as shown in Figure 26. Typically this device is an explosive charge called “pyrobreaker"; this device requires an extra time before operating called “tb”, which is usually equal to 10 [ms] (Figure 28). It is a necessary device because, whenever the CB does not work properly, the discharge time could be longer than the project discharge time, bringing to an overtemperature on the superconductive components and several damages over them.

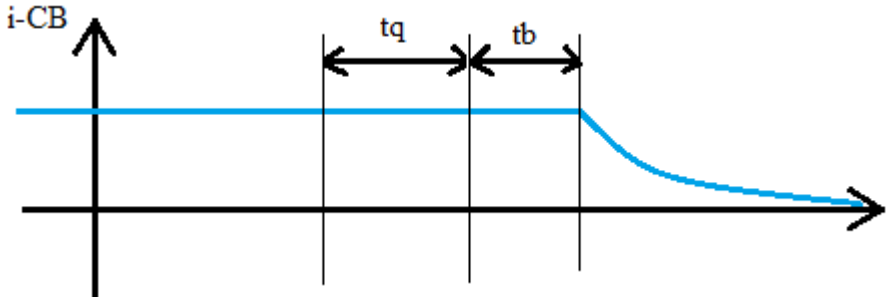

Figure 28 - Backup CB intervention

The energy is not dissipated homogeneously in the winding, with the largest fraction, and hence the largest temperature, at the spot where the quench initiated, also named “hot spot”. [8]
Large temperature gradients are dangerous because of thermal-mechanical induced stress, which can destroy the integrity of the winding. As a design criterion, the hot spot temperature is usually specified

hot spot ≤ 150 K in the rigid parts of the winding, as shown in the case of Figure 29.
In superconducting magnets with stored energy density larger than few [J/g], it is mandatory to extract the stored energy to limit the hot spot temperature.
Another important parameter during quench is pressure. During a quench situation on a coil there is a superconductor to conductor transition, so that area becomes subjected to Joule effect: the QPC is able to detect the quench because a non-resistive component has become resistive. Since the QPC intervention the current goes to zero exponentially, as shown in Figure 29, but during this phase the resistive zone dissipates energy, producing heat all around its position; this heating could be able to bring the liquid cooling helium in its gaseous phase, and this transition raises the pressure, which must not exceed the maximum allowed value (in this case 10^6 [Pa]).

Whenever the maximum temperature value should be exceeded the proposed solution is to raise the copper cross section, in order to increase the thermal inertia and to decrease the Joule effect.

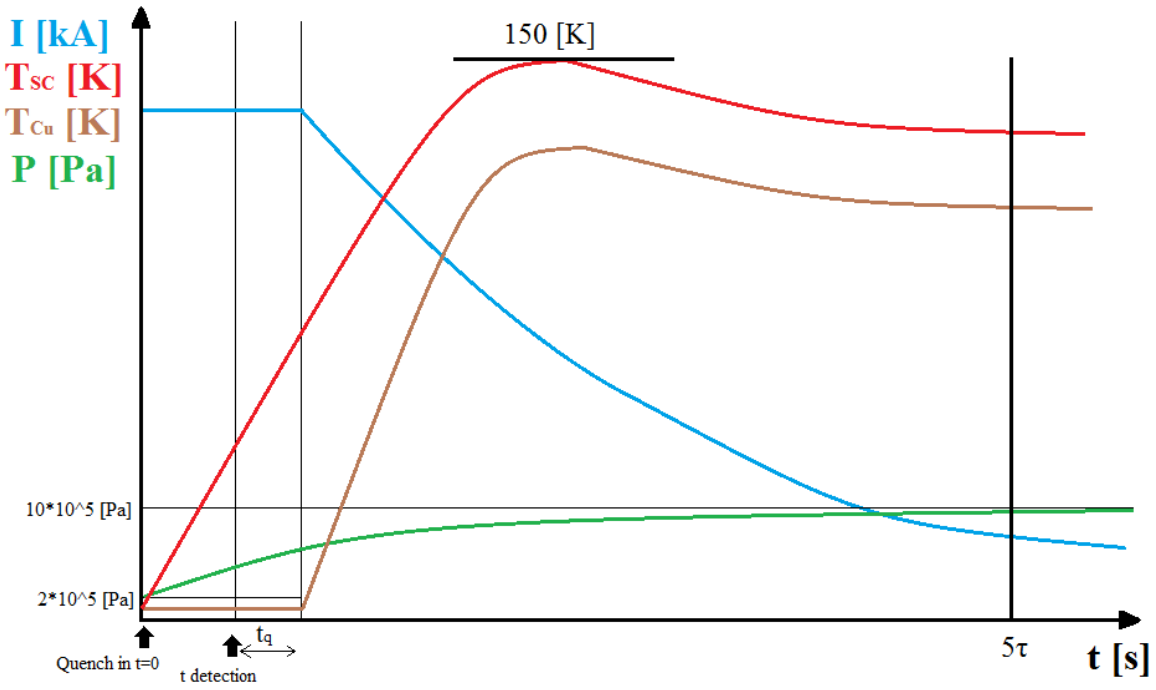

Figure 29- Pressure, temperature and current trends during the QPC intervention

QUENCH PROTECTION STRATEGY

Initially the coils are fully charged of magnetic energy, and whenever a quench occurs there are 136 [GJ] distributed over 18 coils to be disposed in τ = 27 [s] (see 3.2), and this raises the coil voltage (Vd) because the energy is dissipated on the DRs in accordance with:

$$Vd = RI = \frac{L}{\tau} \cdot I$$

$$E = \frac{1}{2} LI^2 \longrightarrow Vd = \frac{2E}{\tau I}$$

and Vd is equal to 150 [kV] if there is only one DR. Instead if each coil is provided with one QPC, the voltage is:

$$Vd = \frac{150}{18} = 8.8 \text{ [kV]}$$

Instead with a two coils per QPC configuration Vd is 16.7 [kV]. These are the maximum voltage values reached during nominal conditions (Op. C. 1: see Table 12). Considering the 18 QPC configuration, the voltage is applied to the coil, as shown in Figure 30.

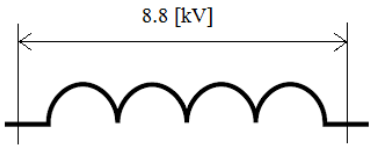

Figure 30 - Voltage applied to the coils during QPC

But with a proper earthing configuration this value can be significantly reduced: in Figure 31 only one terminal is stressed, but the insulation could even be problematic, because in this terminal the voltage to ground (Vg) is still 8.8 [kV]; in fact in ITER and JT-60SA the solution adopted is reported in Figure 32, in which Vd is equally divided on the two terminals (Vg value is half Vd), and this result is shown in Figure 27; in JT-60SA the Terminals Resistors (TR) are used also as Discharge Resistors (DR); in nominal condition the functioning is pretty the same for ITER and JT-60SA configurations, but not during fault conditions.

Figure 31 - A possible earthing solution

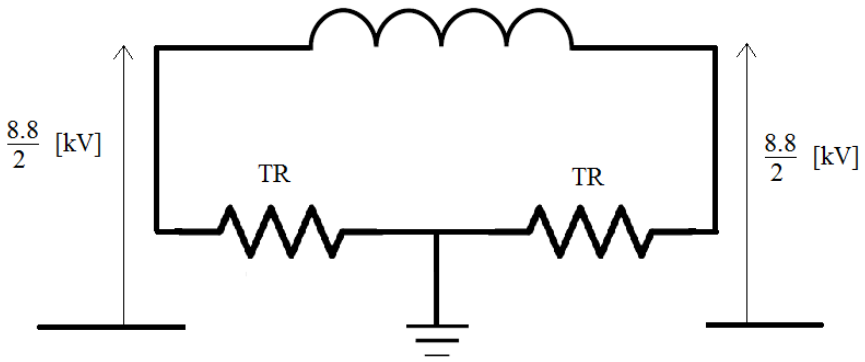

Figure 32 - ITER and JT-60SA earthing

The purpose is to verify if these configurations are valid for DEMO too. Another solution has been found for DEMO, which is to put a DR parallel to each coil (see Chapter 4).

1.5 Fusion Roadmap and DEMO

At the beginning of 2012 the European Commission requested EFDA to prepare a technical roadmap to fusion electricity by 2050. Specific Terms of Reference were elaborated by the EFDA Steering Committee Chair. The roadmap has been developed within a goal-oriented approach articulated in eight different Missions. For each Mission the critical aspects for reactor application, the risks and risk mitigation strategies, the level of readiness now and after ITER and the gaps in the programme have been examined with involvement of experts from the ITER International Organization, Fusion for Energy, EFDA Close Support Units and EFDA Associates.

DEMO is one of the three basilar elements of the European fusion roadmap [10], which are:

- The ITER project as the "essential step towards energy production in a fast track";
- A single step (DEMO) between ITER and the commercial fusion power plant designed "as a credible prototype for a power-producing fusion reactor, although in itself not fully technically or economically optimised";
- The International Fusion Material Irradiation Facility (IFMIF), for material qualification under intense neutron irradiation, in parallel with ITER.

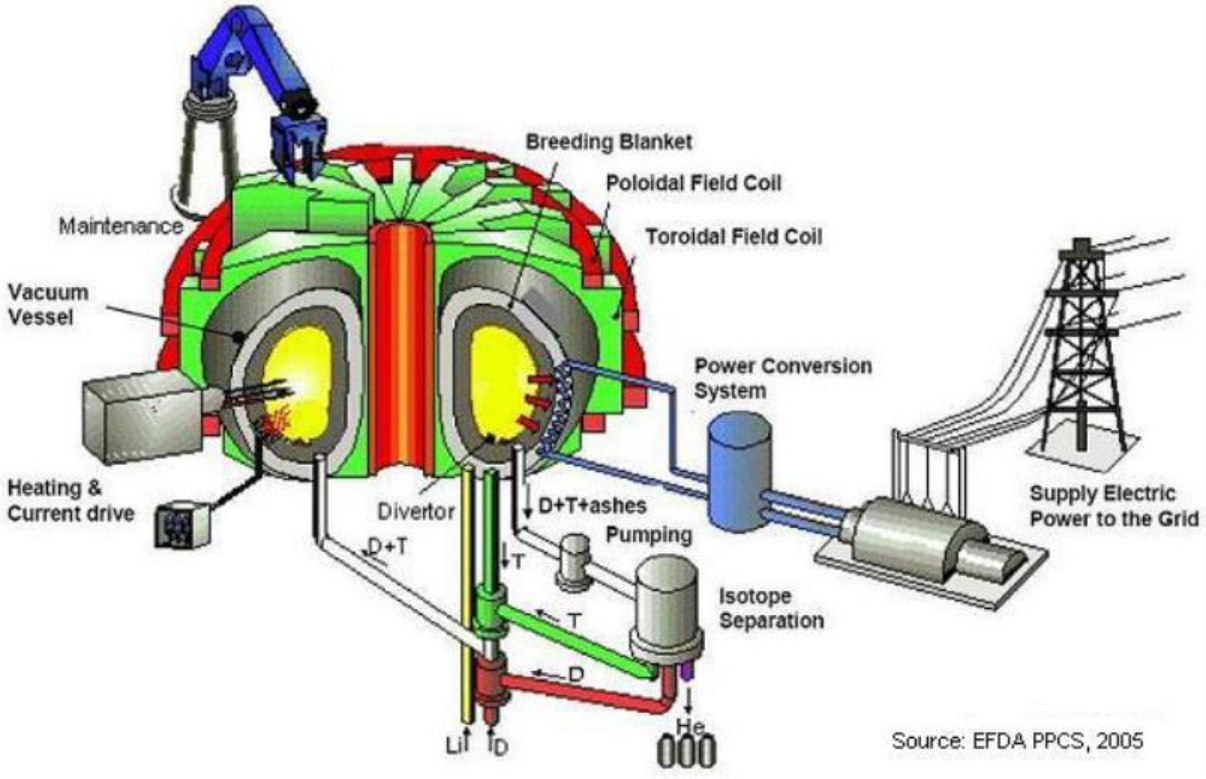

Figure 33 - DEMO, the last step before the commercial reactor

ITER is the key facility in the roadmap; to ensure its success, the preparation of operation on JET (Joint European Torus, first fusion experiment to generate substantial amounts of fusion power) and JT-60SA (Japan Torus-60, currently holds the record for the highest value of the fusion triple product achieved) should be undertaken as main risk mitigation measures. Small and medium sized tokamaks, both in Europe and beyond, with proper capabilities, will play a role in specific work packages.

JET is the world's largest magnetic fusion device; it is the only experiment capable of using tritium and adopting the same first wall material of ITER: Beryllium. About 30 European and international fusion laboratories participate in the JET programme. JET served as a blueprint for the ITER construction and now JET experiments are devoted to validate the ITER design choices and prepare ITER operations. JET's purpose is to try a plasma scenario similar to the ITER one, availing of the same materials for the first wall and the divertor.

JT-60SA is a device being built by Japan and Europe at the Naka Fusion Institute in Japan. JT-60SA is similar in size to JET but in addition features superconducting magnets and CFC first wall and divertor. It will operate in steady-state conditions and at high plasma pressures, both key issues for the preparation of advanced regimes of operation in ITER. JT-60SA first plasma is expected in 2019.

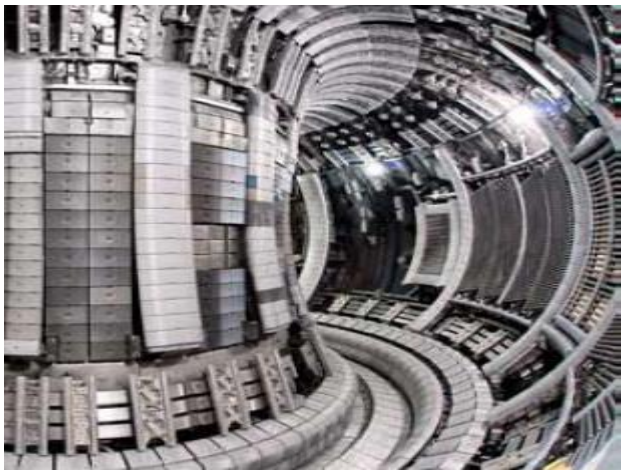

Figure 34 - JET plasma chamber

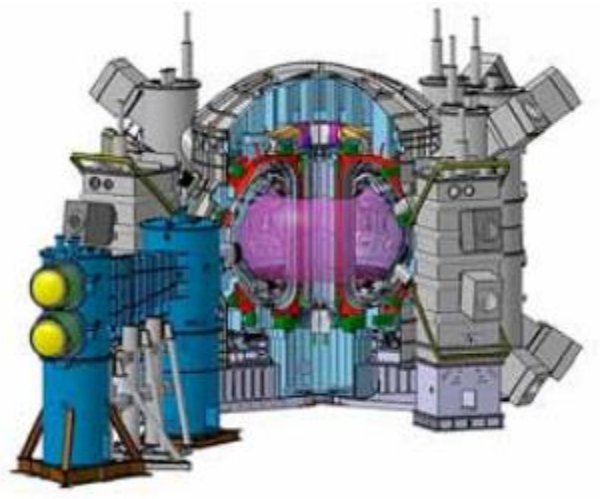

Figure 35 - JT-60SA

DEMO design will benefit largely from the experience that is being gained with the ITER construction., by the way DEMO cannot be defined and designed by research laboratories alone, but requires the full involvement of industry in all technological and systems aspects of the design.

The roadmap addresses three separate periods with distinct main objectives:

- **Horizon 2020 (2014-2020)** with five overarching objectives [9]:
  - Construct ITER;
  - Secure the success of future ITER operation;
  - Prepare the ITER generation of scientists, engineers and operators;
  - Lay the foundation of the fusion power plant;
  - Promote innovation and EU industry competitiveness.
- **Second period (2021-2030)**:
  - Exploit ITER up to its maximum performance and prepare DEMO construction.
- **Third period (2031-2050)**:
  - Complete the ITER exploitation; construct and operate DEMO.

ITER success remains the most important overarching objective of the programme and, in the present roadmap, the vast majority of resources in Horizon 2020 are devoted to ensure that ITER is built within scope, time and budget, that its operation is properly prepared and that a new generation of scientists and engineers is trained for its exploitation. ITER will continue to play the key role over the other two periods of this roadmap. The ITER exploitation up to its maximum performance (demonstration of a fusion gain Q=10) will require focussed effort by scientists and engineers during the period 2020-2030. ITER is currently being built in southern France in the framework of a collaboration between China, Europe, India, Japan, Korea, Russia and the USA.

In the European strategy DEMO is the only step between ITER and a commercial fusion power plant. Its general goals are [11]:

- Produce net electricity for the grid at the level of a few hundred MWs;
- Breed the amount of Tritium needed to close its fuel cycle;
- Demonstrate all the technologies for the construction of a commercial fusion power plant, including an adequate level of availability.

To meet the goal of fusion electricity demonstration by 2050, DEMO construction has to begin in the early 2030s at the latest, to allow the start operation in the early 2040s as indicated in Figure 36 on the DEMO caption, although unfortunately this last target has been postponed.

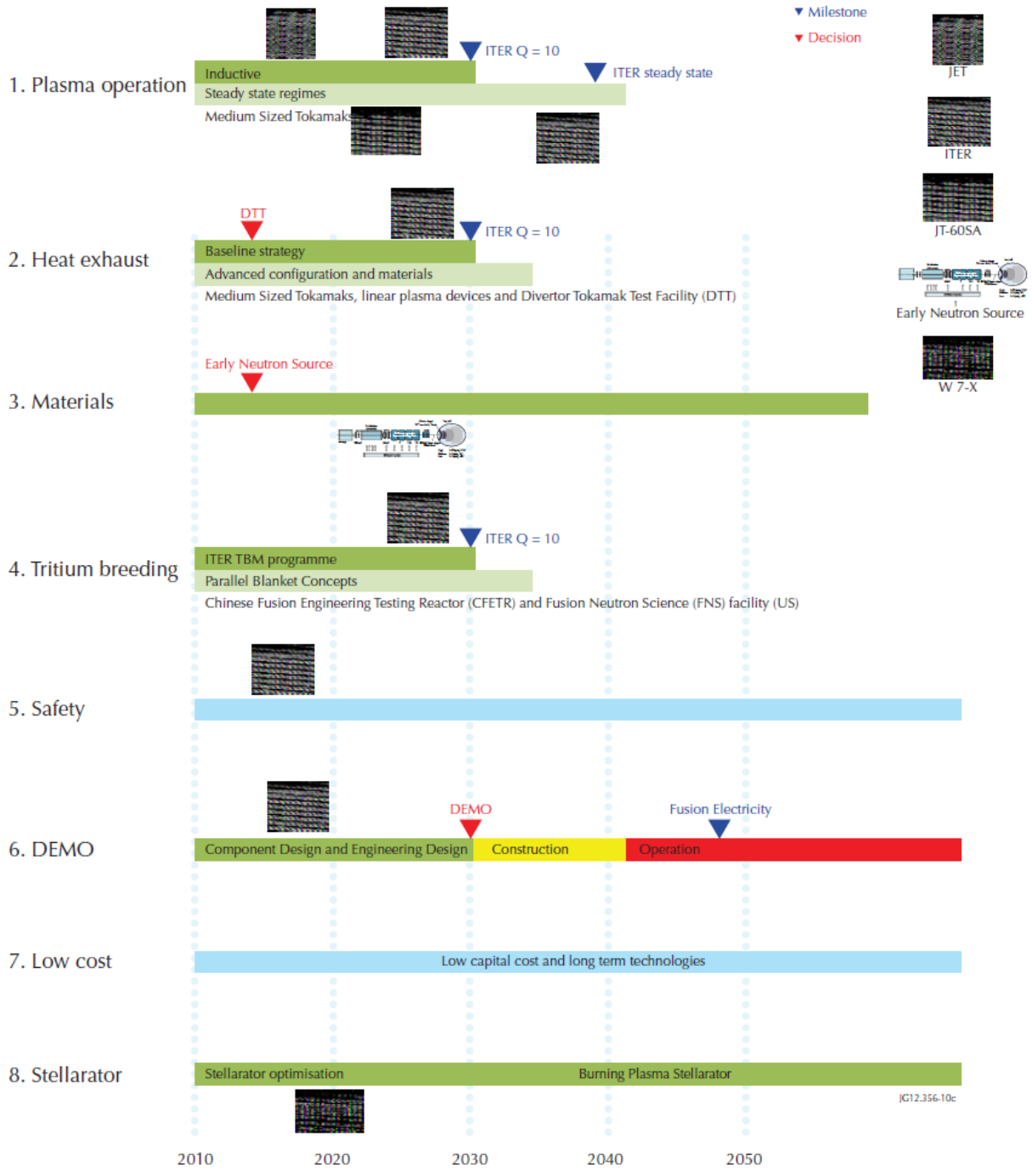

Figure 36 - The conceptual mission to realisation of fusion electricity

DEMO requires a significant amount of innovation in critical areas such as heat exhaust, superconductivity, material and tritium breeding. The technologies desirable for advanced fusion power plants and as risk reduction elements, but not mature enough to be incorporated in DEMO, will have to be pursued in parallel. Innovation is already being pursued in fusion both in industry and in research laboratories but it is only by facing the challenge of the realisation of large projects like ITER and DEMO that their synergy can be fully exploited. For this reason, a close interaction between industry and laboratory through “consortia” is envisaged.

The realisation of fusion energy has to face a number of challenges:

- Plasmas must be confined at temperatures 20 times higher than the temperature of the core of the sun. This requires the minimisation of energy losses due to small-scale turbulence and the taming of plasma instabilities

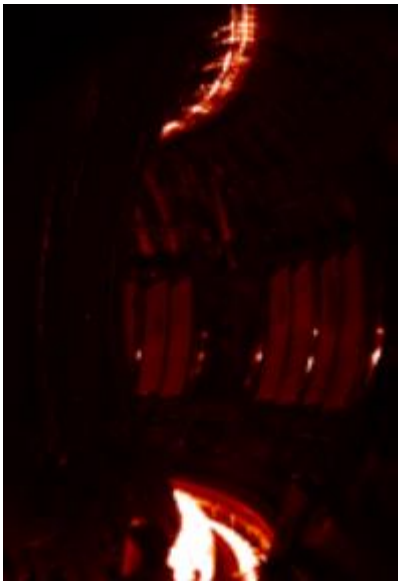

Figure 37- Hot spots on the chamber wall caused by plasma instabilities (JET)

- The power necessary to maintain plasmas at high temperatures is ultimately exhausted in a narrow region of the reaction chamber called the divertor. The need to withstand large heat loads led the development of plasma facing materials and exhaust systems that should be adequate for ITER. However, the development of an adequate solution for the much larger heat exhaust of DEMO is still a challenge
- Neutron resistant materials able to withstand the 14MeV neutron flux and maintain their structural and thermal conduction properties in a sufficiently wide window of operation need to be developed for DEMO to ensure efficient electricity production and adequate plant availability
- Tritium self-sufficiency is mandatory for DEMO, which will burn about 0.4kg of tritium per operational day. Tritium self-sufficiency requires efficient breeding and extraction systems to minimise tritium inventory. The choices of the materials and the coolant of the breeding blanket will have to be made consistently with the choice of the components for the transformation of the high-grade heat into electricity (the so-called Balance of Plant).

Theory and modelling are essential for completing the milestones in this roadmap. Extrapolating solutions to DEMO, for instance, cannot be done without developing and validating suitable models.

1.5.1 DEMO materials and prior R&D

Reduced Activation (RA) – Ferritic/Martensitic steels, included Oxide Dispersion Strengthened alloys (*ODS*)	Database development for reactor use suitable materials
	Breaking resistance decay due to irradiation embrittlement
	High temperature ferritic nano-composites (650 – 750 °C)
Vanadium alloys	Insulation development for induced currents
	Embrittlement due to external impurities adsorption (O, C, N)
	Breaking resistance decay due to irradiation embrittlement
SiC_f/SiC composites	High performance composite structures development
	Irradiation effects on fundamental properties
	Technologies development for fabrication and joints
Tungsten alloys	Technologies development for fabrication and joints
	Radiological properties – Low activation / waste disposal
	Breaking resistance decay due to irradiation embrittlement
Functional materials: Be (neutron multiplier) Lithium ceramics (breeders)	Structural integrity under irradiation
	Uncertainties about Tritium and Helium production
	Fabrication technologies development

2 DEMO reference design

All the input data for the design of DEMO have been obtained from the PROCESS code (Power Reactor Optimisation Code for Environmental and Safety Studies). A picture of DEMO chamber is shown in Figure 38:

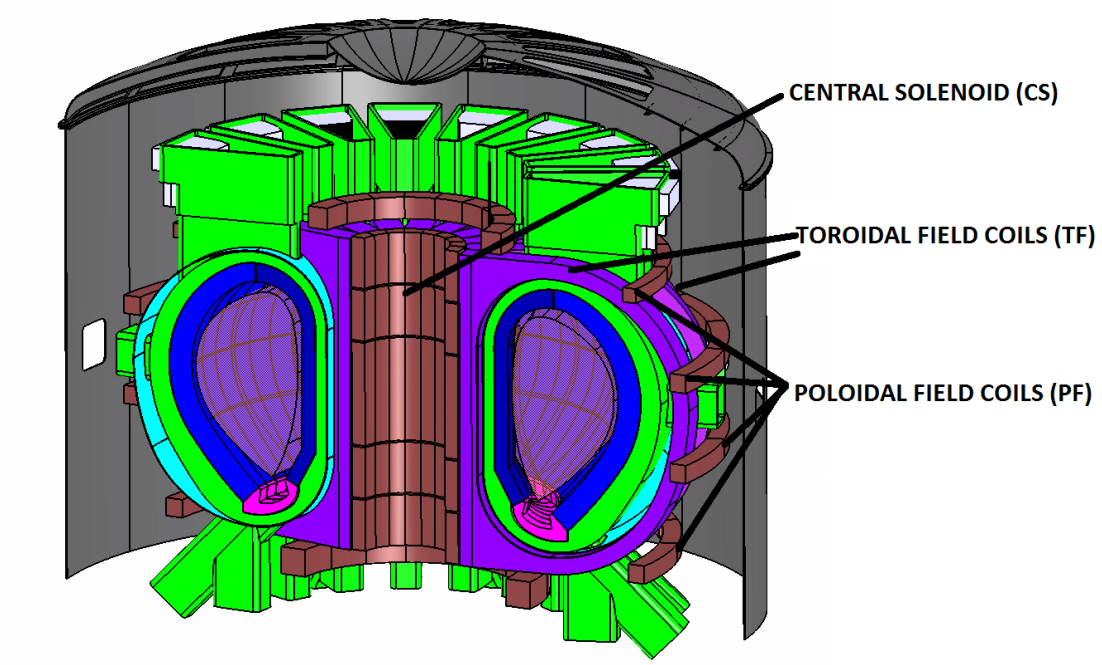

Figure 38 - DEMO overview

PARAMETERS	VALUE	UNIT
Plasma current	19.6	[MA]
Toroidal field	5.667	[T]
Major radius	9.072	[m]
Minor radius	2.927	[m]
Elongation	1.781	/
Triangularity	0.5	/
Aspect ratio	3.1	/
Heating time	10	[s]
Burn time	7200	[s]
Time between pulses	1800	[s]
Ohmic power	1.12	[MW]
Injection power to electrons	29.72	[MW]
Injection power to ions	20.28	[MW]
“Gain” Q	10	/
Nuclear fusion thermal power	2000	[MW]
Net electricity power	500	[MW]

Table 1 - Basic parameters of DEMO

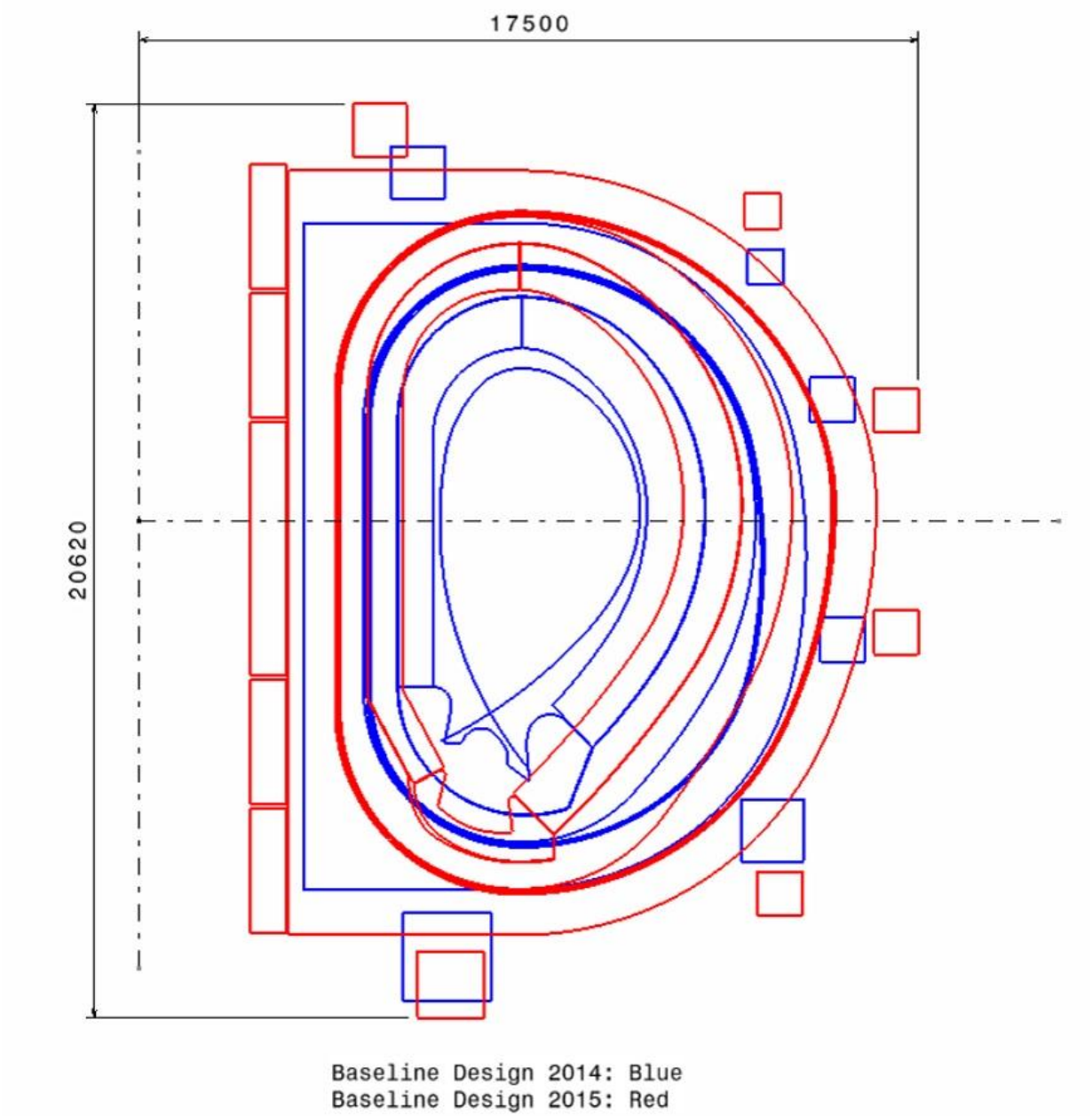

Figure 39 - DEMO coil systems frontal section

CENTRAL SOLENOID (CS)

As studied for ITER, the central solenoid core is in air, due to the unbearable saturation that would occur with a ferromagnetic core. The circuit is protected by a Quench Protection Circuit (QPC) and provided by a Switching Network Unit (SNU), as shown in Figure 40:

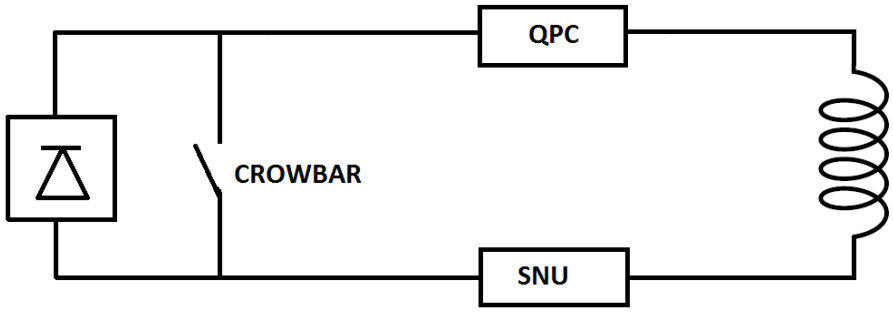

Figure 40 - Central solenoid circuit

PARAMETERS	VALUE	UNIT
Overall cross-sectional area	12.03	[m^2]
Conductor cross-sectional area	5.036	[m^2]
Void cross-sectional area	2.158	[m^2]
Steel cross-sectional area	4.84	[m^2]
Allowable hoop stress in steel	660	[MPa]
Helium coolant temperature	4.75	[K]
CS temperature margin	5.476	[K]

Table 2 - Central solenoid parameters

POLOIDAL FIELD COIL (PF)

There are different PF coils, each one with different functions: for this reason each coil is provided by its own circuit, with different power supplies for each one; each circuit is protected by its own QPC, as shown in Figure 41:

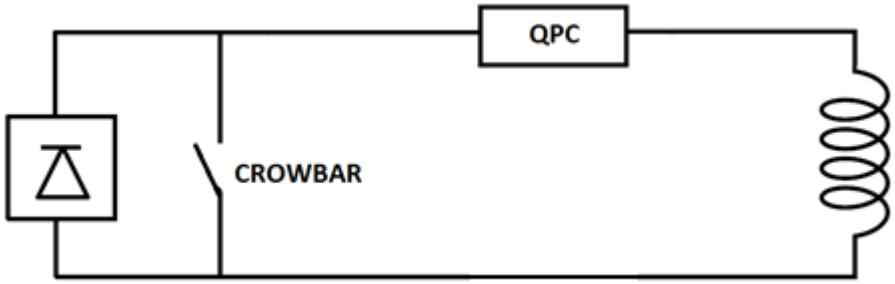

Figure 41 - Poloidal field circuit

Coil	R[m]	Z[m]	R-length [m]	Z-length [m]	turns
PF1	6.40	9.13	1.33	1.33	462.91
PF2	6.40	-10.08	1.42	1.42	526.94
PF3	17.93	2.93	1.22	1.22	210.76
PF4	17.93	-2.93	1.22	1.22	210.76
PF5	16.22	8.19	0.80	0.80	118.17
PF6	16.22	-8.19	0.80	0.80	118.17
CS	2.89	0	0.82	14.71	3790.08
Plasma	9.07	0	5.85	10.42	/

Table 3 - Geometry of PF coils, central solenoid and plasma (referred to the centre of plasma)

Coil	Total current * turns [MA]	Conductor mass [t]	Steel mass [t]	Field [T]
PF1	19.53	450	275	6.35
PF2	22.24	512	330	6.78
PF3	8.89	1052	444	2.82
PF4	8.89	1052	444	2.82
PF5	5.08	407	181	2.53
PF6	5.08	407	181	2.53
CS	162.97	823	686	12.92

Table 4 - PF coils and CS parameters

TOROIDAL FIELD (TF) COILS

There is a common power supply for all the coils connected in series, with QPC units interposed in between them. A crowbar short-circuits the power supply when the QPC units intervenes. Figure 42 shows the typical circuit.

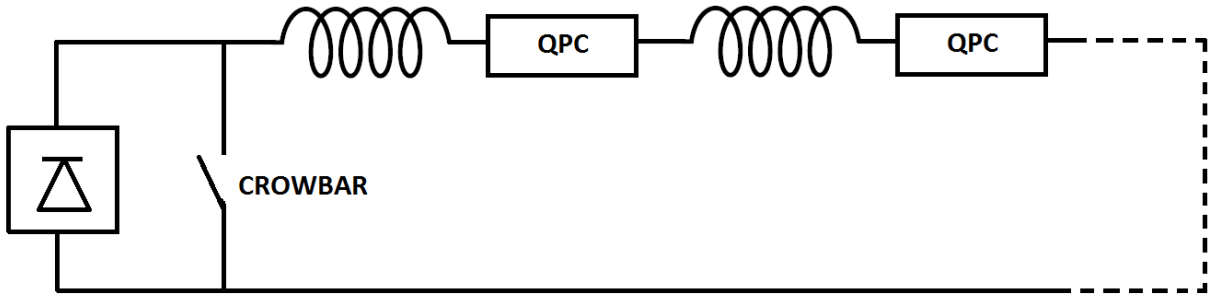

Figure 42 - Toroidal field circuit

The main parameters of the TF coils are listed in Table 5, where Vg max is the maximum voltage value between the coil terminals and the ground, due to the insulation design.

PARAMETERS	VALUE	UNIT
NTFC	18	/
Ec (Stored energy per coil)	7.54	[GJ]
Iop	65	[kA]
τ (discharge time)	27	[s]
Cross-sectional area per coil	1.42	[m^2]
Mean coil circumference	46.2	[m]
Peak field	12.32	[T]
Vg max	28	[kV]

Table 5 - Toroidal field parameters

3 Power supply

The toroidal field circuit has to be interfaced with the network by and AC/DC converter; in fact the coil current must be provided 24 hours a day, 7 days a week, while the charging process must be done in reasonable time. Then the system is supplied by a two quadrants three-phase thyristor converter; the first quadrant is used for the superconductive coils charging process and for the maintaining of the charge, the second one instead is used for the shutdown slow discharge for example for maintenance, in order to give back to the network the stored energy, instead of dissipating it on the DRs.

The charging process is exposed in the following chapter, and so the discharging process, which is pretty the same except for the inverted voltage; in fact the converter operates on the first and the fourth quadrants.

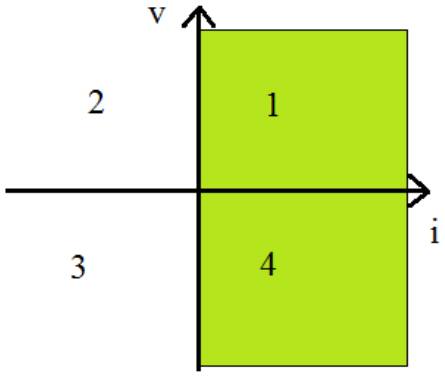

Figure 43 - ACDC converter operating quadrants

3.1 Charging process

The charging process is modelled in ideal conditions by a single converter for the 18 coils as a DC voltage source:

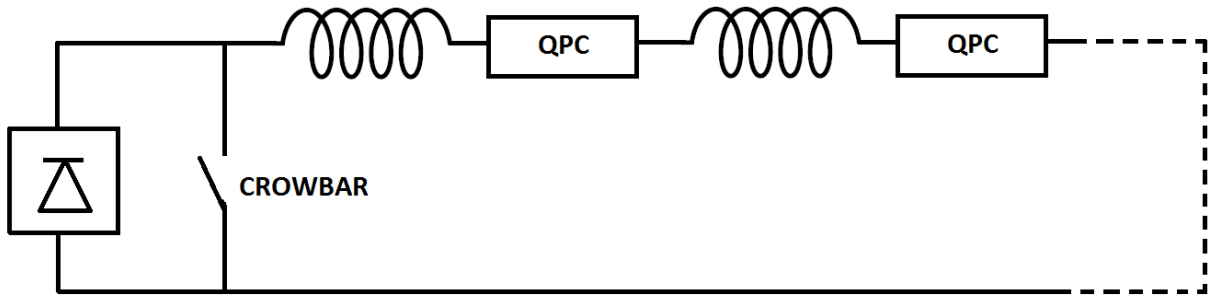

Figure 44- Ideal charging configuration

Assuming Lc = 3.57 [H] (Table 10), we need to find the source voltage Vs assuming a charging time equal to 3600 [s]; applying the Kirchhoff Voltage Law (KVL):

$$Vs = vl;\ vl = (18Lc)\ \frac{di}{dt}$$

Substituting:

$$Vs = (18 * 3.57) * \frac{di}{dt}$$

Since Iop = 65 [kA] and T = 3600 [s] (see Figure 45), then:

$$Vs = \frac{64.26 * 65000}{3600} = 1160\ [V]$$

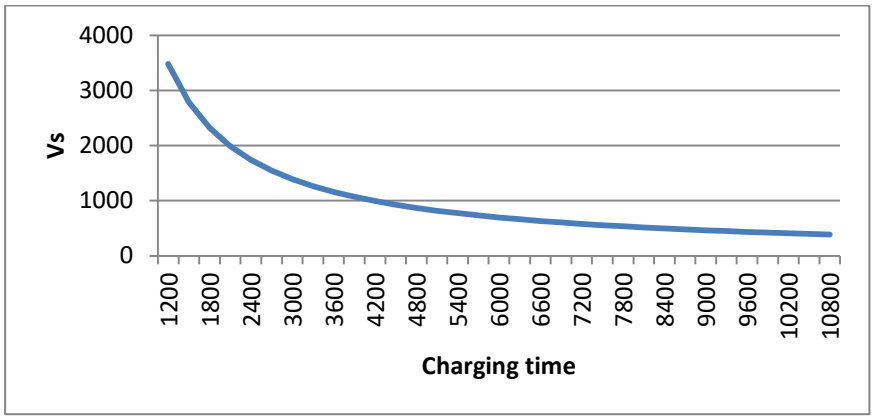

Figure 45 - Voltage needed depending on the charging time

3.2 Toroidal field circuit power supply

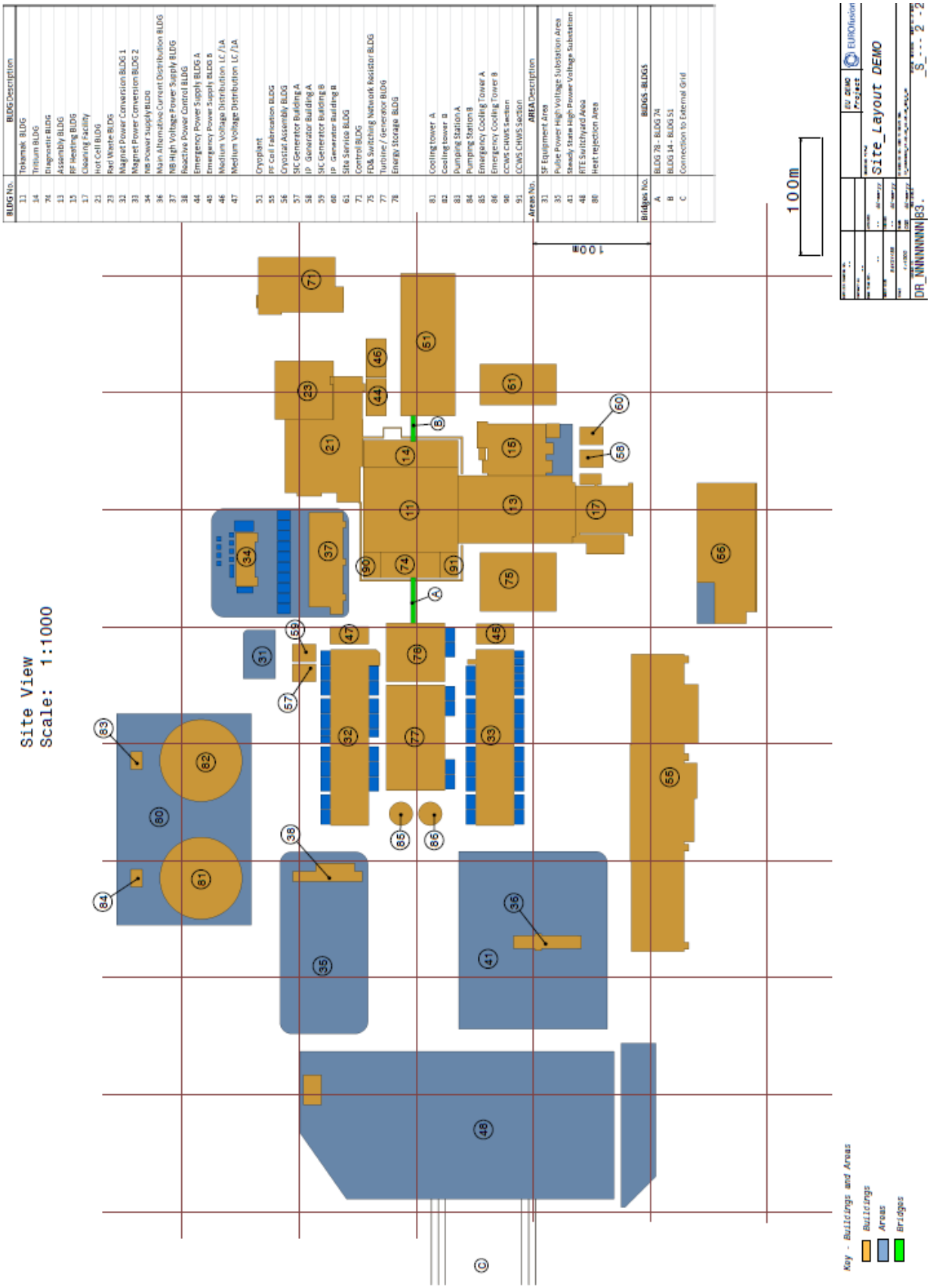

Figure 46 - DEMO plant

3.2.1 Ideal case

The coil power supply is modeled by an AC/DC ideal thyristor converter, with an imposed value of 1160 [V] for the DC voltage, as calculated in 3.1; assuming a trigger angle α equal to 0°, the line-to-line maximum voltage V_{LL} required by the converter is [12]:

$$V_{LL} = \frac{Vs}{1.35 * \cos(\alpha)} = \frac{1160}{1.35} = 860\ [V]$$

This system is powered by a 22 [kV] concatenated voltage line, which is moreover fed by a 380 [kV] high voltage system; including in this analysis just the low voltage segment, the 22 [kV] – to – V_{LL} transformer transformation ratio will be:

$$k = \frac{22000}{860} = 25.58$$

The converting system requires a dedicated α-control block set in such a way that the coil current Iop is fixed at 65 [kA]. Moreover the α-control needs to be synchronized with the V_{LL} waveform.
The synchronization is obtained sending into the α-control block a signal which is synchronized with V_{LL}, based on the comparison between the waveforms of two of the three lines of the low-voltage three-phase line, as shown below in Figure 47 [13].

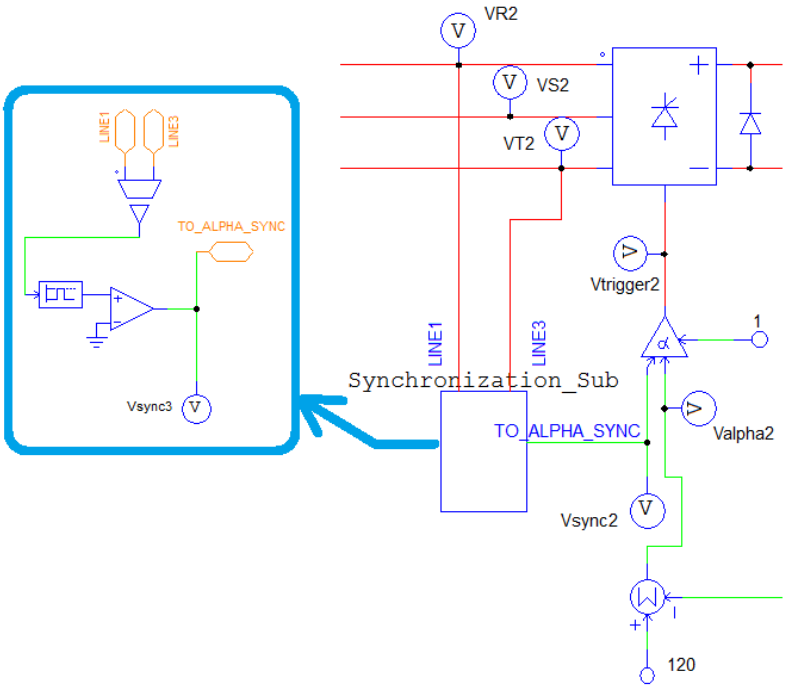

Figure 47 - Alpha-control synchronization subcircuit

The logic behind the α value is based on a feedback control over the operative current instantaneous value (Figure 48):

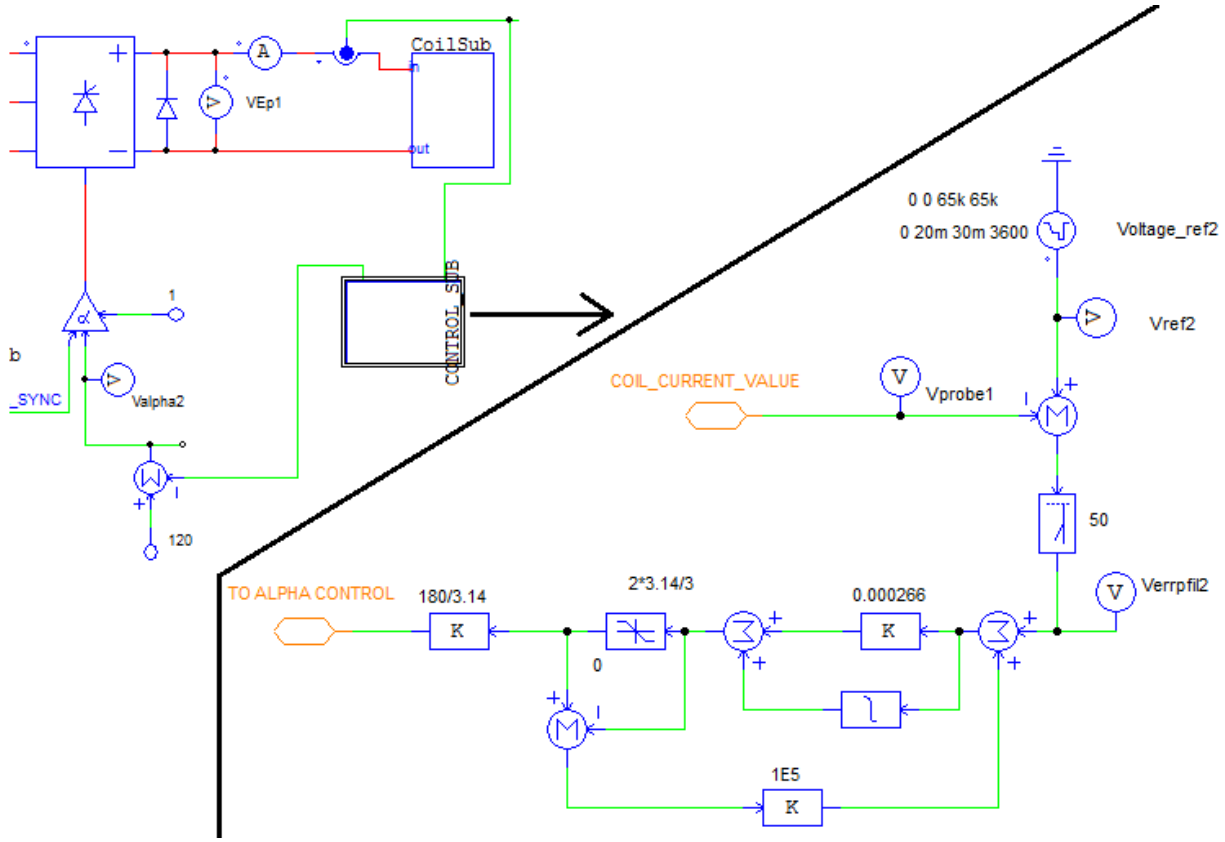

Figure 48 - Alpha value control subcircuit

The operative current value is compared to the fixed value 65000; their difference is low-pass filtered and sent to a PI control and then to a limiter, in order to obtain a degree value; this value is finally sent to the α-control, where it is compared to the maximum α-value, 120; if the result is 120 or near, it means that the Iop value is very close to the desired value 65000; instead if the value sent to the α-block is near to 0 it means that the Iop value is quite far from 65000.

3.2.2 Actual case

There are various contributions to the losses inside the system:

- Medium voltage three-phase transmission cable
- DC busbars between the converters, the QPCs, the Dump Resistors and the coils, modelled by a resistor and an inductance
- The losses inside the QPCs, modelled by a resistor and an inductance
- Medium-to-low voltage transformer
- Thyristor converter

MEDIUM VOLTAGE THREE-PHASE TRANSMISSION CABLE

First of all, we need to know which is the current value needed by the system; the toroidal field circuit presents an operative current Iop = 65 [kA], and during the charge it requires a DC voltage Vs equal to

1160 [V] without taking into account the losses, so it is immediate to obtain the order of magnitude of the apparent power from:

$$Iop * Vs = 65000\ [A] * 1160[V] = 75.4\ [MVA]$$

It is reasonable to assume 80 [MVA] due to the losses. With a line voltage equal to 22 [kV], the resulting current flowing per cable is approximately:

$$\frac{1}{3} * \frac{80 * 10^6}{\sqrt{3} * (22 * 10^3)} = 700\ [A]$$

According to the apparent power, the cable section can be found from the catalogues [14]:

3 horizontally aligned *RG7H1R 18/30 kV* cables in air, copper conductor, 300 [mm^2] section; with these parameters the capacity of the cables is 790 [A]. For the 18/30 [kV] and 400 [mm^2] cables the resistance is r = 0.0623 [Ω/km], and the reactance is x_L = 0.16 Ω/km; consequently the inductance is:

$$l = \frac{0.16}{2\pi * 50} = 5.09 * 10^{-4}\ [\mathrm{H/km}]$$

The assumed line length is 300[m], so the total is resistance and the total inductance are:

$$R = 0.3 * r = 18.7\ [\mathrm{m\Omega}]$$

$$L = 0.3 * l = 0.153\ [\mathrm{mH}]$$

DC BUSBARS

There will be considered typical copper busbars instead of superconductive ones, in order to verify the big amount of losses; this is a conservative condition because, in order to bring to the superconductive solution it is sufficient to neglect the resistances.

Assuming a typical value of 4.5 [A/mm^2] for a copper DC busbar, the required section is:

$$S = \frac{65000}{4.5} = 14444\ [\mathrm{mm^2}]$$

The resistance value for each busbar can be now found with the well-known:

$$R\ [\Omega] = \frac{l[\mathrm{m}] * \rho[\Omega * \mathrm{m}]}{S[\mathrm{m^2}]}$$

It is reasonable to assume 1 [μH/m] for the DC busbar inductance.

We refer to Figure 49 for the DC busbars lengths; in addition to that, we also consider 6 [m] DC busbars on the DR terminals and 2 [m] DC busbars on the QPCs terminals:

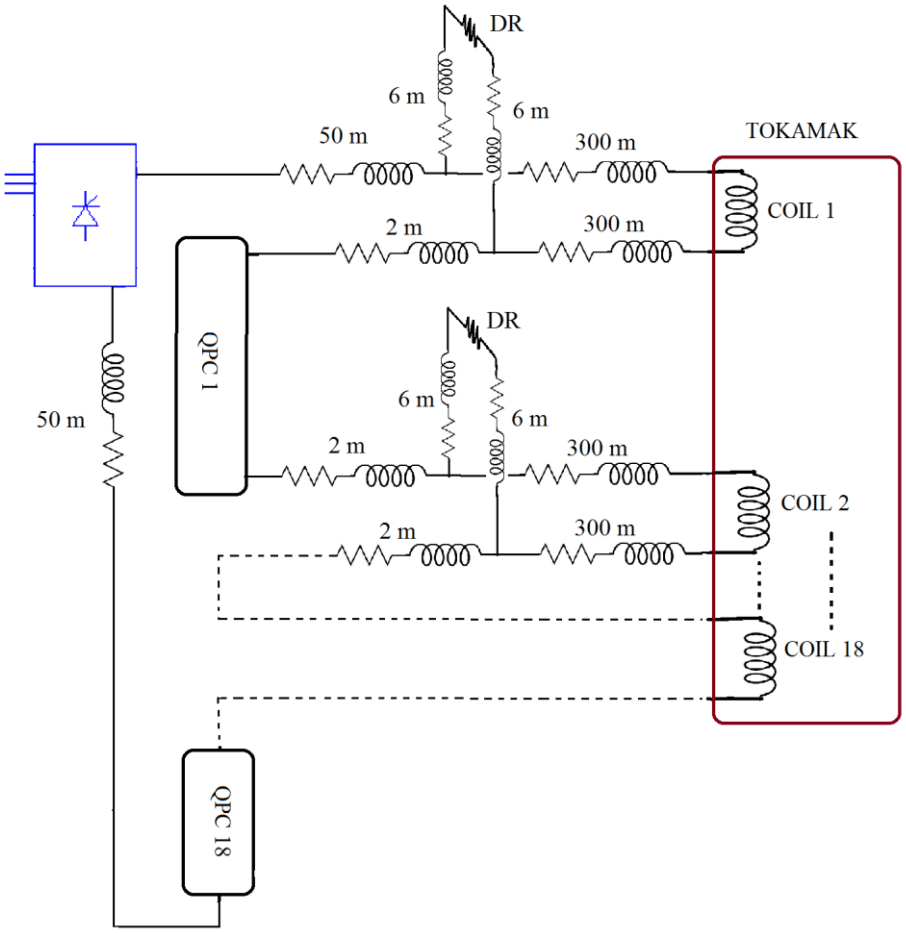

Figure 49 - DC buses lengths

Now, assuming a QPC-resistance value of 0.5 [μΩ] and a QPC-inductance value of 1.5 [μH], the total resistance and inductance along the DC buses calculation is immediate:

$$Rtot + Ltot = 2(R50 + L50) + 36(R300 + L300) + 36(R2 + X2) + 18(Rqpc + Lqpc)$$
$$= 0.0128\ [\Omega] + 0.011[\mathrm{H}]$$

Taking into account these values, the Vs value must increase to keep the charging time constant, otherwise the charging time would be longer, and can be found with the solution of a RL circuit, where R = 0.0128 [Ω] and L = 18Lc + 0.011 = 64.27 [H]

The circuit can be solved as follows: [15]

$v_L + v_R = E$
$v_R = Ri_L$
$v_L = Ldi_L/dt$

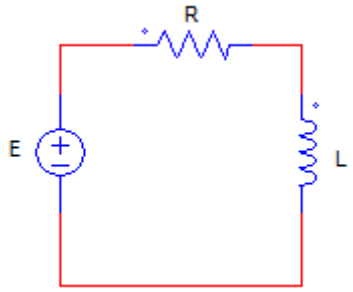

Figure 50 - Configuration

$$L\frac{di_L}{dt} + Ri_L = E$$

$$Stationary\ solution: i_P(t) = i_L = \frac{E}{R}$$

$$Associated\ homogeneous\ equation: Ls + R = 0 \longrightarrow s = -\frac{R}{L}$$

$$Associated\ homogeneous\ integral: i_0(t) = I_0 e^{st} = I_0 e^{-\frac{Rt}{L}}$$

$$Associated\ homogeneous\ solution: i(t) = \ i_P(t) + i_0(t) = \frac{E}{R} + I_0 e^{-\frac{Rt}{L}}$$

$$For\ t = 0 \longrightarrow i(0) = 0 = \frac{E}{R} + I_0 \longrightarrow \ I_0 = -\frac{E}{R}$$

$$i(t) = \frac{E}{R}\left(1 - e^{\frac{Rt}{L}}\right)$$

$$\longrightarrow i(3600) = \frac{E}{R}\left(1 - e^{-\frac{0.0128*3600}{64.27}}\right) \longrightarrow 65000 = E * 39.98$$

$$\longrightarrow E = \frac{65000}{39.98} = 1626\ [V]$$

Where E, in our case, is Vs. So, from the initial value of 1160, we are able to see that the losses along the DC busbars involve a voltage increase of 40% in order to reach the same Iop in one hour of charging.

MEDIUM-TO-LOW VOLTAGE TRANSFORMER

With this new value of Vs, the transformation ratio should be updated:

$$V_{LL} = 1.35Vs \longrightarrow \frac{1626}{1.35} = 1210\ [V]$$

$$k = \frac{22000}{1210} \approx 18$$

Assuming typical values for the transformers as Pcc = 5% and $\cos\varphi_{cc}$ = 0.4, the next step is to evaluate the transformer loss parameters [16].
As seen for the medium voltage three-phase transmission cable losses evaluation, the apparent power S is about 80 [MVA], then:

$$Pcc = \frac{80}{100} * 5 = 4\ [MVA]$$

$$R' = \frac{Pcc}{3In^2}, \text{where } In = \frac{S}{\sqrt{3} * V_{LL}} = \frac{80 * 10^6}{\sqrt{3} * 22 * 10^3} = 2101[A]$$

$$R' = \frac{4 * 10^6}{3 * 2101^2} = 0.302\ [\Omega]$$

$$\text{Now } \frac{X'}{R'} = tg\varphi cc, \text{and } \varphi cc = cos^{-1}(0.4) = 66.42 \longrightarrow tg\varphi cc = 2.29$$

$$\longrightarrow X' = R' * 2.29 = 0.69\ [\Omega] \longrightarrow L' = \frac{X'}{2\pi * 50} = 2.2\ [\text{mH}]$$

The voltage drop due to these losses can be calculated by the well-known formula:

$$\Delta E = R'Icos\varphi + X'\text{Isin}\varphi$$

in order to evaluate $E_1 = E_{12} + \Delta E$.

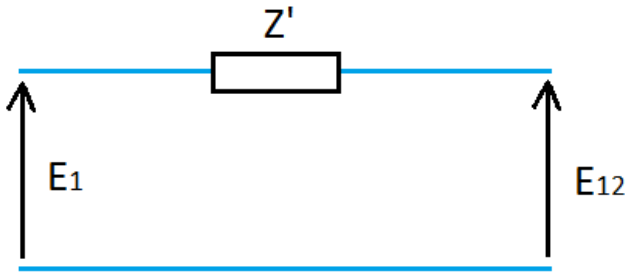

Figure 51 - Voltage drop ($Z' = \sqrt{R'^2 + X'^2}$)

E_{12} is the line-to-neutral voltage from the line-to-line V_{LL} which is equal to 1626; then:

$$E_{12} = \frac{1626}{\sqrt{3}} = 1210\ [V]$$

The value of I was previously calculated, which was 2101 [A].
The value of φ has been evaluated with PSIM10, plotting in the same graph E_1 and I:

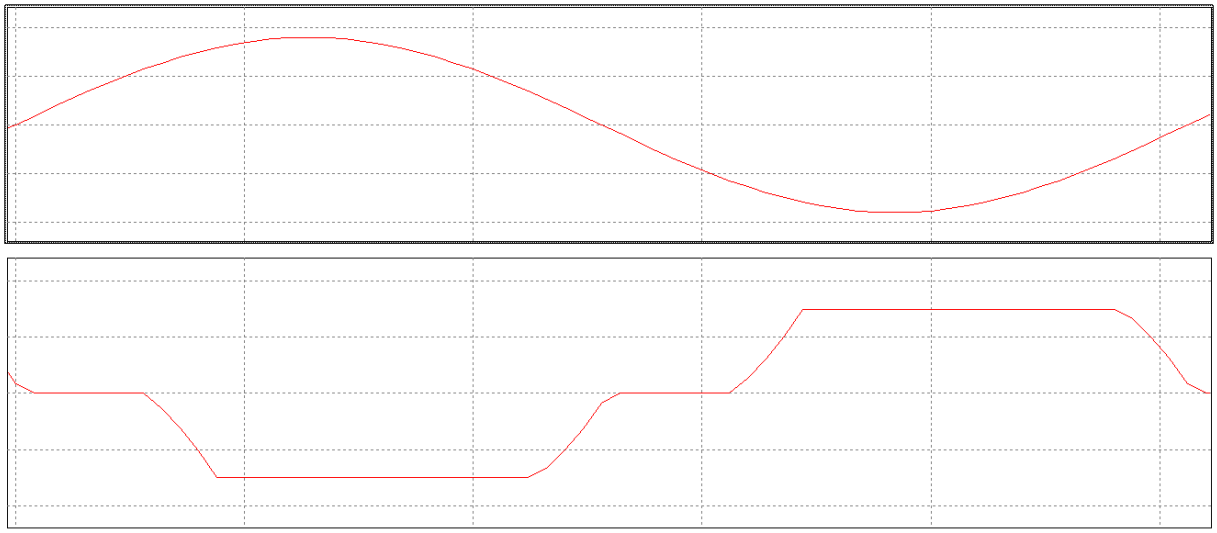

Figure 52 - Voltage and current waveforms displacement

While the voltage zero crossing is easily obtainable, for the current wave it is possible to deduce the fundamental waveform zero crossing, in the middle of the current zero trait of the quasi-trapezoidal current waveform.

The waveforms are not constant during the charge, so the best solution to evaluate the value of φ is to collect many temporal shift values during different charging states:

Current value [kA]	Displacement [s]	Displacement [°]
0	$3.33*10^{-4}$	6
10	$8.46*10^{-4}$	15
20	$1.05*10^{-3}$	18.9
30	$1.20*10^{-3}$	21.6
40	$1.22*10^{-3}$	22
50	$1.24*10^{-3}$	22.3
60	$1.27*10^{-3}$	22.8

Table 6 - Voltage and current displacement for different charging states

From the plotting of these values it is possible to identify an asymptote for the value of 23°:

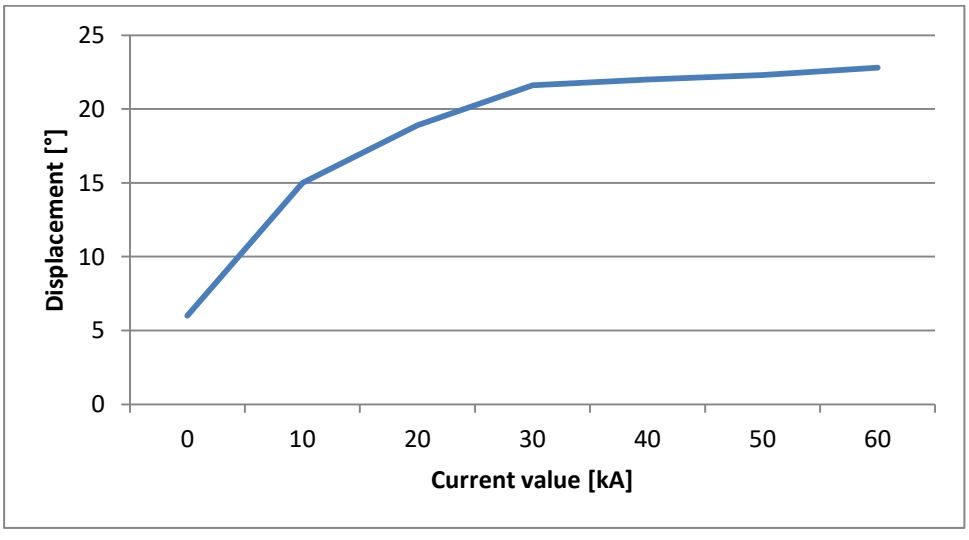

Figure 53 - Voltage and current displacement for different charging states

$$\cos\varphi = 0.93$$
$$\sin\varphi = 0.38$$

Assuming these values it is now possible to evaluate the voltage drop:

$$\Delta E = 2099 * (0.302 * 0.93 + 0.69 * 0.38) = 1139\ [V]$$

The ideal configuration would be:

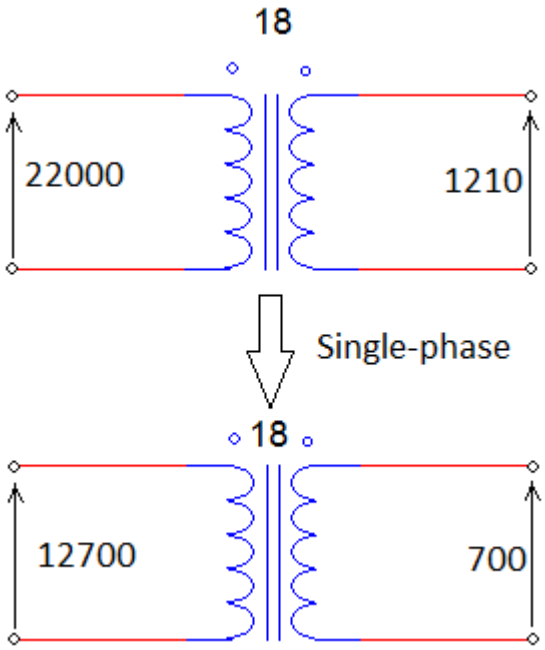

But considering the losses inside the transformer:

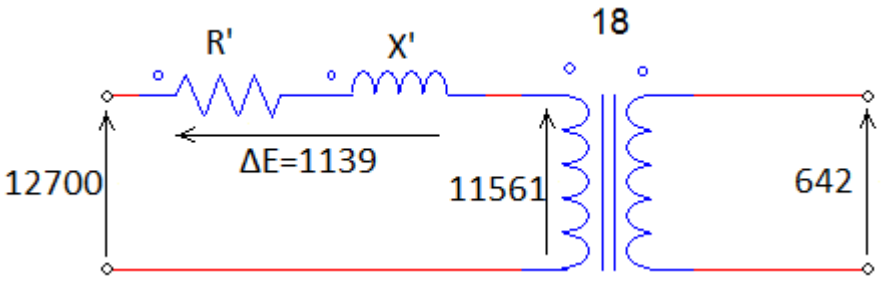

Indeed the desired configuration is:

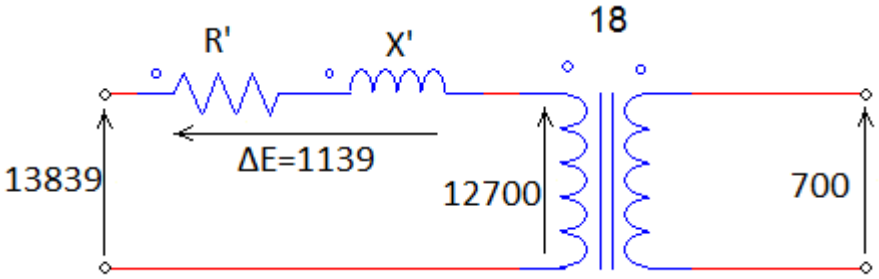

Reporting the losses to the secondary winding:

$$700 + \frac{1139}{18} = 763\ [V]$$

Reporting the line-to-line voltage: $763 * \sqrt{3} = 1332\ [V]$

Then, fixed the primary voltage to 22 [kV], the required new transformation ratio will be:

$$k = \frac{22000}{1332} = 16.5$$

THYRISTOR CONVERTER

The first step to choose the type of thyristor from the catalogues is to identify the required specifics, first of all the average on-state current and the rate of rise of on-state current.
The on-state current is the Iop, which is equal to 65 [kA]; the rate of rise of on-state current can be obtained from PSIM10 measuring the time interval of the current rising (Figure 54):

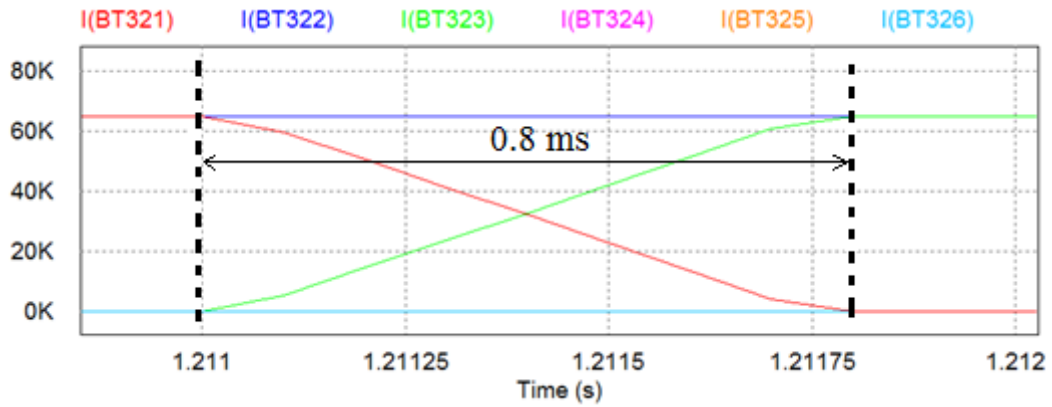

Figure 54 - Thyristor converter commutation time

Commutation time ≈ 0.8 [ms]

Since ΔI = 65 [kA], the rate of rise of on-state current is:

$$\frac{di}{dt} = \frac{65000}{0.8 * 10^{-3}} = 81.25\ [\frac{A}{\mu s}]$$

A good choice could be the Phase Control Thyristor 5STP 45Q2800 from the ABB catalogue, which presents a critical rate of rise of on-state current of 250 [A/μs], a maximum repetitive peak forward voltage of 2800 [V], but the maximum average on-state current is 5490, so our converter will require at least 12 thyristors for each branch of the bridge.

Due to the huge amount of current it is necessary to evaluate the thermal regime of the converter, availing from the catalogue data:

i	1	2	3	4
R_i(K/kW)	3.560	0.680	0.460	0.280
τ_i(s)	0.4069	0.0559	0.0075	0.0018

Table 7 - Thyristor thermal data

In Table 7 i = 1,2,3,4 are the thermal parameters of the thyristor converter layers given by the ABB catalogue, R_i is the thermal resistance of each layer and τ_i is the thermal time constant, from which it is possible to evaluate the thermal capacitance of the layers.

A thermal model was developed inside the circuit on PSIM 10 considering the previous parameters:

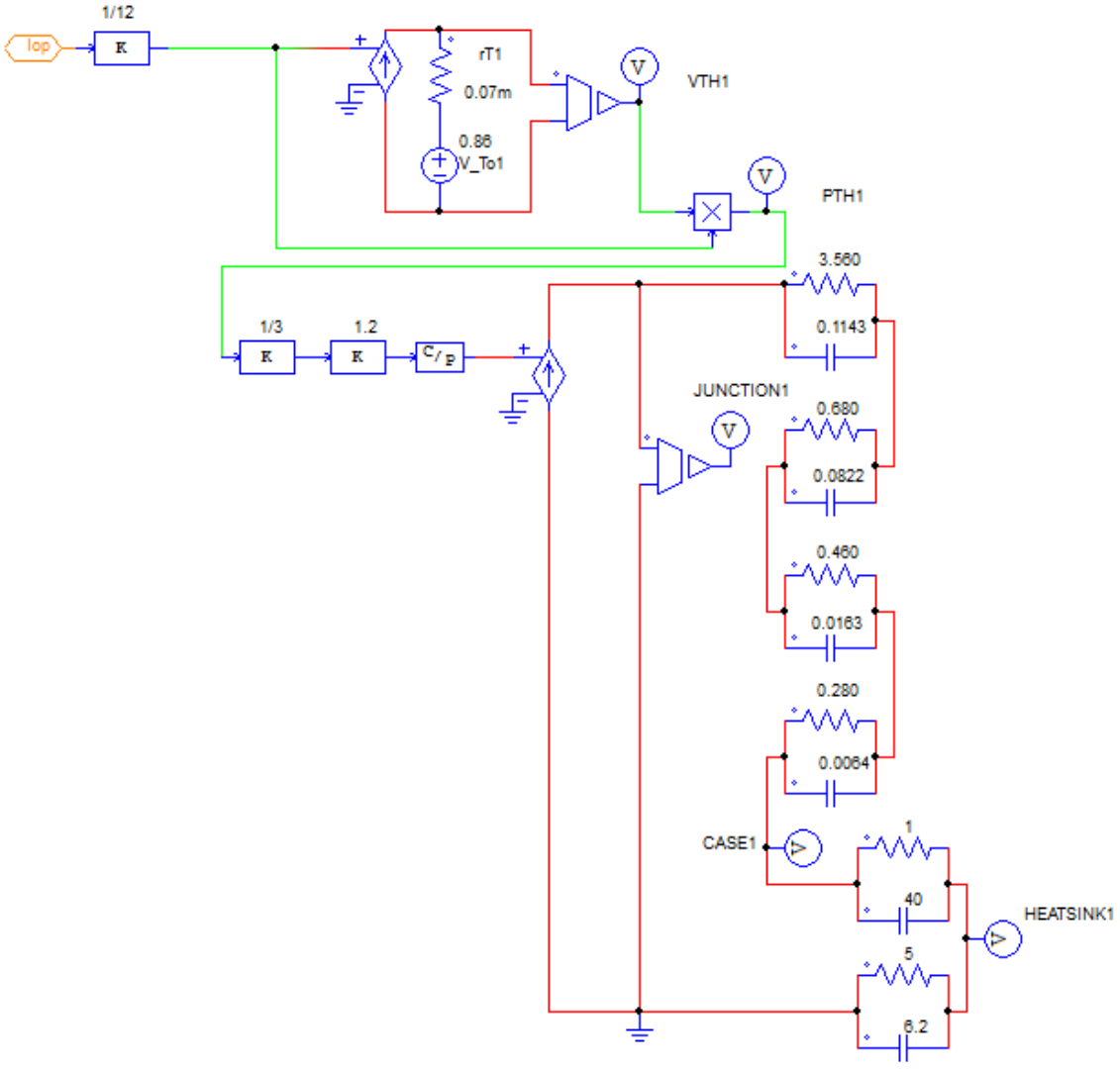

Figure 55- PSIM 10 thermal model

In this model the current value of Iop is divided by the number of components (12) and sent to a voltage-controlled current source put in parallel with the series of the slope resistance r_{T1} = 0.07 [mΩ] and the threshold voltage V_{TO} = 0.86 [V]; the resulting voltage V_{TH1} is multiplied by the current value divided per 12, in order to obtain the thermal power P_{TH1}. But each branch operates just for one third of the period thanks to the three-phase supply of the converter, so the thermal power is divided by 3; it is also increased of 20% for security reasons; finally this thermal power value goes into different blocks

which represent the different layers of the thyristor, whose values are given by the schematics. The last two blocks are the models of a water cooling system [17].

For each block the thermal capacitance is calculated from:

$$\tau = RC \longrightarrow C = \frac{\tau}{R}$$

The temperature increase can be evaluated from the thermal model:

$$\Delta T = P_T \cdot (R_T \,//\, C_T)$$

where P_T is the thermal power, given by the product of I_T and V_T, since:

$$I_T = \frac{I_{OP}}{12} = 5.42 \cdot 10^3 \; [A]$$

$$V_T = V_{T0} + (I_T \cdot r_{T1}) = 1.24[V]$$

Since there is a very long charging time, C_T can be neglected. Then:

$$P_T = 5.42 \cdot 10^3 \cdot 1.24 = 6.72 \; [kW]$$

For each branch:

$$\frac{P_T}{3} = 2.24 \; [kW]$$

Now:

$$R_T = 3.56 + 0.68 + 0.46 + 0.28 + 1 + 5 = 10.98 \; [\frac{K}{kW}]$$

And finally:

$$\Delta T = \frac{P_T}{3} \cdot R_T = 24.6 \; [K]$$

Assuming as the worst condition an external temperature of 40°C, the final temperature is equal to 40+24.6 = 64.6 °C, so the critical temperature of 125°C is not exceeded; the simulation results confirm the feasibility of the choice of these components and of this layout.

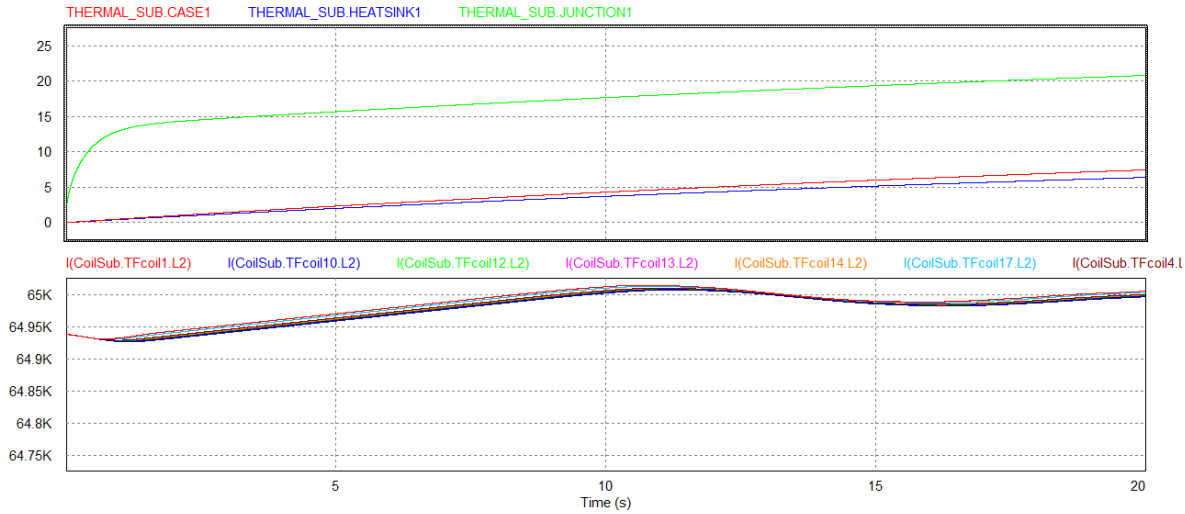

Figure 56 - Thermal transient of the converter

3.3 Snubber design

During the shutdown the thyristors are subject to the line-to-line voltage $-V_R$, which is 22000/17 = 1300 [V].

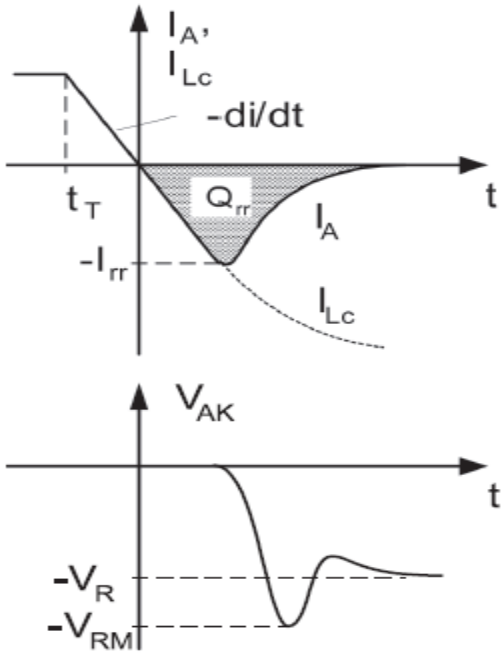

Figure 57 - Reverse current and voltage applied to the thyristor

It is also known that di/dt = 53 [A/μs]; from the ABB catalogue for the Phase Control Thyristor 5STP 45Q2800 we impose Q_{rr} equal to 30000 [μAs] [18]:

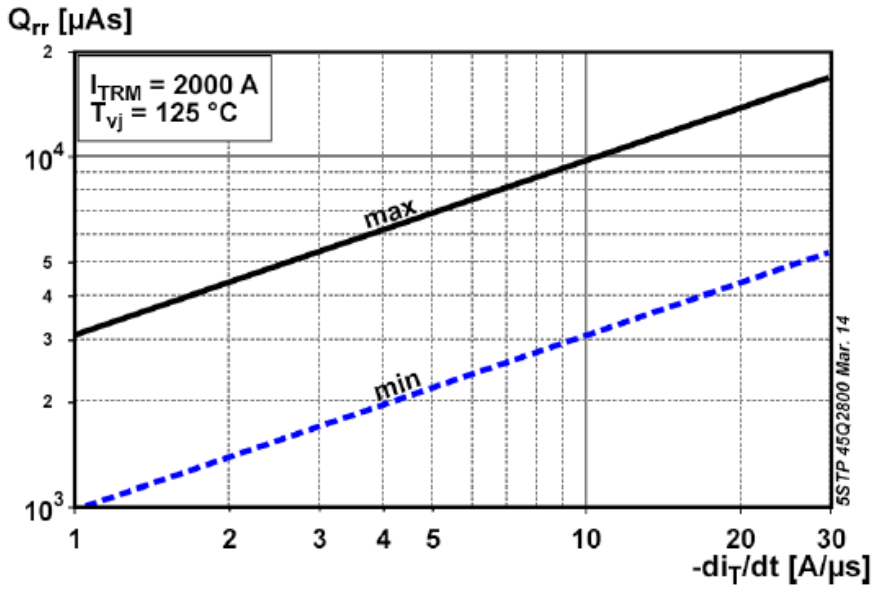

Figure 58 – Qrr for the Phase Control Thyristor 5STP 45Q2800

From the catalogue the maximum peak reversed voltage V_{RM} is 2800 [V], so:

$$\frac{V_{RM}}{V_R} = \frac{2800}{1300} = 2.15$$

Now it is possible to evaluate the R and C for the snubber:

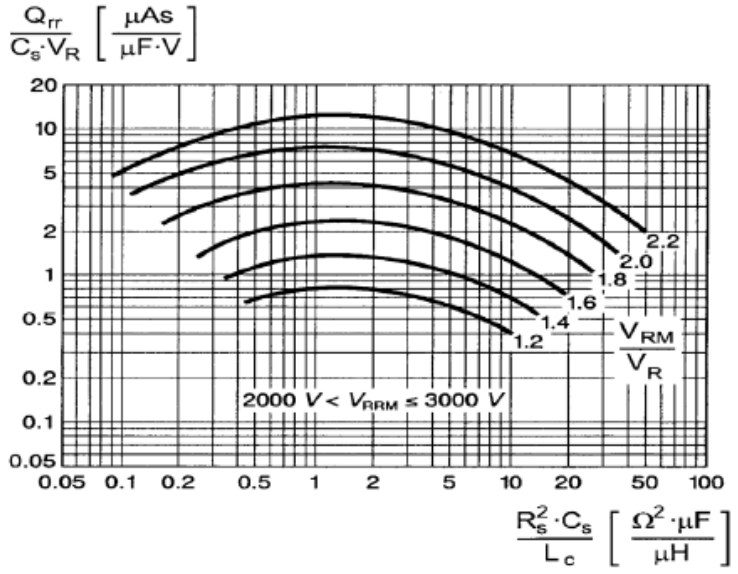

Figure 59 - From ABB catalogue

$$\frac{Q_{RR}}{C_S * V_R} = 8$$

$$L_C = \frac{V_R}{\frac{di}{dt}} = \frac{1300}{53} = 24.53\ [\mu H]$$

$$C_{eq} = \frac{Q_{RR}}{8 * V_R} = \frac{30000}{8 * 1300} = 2.9\ [\mu F]$$

$$R_{eq} = \frac{L_C}{C_{eq}} = \frac{24.53}{2.9} = 8.45\ [\Omega]$$

Considering our 6-pulse bridge configuration, the RC snubbers will communicate with each other at turn-off, if each thyristor has its own RC snubber.

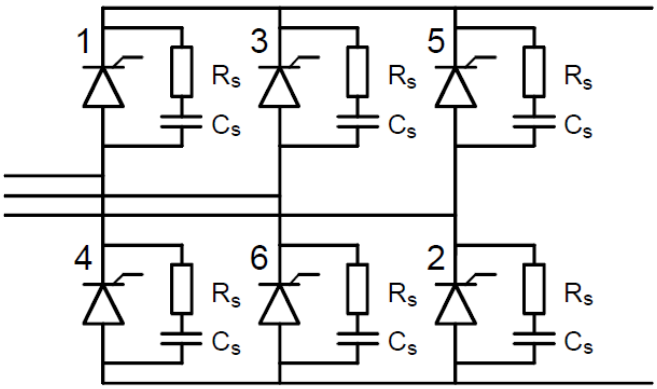

Figure 60 - Bridge configuration

At turn-off of thyristor 1, thyristors 2 and 3 are conducting and are thus short-circuiting their RC snubbers but thyristors 4, 5 and 6 are blocking and thus their RC snubbers influence the turn-off of thyristor 1:

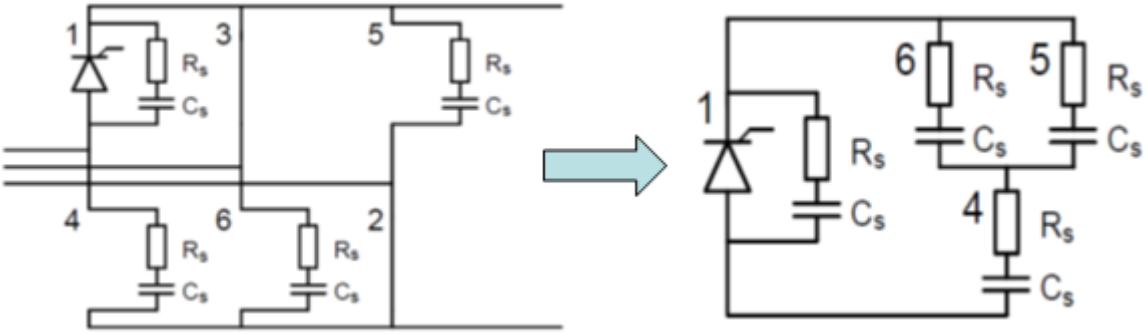

Figure 61 - Turn-off configuration

$$C_S = \frac{3}{5} C_{eq}$$
$$R_S = \frac{5}{3} R_{eq}$$

In our bridge we have 12 thyristors in parallel for each position, so:

$$C = 12 C_S = 20.76\ [\mu F]$$
$$R = \frac{R_S}{12} = 1.17\ [\Omega]$$

Converter analysis conclusions

After the previous analysis the resulting converter is reasonable if compared to the ITER configuration; obviously the losses due to the busbars are too high, and different solutions can be approached:

- increasing the cross section of the busbars, but for a good result the busbars become too big for the layout
- reducing the distance between the converters and QPC building and the tokamak building
- adopting high temperature superconducting busbars: as introduced in 1.3.1 the cooling plant cost becomes much lower when working at liquid nitrogen temperature (77 K); this solution is useful also for the interface between ambient temperature conductors (Cu or Al) and superconductive links: in fact a simple copper connection between the two zones is unsustainable due to the high thermal conductivity of copper; instead the adoption of high temperature superconductive current leads between the two zones drastically reduces the thermal losses.

4 DEMO Toroidal Field Circuit

The TF coils (TFCs) produce the toroidal field Bφ in order to guide the plasma along the reactor chamber. It was studied the possibility to group TFCs into sectors, in order to minimize the number of Quench Protection Circuits (QPC), Current Leads and busbars which can result both in investment reduction and in efficiency increase due to the limitation of the recirculating power. Furthermore, the crowded area of the cryostat would see the presence of only half of the connections to the coils. The price to pay is a higher voltage to ground of the coil terminals, that could be afforded by a suitable design of the insulation of the coils.

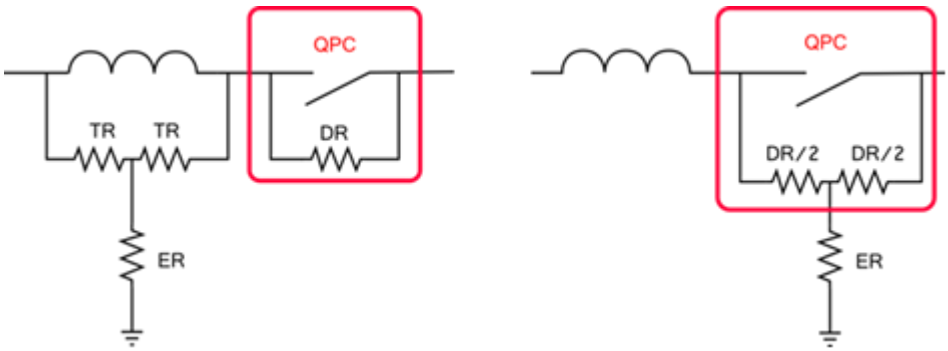

Figure 62 - One sector of ITER TF Circuit (left), one sector of JT-60SA TF Circuit (right)

Acronym	Description
TF	Toroidal Field
TFC	Toroidal Field Coil
QPC	Quench Protection Circuit
DR	Dump (Discharge) Resistor
ER	Earthing Resistor
CB	Circuit Breaker
TR	Terminal Resistor
Vg	Voltage from coil terminal to ground
Vd	Voltage across the coil

Table 8 - Acronyms and abbreviation used in the analysis

Four different topologies have been studied for the TF circuit in normal operation of QPCs and in fault conditions, with different earthing circuit for the ground reference and with a different connection of the Dump Resistor (DR) in the circuit. The aim of the analysis was to estimate the maximum voltage applied at the coils terminals with respect to ground, the voltage across each coil and the equivalent time constant for the discharge. The quantification of the peak voltage reached is important to verify the margins of the coil insulation, while the time constant of the discharge is important for the winding pack designers to verify if the coil can survive the quench.

The analysed earthing circuit topologies derive from those adopted in ITER and JT-60SA; the first consisting in a couple of terminal resistors connected one side to the coil terminals and the other side to a common earthing resistor grounded (Figure 62).

The earthing system topology ITER-like seems to lead to lower peak voltages in most of the case analysed with numerical simulations.

As far as the connection of the DR is concerned, in both ITER and JT-60SA the DR are connected in parallel the Circuit Breaker (CB) of the QPC; other possibilities are the connection of the DR to the coil terminals (Figure 63) or a mix of the two approaches; these case have been analysed to identify the most suitable solution for DEMO.

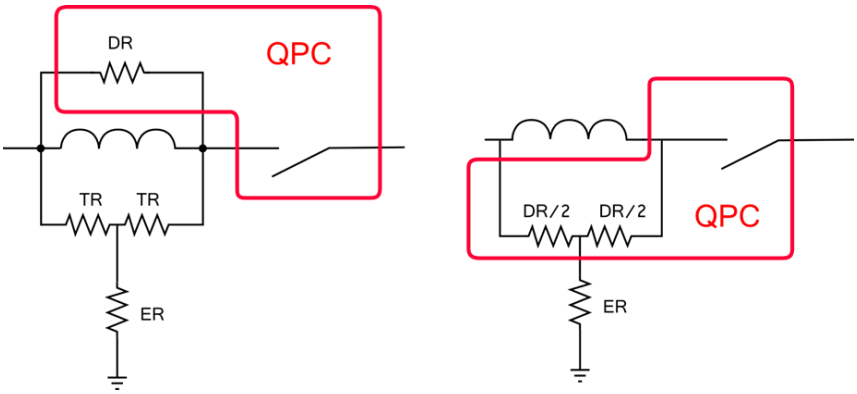

Figure 63 - Dump resistor in series to the main circuit breaker, earthing circuits used in ITER (left) and JT-60SA (right)

The conceptual design of TF QPC has been started making reference to the design of ITER Fast Discharge Units, which make use of a mechanical Bypass Switch to sustain the TFC current, a Vacuum Circuit Breaker and a Counter-Pulse Network to interrupt the dc current, a Dump Resistor to discharge the coil energy and a Pyro-Breaker as backup protection.

4.1 Model circuit analysis setting

The analysis has been done simulating many operative conditions on PSIM 10 software, starting considering an ideal TFC with 18 sectors, as already done for ITER; at the end of the study there will be evaluated the possibility of a 9 sectors TFC.
As shown in chapter 4, there are four possible topologies to supply the TF circuit coils:

TOPOLOGY	DESCRIPTION
A	ITER-like earthing, DR parallel to the CB
B	ITER-like earthing, DR parallel to the coil
C	JT60-SA-like earthing, DR parallel to the CB
D	JT60-SA-like earthing, DR parallel to the coil

Table 9 - Possible topologies

The coil is modelled by an adequate inductance, across which it is possible to measure the voltage applied and the voltages between the terminals and ground; for example, in Figure 64 it is reported the case of topology A. In order to lead us back to the case of QPC intervention the coil was imposed fully charged and subjected to the operative current.

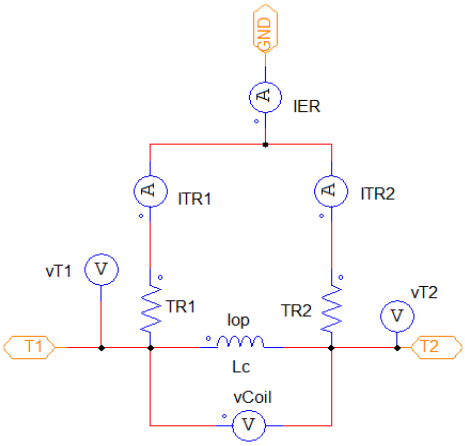

Figure 64 - Coil subcircuit

The CB is modelled by an adequate logic piloted switch, which simulate the QPC intervention; in Figure 65 the DR is put parallel to the CB.

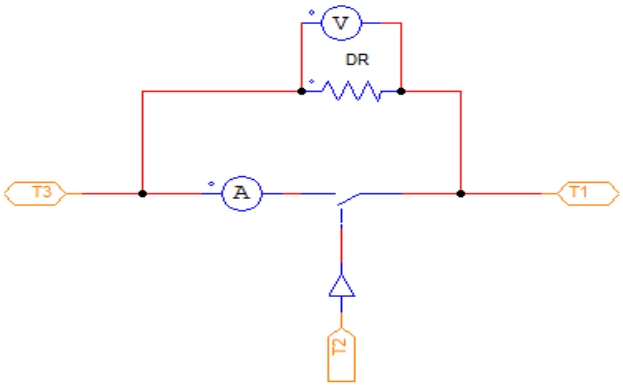

Figure 65 - Circuit Breaker subcircuit

4.2 Model circuit input data

Below are reported the input values for the 18 and 9 sectors analysis [19]:

Symbol	Description	PROCESS data	Unit	Input	Calculated value
NTFC	Number of toroidal field coils	18	-	✓	
Ec	Stored energy per coil	7.54	[GJ]		✓
Iop	Operative coil current	65	[kA]	✓	
Lc	Inductance per TF coil	3.57	[H]		✓
τ	Constant time for discharge	27	[s]	✓	
DR	Dump resistor	0.132	[Ω]		✓
TR	Grounding resistor	500	[Ω]		✓
ER	Earthing resistor	500	[Ω]		✓

Table 10 – 18 sectors input data

Symbol	Description	PROCESS data	Unit	Input	Calculated value
NTFC	Number of toroidal field coils	9	-	✓	
Ec	Stored energy per sector	15.08	[GJ]		✓
Iop	Operative coil current	65	[kA]	✓	
Lc	Inductance per TF coil	7.14	[H]		✓
τ	Constant time for discharge	27	[s]	✓	
DR	Dump resistor	0.264	[Ω]		✓
TR	Grounding resistor	500	[Ω]		✓
ER	Earthing resistor	500	[Ω]		✓

Table 11 - 9 sectors input data

Here are reported all the procedures to obtain the values of Ec, Lc and DR:

$$Ec = \frac{Total\ Energy}{NTFC} = \frac{135.7}{NTFC}\ [20]$$

$$Lc = \frac{2 * Ec}{Iop^2}$$

$$DR = \frac{Lc}{\tau}$$

4.3 Normal operation and fault analysis

To identify the stresses on the coils in terms of maximum voltage applied at the coils terminals with respect to ground, the voltage across each coil and the i^2t for the discharge, six different operating conditions (Op.C.) have been identified as worst conditions for ITER and JT-60SA; after having done the analysis on the four topologies (see Table 9) other fault conditions cannot be excluded, just like Op.C. 7:

Op.C. id	Description
1	QPC intervention
2	QPC intervention + ground fault at one QPC terminal
3	QPC intervention + QPC 1 does not work
4	QPC intervention + QPC 2 opens with a delay of 10ms
5	QPC intervention + QPC 1 does not work + ground fault near faulted QPC
6	QPC intervention + QPC 1 does not work + ground fault opposite to faulted QPC
7	QPC intervention + QPC 1 does not work + ground fault after subsequent coil

Table 12 - TFC operating conditions

At the beginning all the sectors are charged, imposing an operative current value of 65 [kA] as shown in Table 10; in case of quench detection inside the circuit, we suppose the QPC intervention after 1 [ms]; after that time the CB is opened, so the coils are able to discharge on the DRs. It is fundamental that all the QPC intervene at the same time, in order to avoid overvoltages inside the TF circuit; the system must be able to sustain these overvoltages whenever a fault occurs during the QPCs intervention. For this reason those fault conditions besides the normal QPC intervention have been simulated and analysed, in order to verify the functioning of the system with different topologies.

The first operating condition (Op.C.1) concerns the QPC intervention after a quench detection over the superconductors; Op.C.2 provides that, after the QPCs intervention, there is a ground fault near one of

the QPC's terminals 10 [ms] after the intervention; Op.C.3 concerns the non-intervention of one of the QPCs after a quench detection; Op.C.4 consists of a 10 [ms] delayed intervention of one of the QPCs respect to all the others, and this event well represents the Bypass Switch intervention (Pyro-breaker) next to the failure of one protection; Op.C.5 provides the non-intervention of one QPC and also a ground fault near one of its terminals; finally Op.C.6 is similar to the previous, except for the location of the ground fault, which is not near to the faulted QPC terminals in this case, but near to the opposite QPC terminals with respect to the circuit.
In Op.C. 7 there is the non-intervention of one QPC just like Op.C. 3 but the ground fault is not near to one of its terminals, but after the subsequent coil: this situation could involve other fault conditions in other critical points of the circuit.

4.4 Numerical analysis

The analysis of the various solutions listed about the toroidal field circuit coils topology has been done through numerical simulations (PSIM 10); this study highlights the pros and cons of the alternatives in terms of overvoltages, coils protection and energy disposal from the numerical and graphical points of view.
Reference:

- "PROCESS" data (Table 10 and Table 11)
- Operating conditions from Table 12
- Topologies from Table 9

4.4.1 18 sectors TOPOLOGY "A"

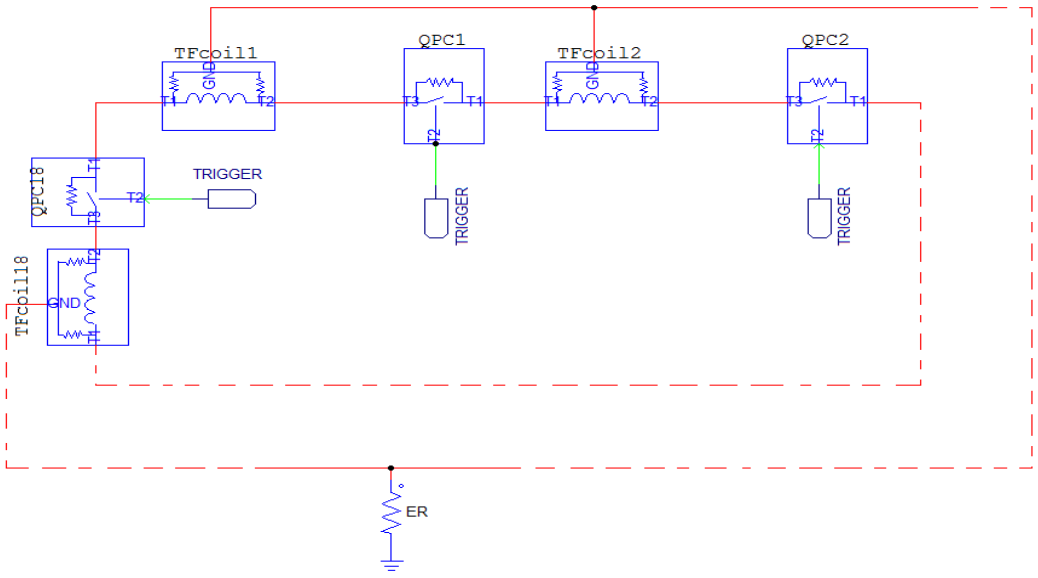

Figure 66 - 18 sectors TOPOLOGY "A"

Abbreviations: T ⟶ Terminal, C ⟶ Coil

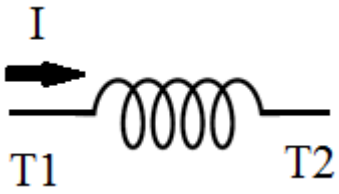

Figure 67 - Coil terminals reference

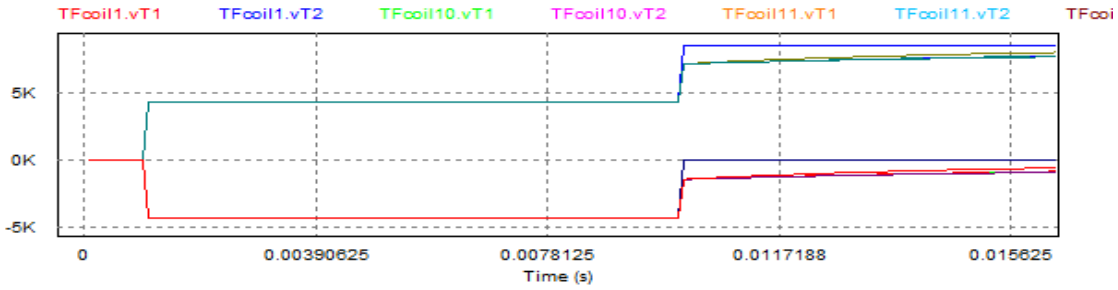

Figure 68 - 18 sectors TOPOLOGY "A" – Op.C. 2 – Vg

The voltage on C2:T1 goes to zero after the ground fault; the maximum value is reached on C1:T2; in short times all the terminals "1" voltages of the coils go to zero, while the others follow the trend of C1:T2.

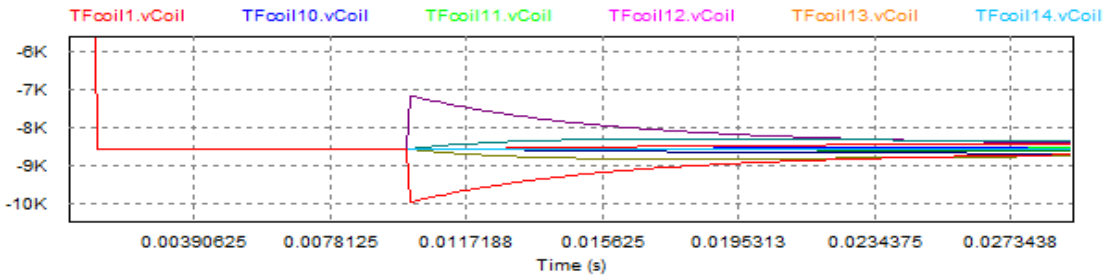

Figure 69 - 18 sectors TOPOLOGY "A" – Op.C. 2 – Vd

After the fault the highest value is reached by C1, but in short times all the coils tend to the before-fault Vd.

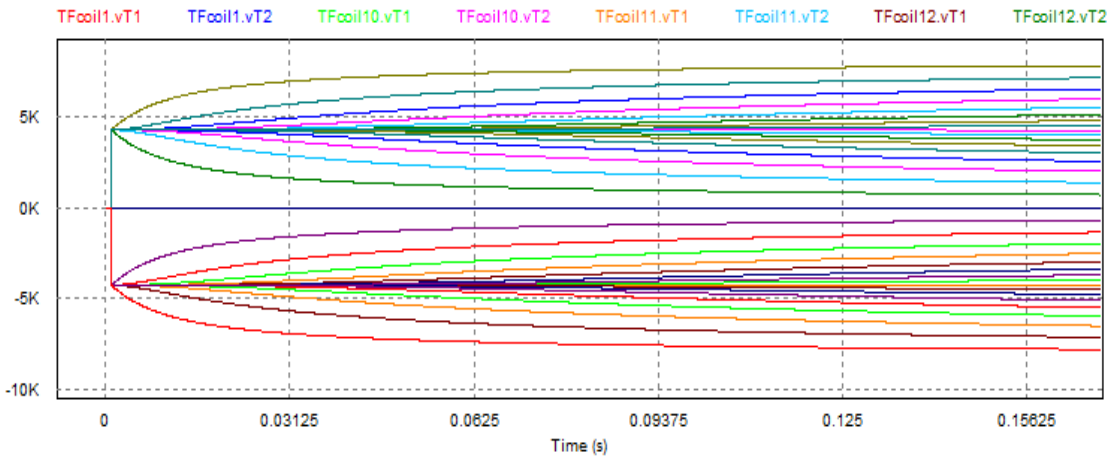

Figure 70 - 18 sectors TOPOLOGY "A" – Op.C. 3 – Vg

After the fault C1:T2 and C2:T1 go to zero, while all the other voltages reach different values for each coil, where the most stressed are C1:T1 and C2:T2.

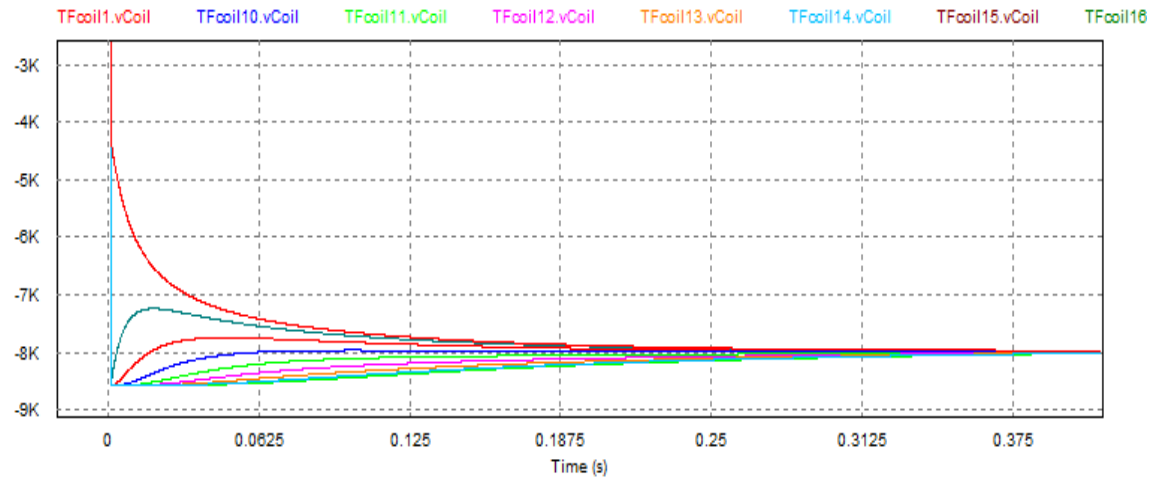

Figure 71- 18 sectors TOPOLOGY "A" – Op.C. 3 – Vd

Each coil is subjected to a different voltage value, but in short times all of them tend to the nominal Vd.

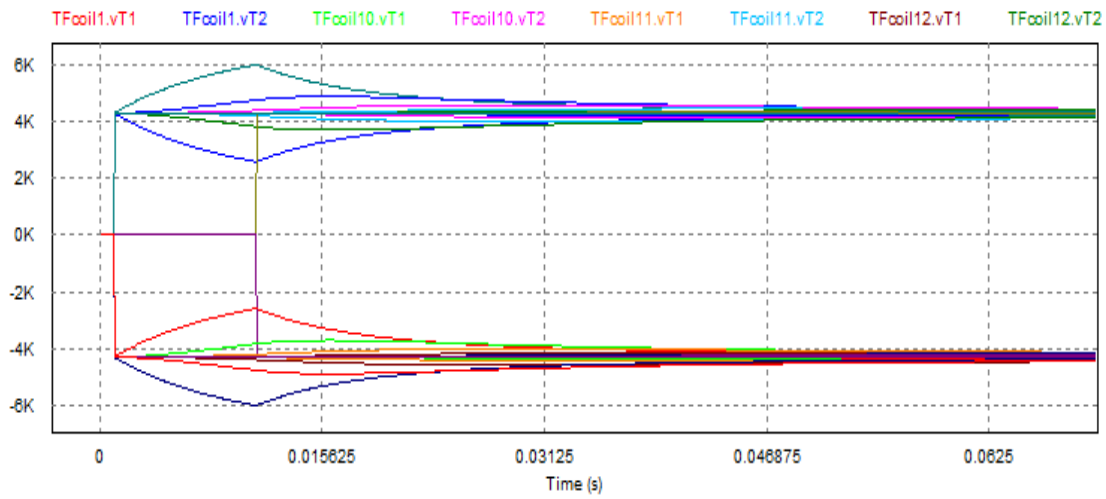

Figure 72 - 18 sectors TOPOLOGY "A" – Op.C. 4 – Vg

During the first 11 [ms] the trends are the same of Op.C.3, but when the delayed QPC intervene all the voltage rapidly reach the nominal Vg.

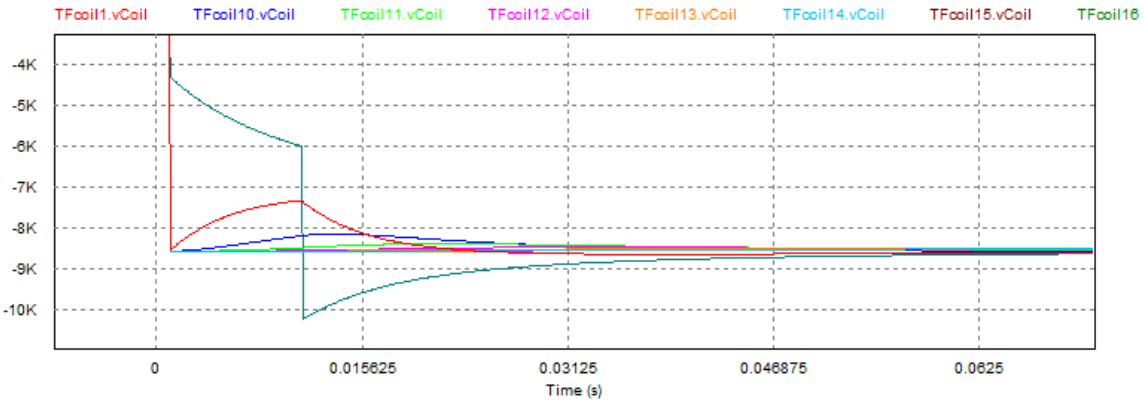

Figure 73 - 18 sectors TOPOLOGY "A" – Op.C. 4 – Vd

Same as said for Vg; notice that after the delayed QPC intervention C2 and C3 reach the highest Vd value.

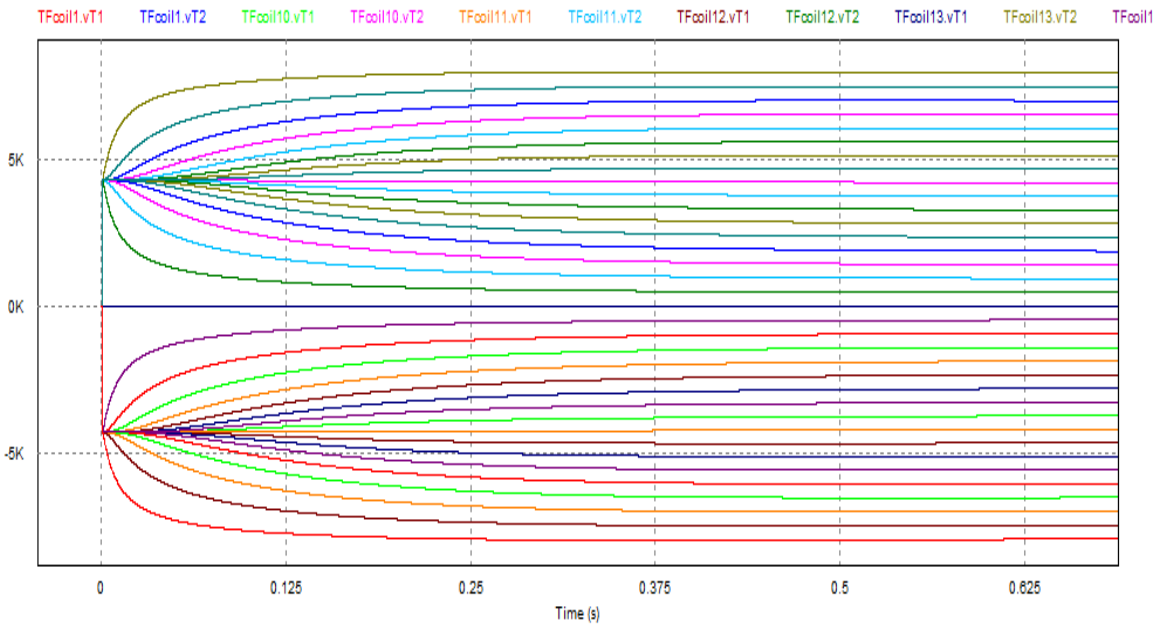

Figure 74 - 18 sectors TOPOLOGY "A" – Op.C. 5 – Vg

The trends for Op.C. 5 are pretty similar to Op.C.3.

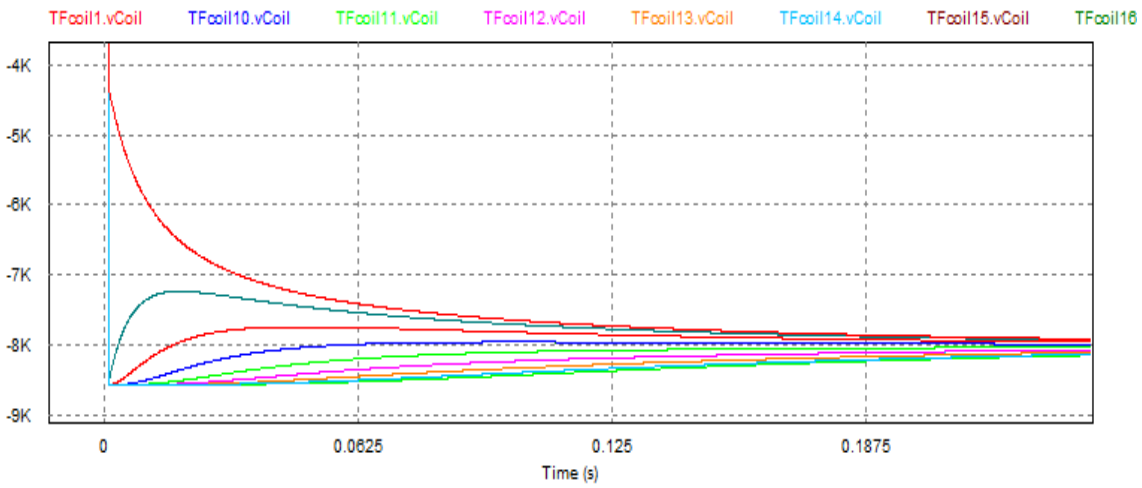

Figure 75 - 18 sectors TOPOLOGY "A" – Op.C. 5 – Vd

Same as said for Vg.

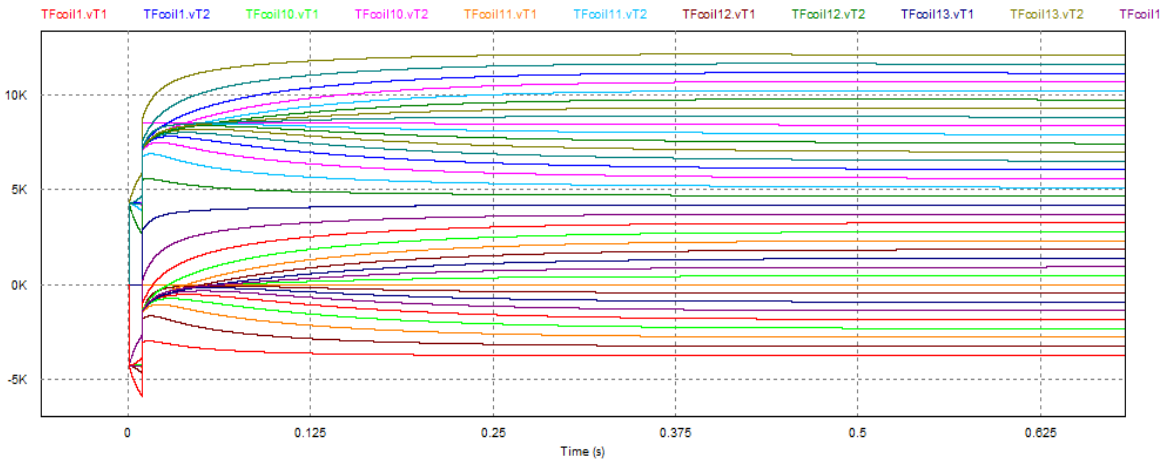

Figure 76 - 18 sectors TOPOLOGY "A" – Op.C. 6 – Vg

Initially the trends are the same as seen for Op.C.3, but after 10 [ms] the effect of the opposite ground fault is evident.

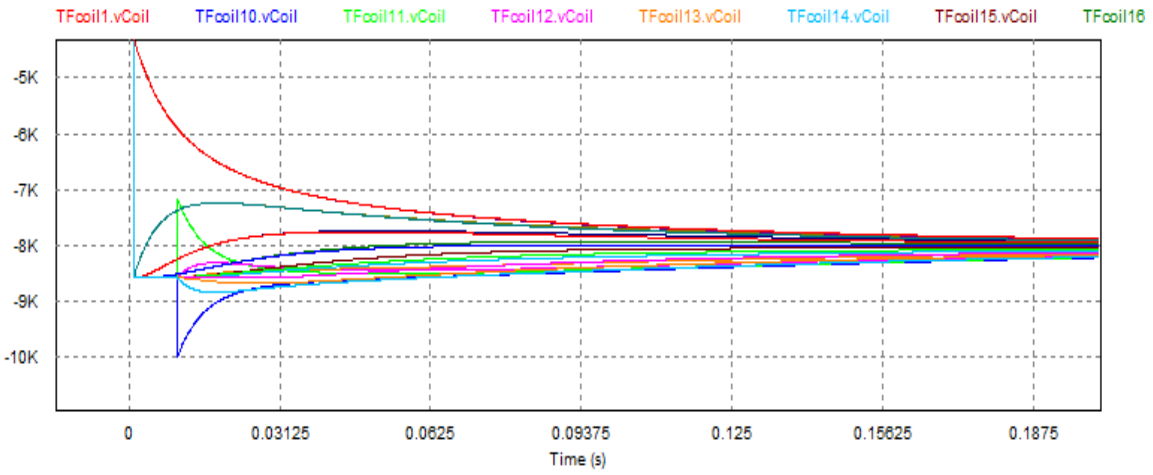

Figure 77 - 18 sectors TOPOLOGY "A" – Op.C. 6 – Vd

Same as said for Vg.

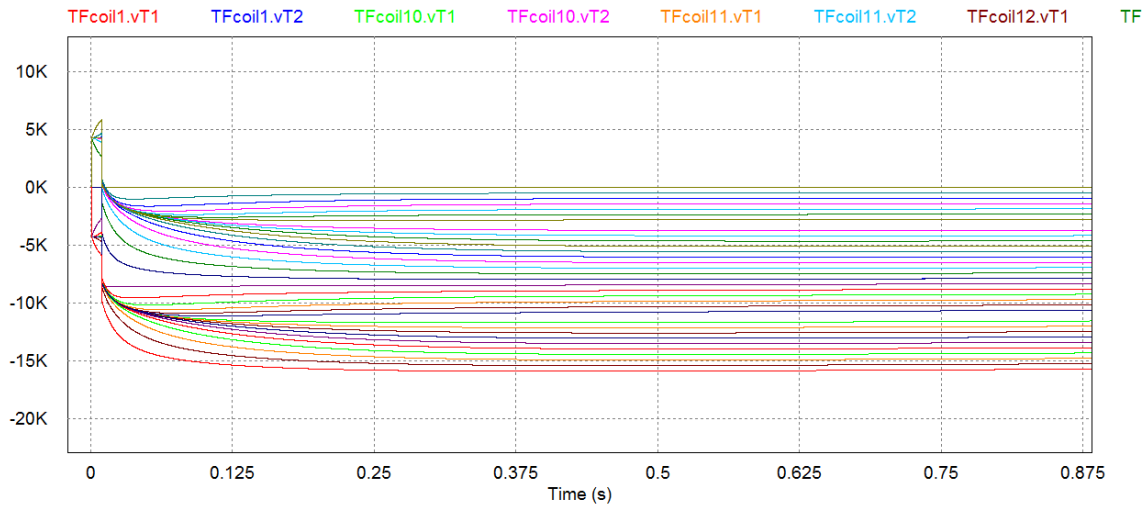

Figure 78 - 18 sectors TOPOLOGY "A" – Op.C. 7 – Vg

In this case there are the same considerations seen for Op.C.6, except for the different and higher voltage values that have been reached; during the first phase C2:T1 stays at zero, but after the ground fault it is C2:T2 which goes to zero.

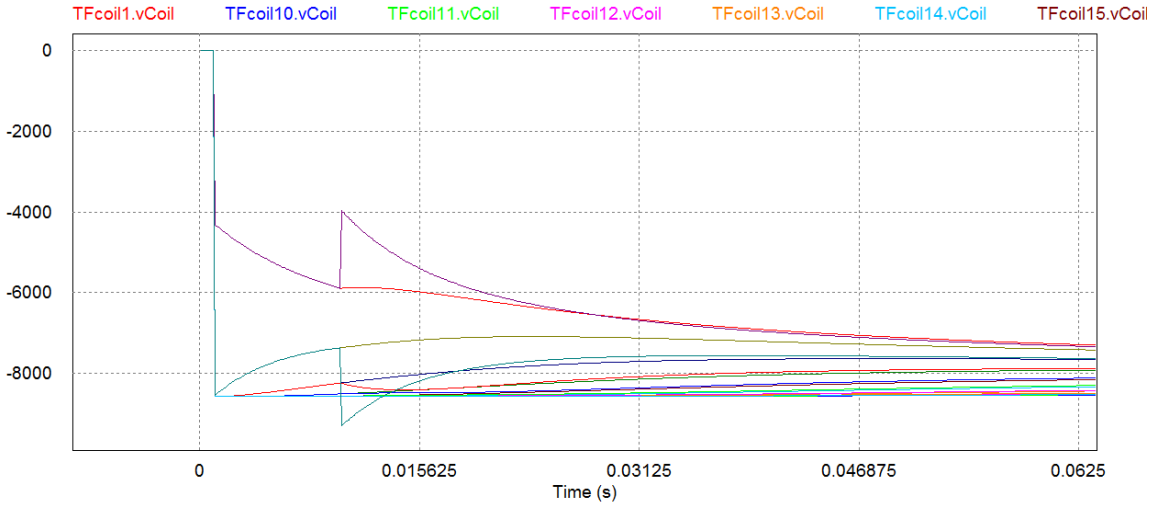

Figure 79 - 18 sectors TOPOLOGY "A" – Op.C. 7 – Vd

C3 reaches the highest Vd.

Op.C.	Vg peak module [kV]	Time (Vg peak) [s]	Location (Vg peak)
1	4.289	0.00101	Each coil
2	8.575	0.01001	C1:T2
3	7.963	0.39487	C1:T1, C2:T2
4	5.997	0.0110	C2:T2, C3:T1
5	7.963	0.39487	C2:T2, C1:T1
6	12.200	0.3990	C2:T2
7	15.917	0.4110	C1:T1

Table 13 - Vg, times to be reached and location for 18 sectors TOPOLOGY "A"

Op.C.	Vd peak module [kV]	Time (Vd peak) [s]	Location (Vd peak)
1	8.579	0.00101	Each coil
2	10.003	0.01001	C1
3	8.579	0.00101	each one except C1 and C2
4	10.280	0.01101	nearest two coils
5	8.579	0.00101	each one except the nearest coil
6	10.003	0.01001	coils nearest to the fault
7	9.294	0.01010	C3

Table 14 - Vd, times to be reached and location for 18 sectors TOPOLOGY "A"

I^2t analysis

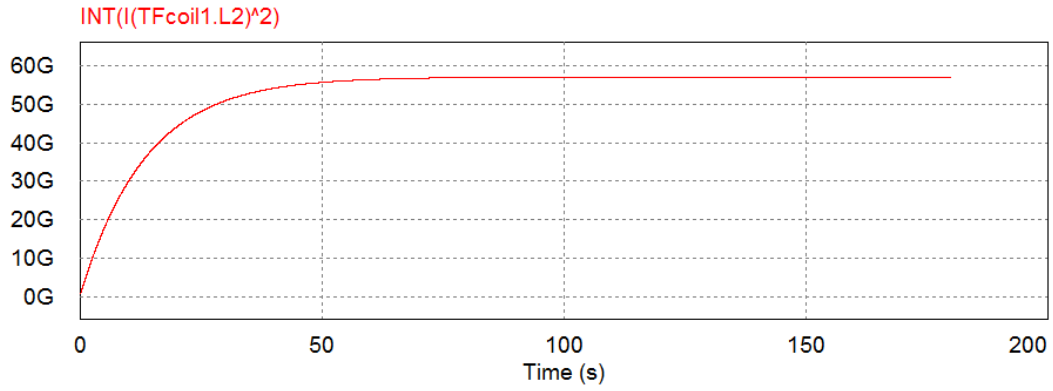

Figure 80 - I2t, Op.C.1, TOPOLOGY "A"

We suppose the QPC intervention one second after the quench detection (Tq); so we must add to the calculated I^2t value also the contribution of the first second, which is equal to Iop^2*1:

$$Regime\ value: 57.11 * 10^9\ [A^2 s]$$

$$Tq = 1\ [s]$$

$$Iop = 65\ [kA]$$

$$I^2t = 57.1 * 10^9 + 65000^2 * 1 = 61.3 * 10^9\ [A^2 s]$$

The I^2t and coil current trends are always the same with the various operative conditions analysed, except for their regime values:

Op.C.	Regime value [A^2s]	Tq [s]	Iop [kA]	I^2t [A^2s]
1	$57.11*10^9$	1	65	$61.3*10^9$
2	$57.11*10^9$	1	65	$61.3*10^9$
3	$60.55*10^9$	1	65	$64.8*10^9$
4	$57.11*10^9$	1	65	$61.3*10^9$
5	$60.55*10^9$	1	65	$64.8*10^9$
6	$60.55*10^9$	1	65	$64.8*10^9$
7	$60.55*10^9$	1	65	$64.8*10^9$

Table 15 - I2t for TOPOLOGY "A"

In most of cases the maximum I^2t is exceeded; for this reason the ITER scheme need a pyrobreaker to avoid dangerous high temperature inside the circuit; we could think about modifying the τ of the circuit changing the value of some parameters, but we need to consider the electrodynamic forces that would be created, and for this reason this solution is impossible.

4.4.2 18 sectors TOPOLOGY “B”

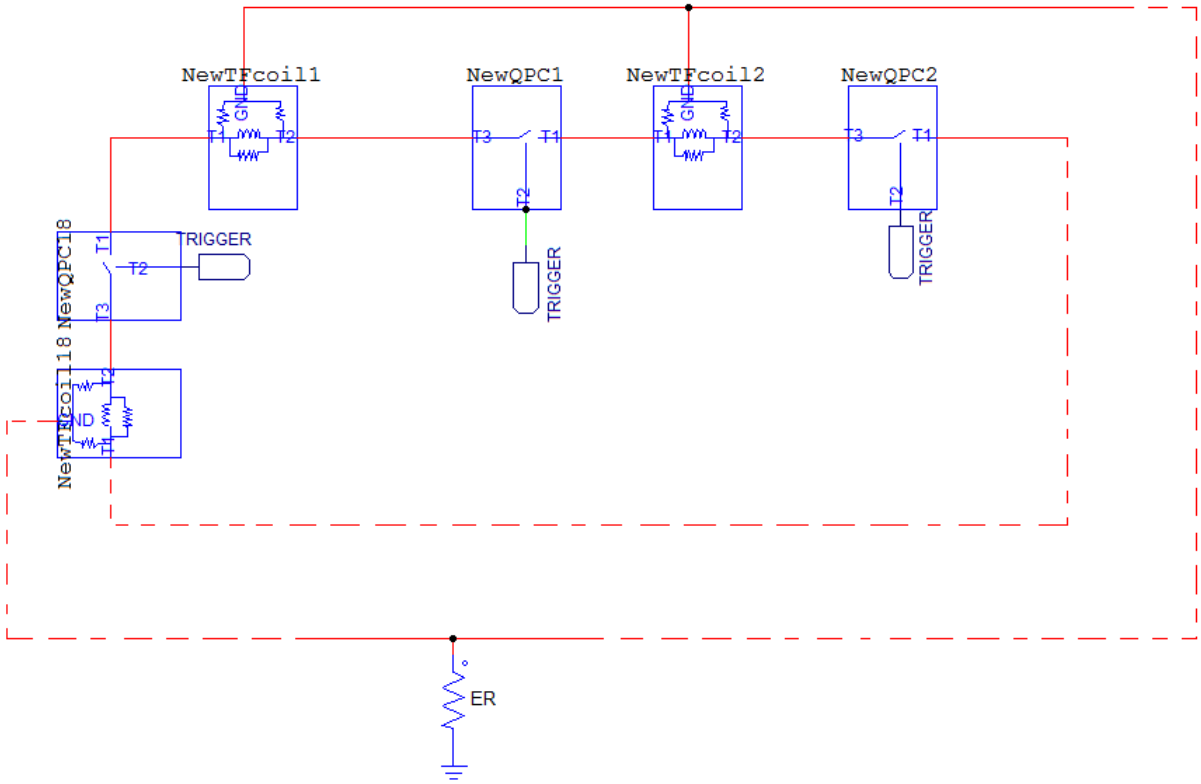

Figure 81 - 18 sectors TOPOLOGY "B"

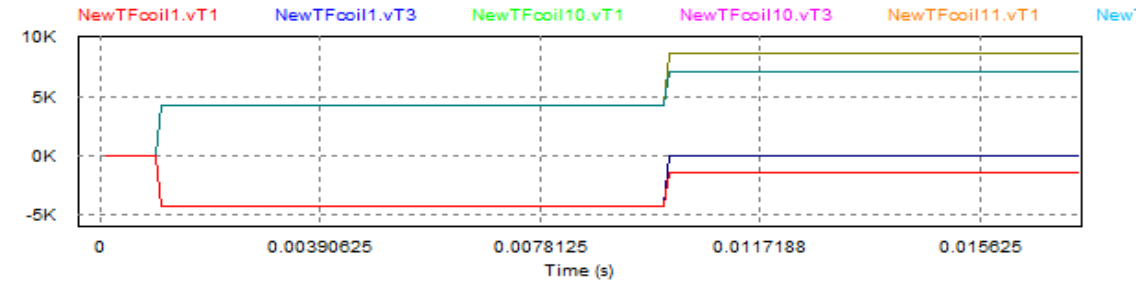

Figure 82 - 18 sectors TOPOLOGY "B" – Op.C. 2 – Vg

The voltage on C2:T1 goes to zero after the ground fault; the maximum value is reached on C2:T2. Except for these two terminals, for all the others half reaches a value which is a bit lower than C2:T2, and the other half reach a value a little higher than zero in module.

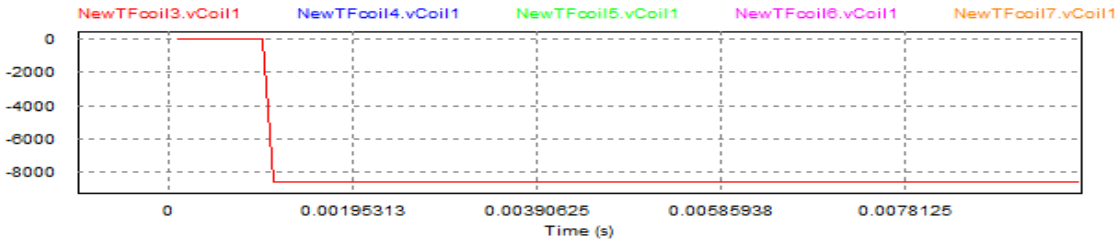

Figure 83 - 18 sectors TOPOLOGY "B" – Op.C. 2 – Vd

The Vd trend is always the same in all the operative conditions of TOPOLOGY "B" for each coil.

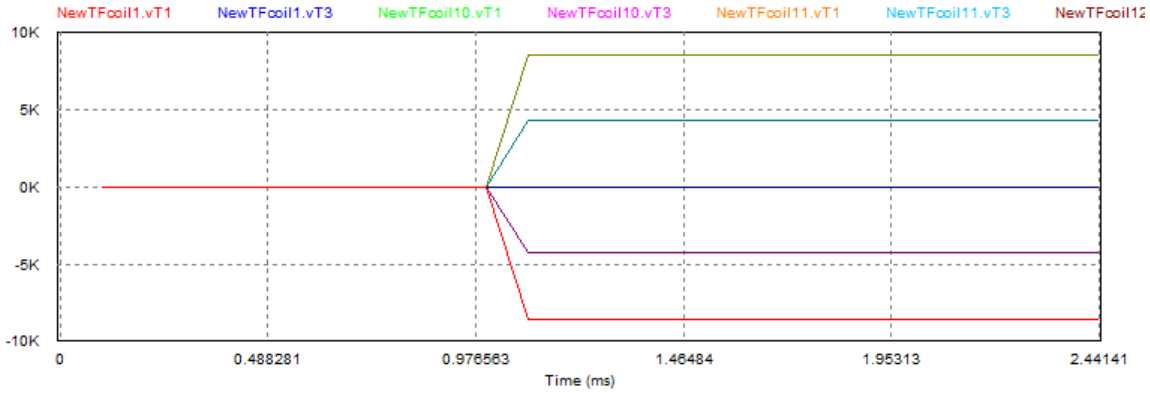

Figure 84 - 18 sectors TOPOLOGY "B" – Op.C. 3 – Vg

C1:T2 and C2:T1 remain at zero after the non-intervention of QPC1. The most stressed are C1:T1 and C2:T2.

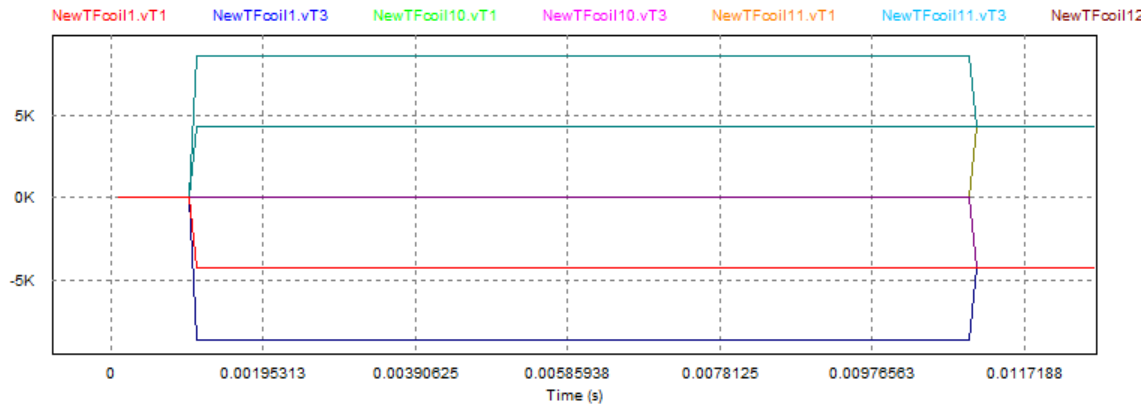

Figure 85 - 18 sectors TOPOLOGY "B" – Op.C. 4 – Vg

During the first 11 [ms] the trends are the same of Op.C.3, but when the delayed QPC intervene all the voltage rapidly reach the nominal Vg.

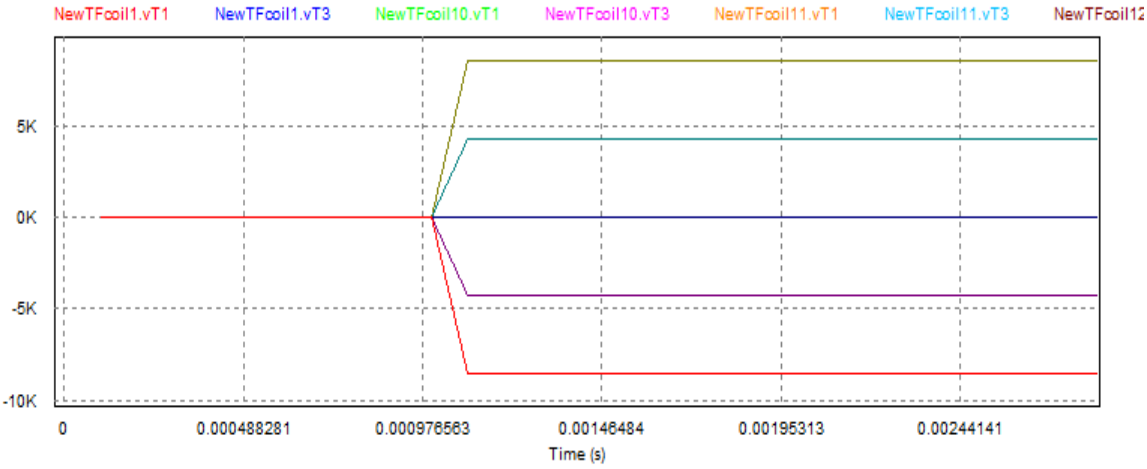

Figure 86 - 18 sectors TOPOLOGY "B" – Op.C. 5 – Vg

The trends for Op.C. 5 are pretty similar to Op.C.3.

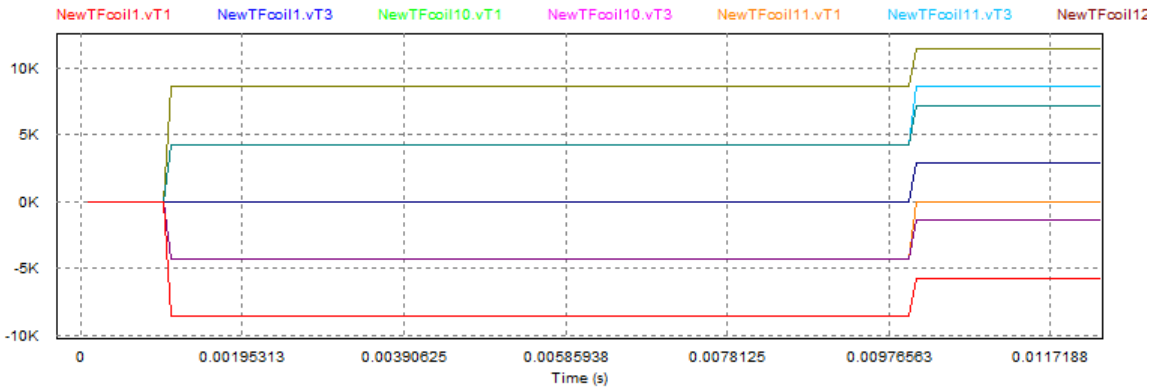

Figure 87 - 18 sectors TOPOLOGY "B" – Op.C. 6 – Vg

Initially the trends are the same as seen for Op.C.3, but after 10 [ms] the effect of the opposite ground fault is evident.

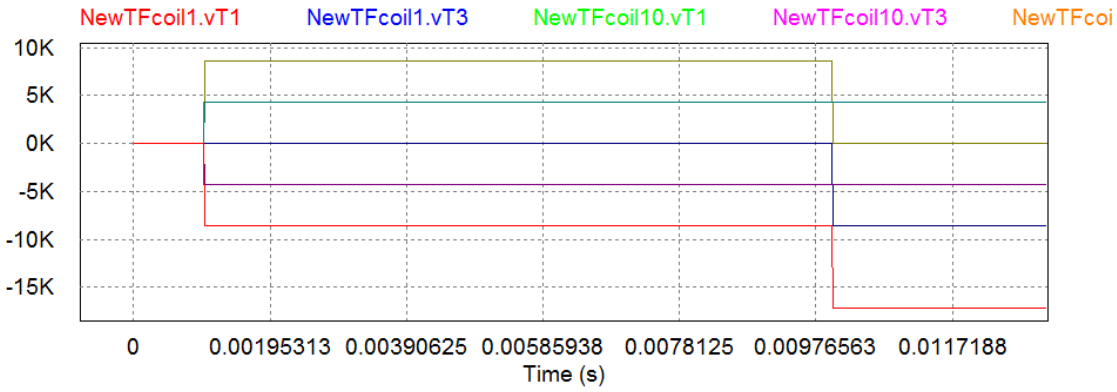

Figure 88 - 18 sectors TOPOLOGY "B" – Op.C. 7 – Vg

The highest value is reached on C1:T1.

Op.C.	Vg peak module [kV]	Time (Vg peak) [s]	Location (Vg peak)
1	4.289	0.0010	Each coil
2	8.576	0.0100	C2:T2
3	8.578	0.0010	C2:T2, C1:T1
4	8.578	0.0010	C3:T2, C2:T1
5	8.578	0.0010	C2:T2, C1:T1
6	11.433	0.0100	C2:T2
7	17.141	0.0100	C1:T1

Table 16 - Vg, times to be reached and location for 18 sectors TOPOLOGY "B"

Op.C.	Vd peak module [kV]	Time (Vd peak) [s]	Location (Vd peak)
1	8.579	0.0010	each coil
2	8.579	0.0010	each coil
3	8.578	0.0010	each coil
4	8.579	0.0010	each coil
5	8.578	0.0010	each coil
6	8.578	0.0010	each coil
7	8.578	0.0010	each coil

Table 17 - Vd, times to be reached and location for 18 sectors TOPOLOGY “B”

I^2t analysis

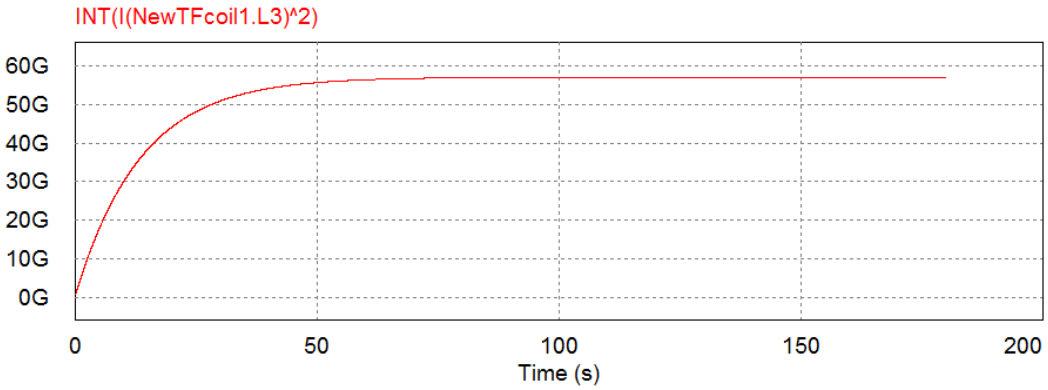

Figure 89 - I2t, Op.C.1, TOPOLOGY “B”

Op.C.	Regime value [A^2s]	Tq [s]	Iop [kA]	I^2t [A^2s]
1	$57.11*10^9$	1	65	$61.3*10^9$
2	$57.11*10^9$	1	65	$61.3*10^9$
3	$57.11*10^9$	1	65	$61.3*10^9$
4	$57.11*10^9$	1	65	$61.3*10^9$
5	$57.11*10^9$	1	65	$61.3*10^9$
6	$57.11*10^9$	1	65	$61.3*10^9$
7	$57.11*10^9$	1	65	$61.3*10^9$

Table 18 - I2t for TOPOLOGY "B"

Independently from the fault condition, there is always the same I^2t, and this is a reliable safety margin in the operation.

4.4.3 18 sectors TOPOLOGY “C”

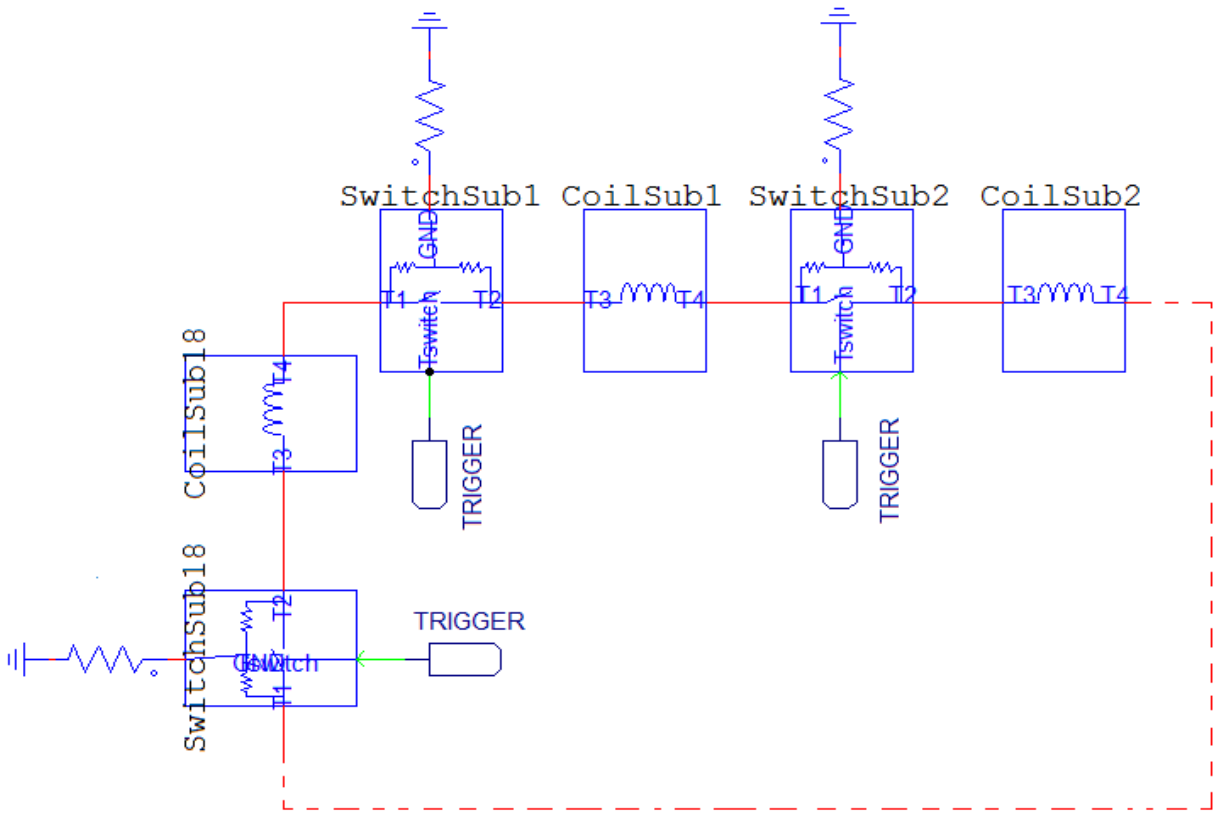

Figure 90 - 18 sectors TOPOLOGY "C"

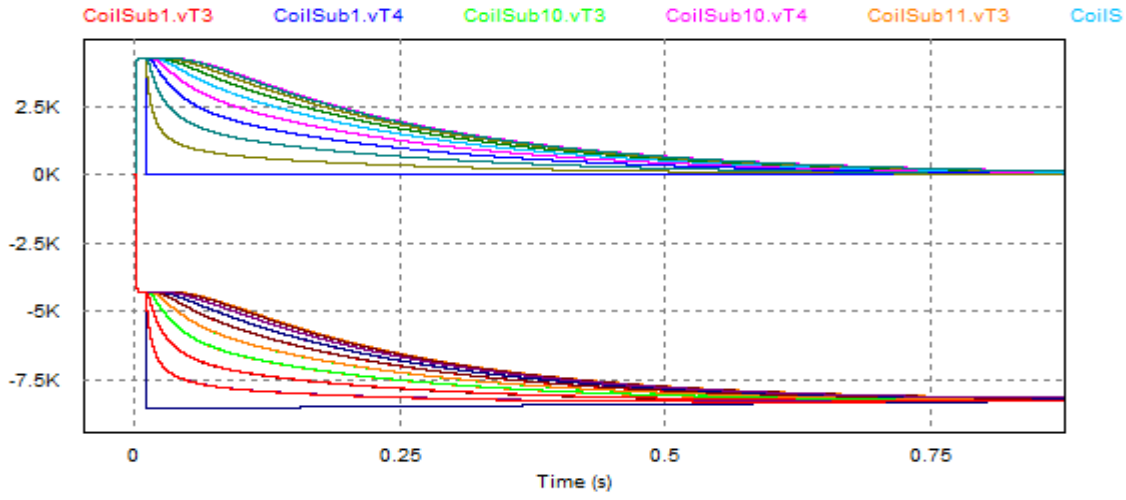

Figure 91 – 18 sectors TOPOLOGY “C” – Op.C. 2 – Vg

C1:T2 goes to zero after the fault, while half of the other terminals goes to zero after the initial peak, and the other half rapidly reach the highest value that have been reached on C2:T1.

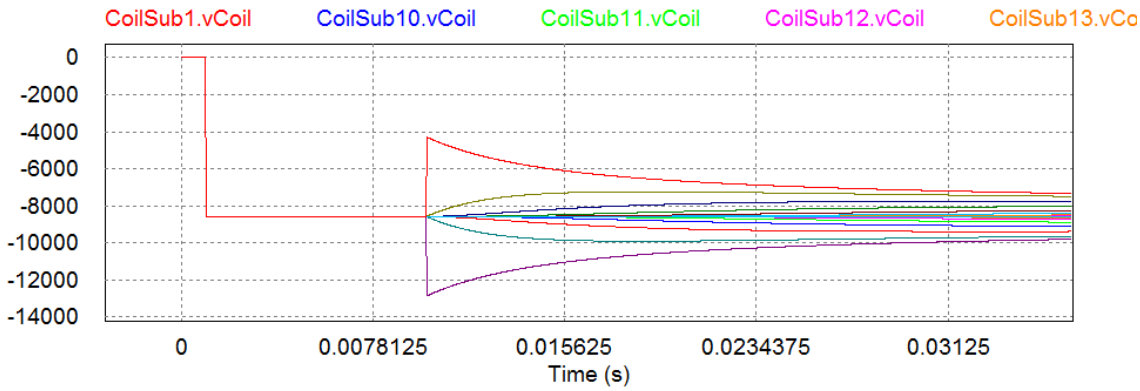

Figure 92 - 18 sectors TOPOLOGY "C" – Op.C. 2 – Vd

C2 reaches the highest Vd, but all the coils reach in short times the nominal Vd.

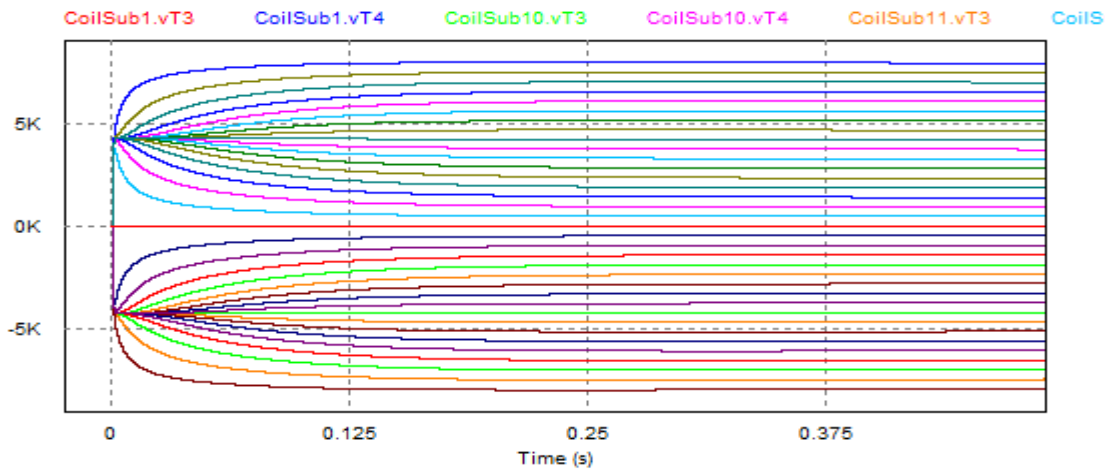

Figure 93 - 18 sectors TOPOLOGY "C" – Op.C. 3 – Vg

C1:T1 and C18:T2 stay at zero, while all the other terminals reach different Vgs.

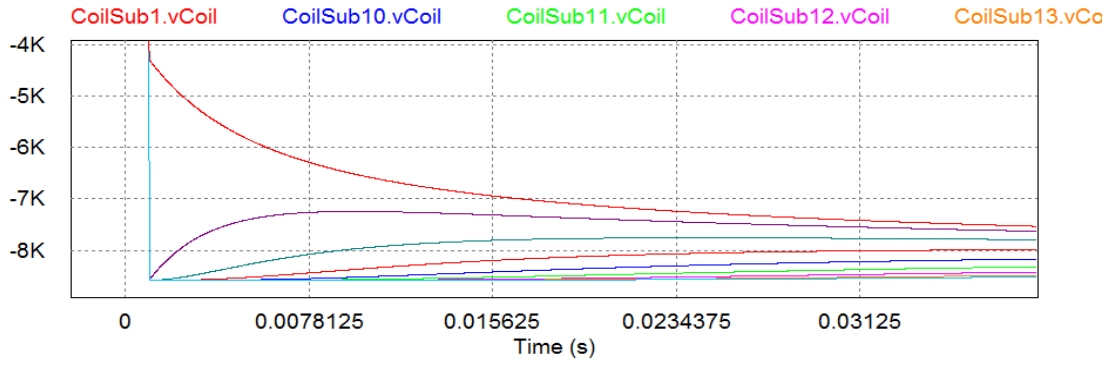

Figure 94 - 18 sectors TOPOLOGY "C" – Op.C. 3 – Vd

Each coil reaches a different Vd value, but in short times they reach the nominal Vd.

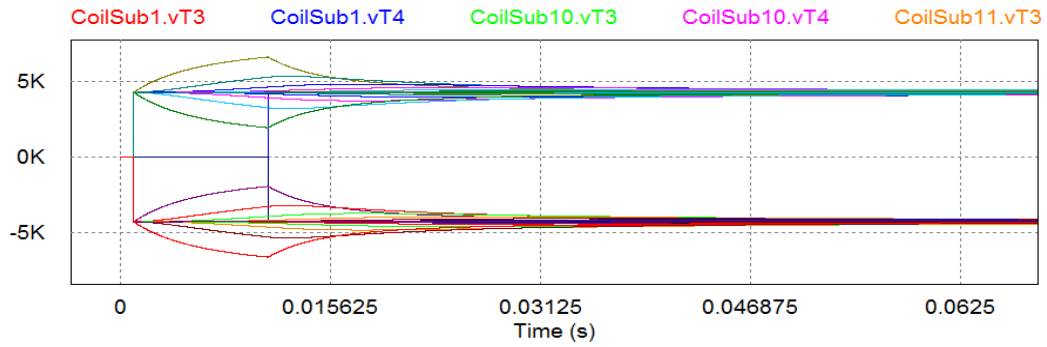

Figure 95 - 18 sectors TOPOLOGY "C" – Op.C. 4 – Vg

During the first 11 [ms] the trends are the same of Op.C.3, but when the delayed QPC intervene all the voltage rapidly reach the nominal Vg.

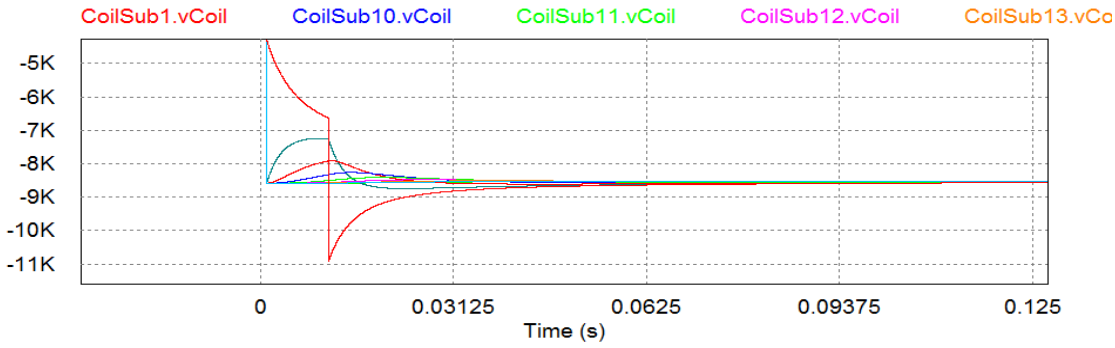

Figure 96 - 18 sectors TOPOLOGY "C" – Op.C. 4 – Vd

After the delayed intervention C1 reach the highest value.

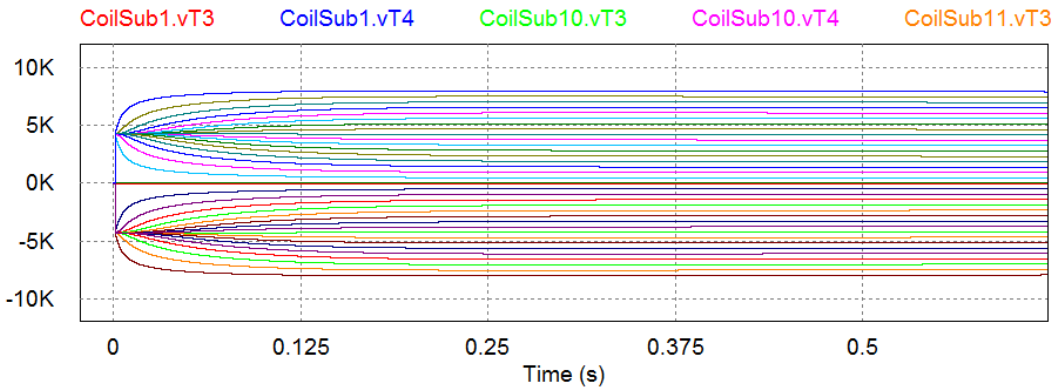

Figure 97 - 18 sectors TOPOLOGY "C" – Op.C. 5 – Vg

C1:T1 and C18:T2 remain at zero, while all the other terminals reach different values.

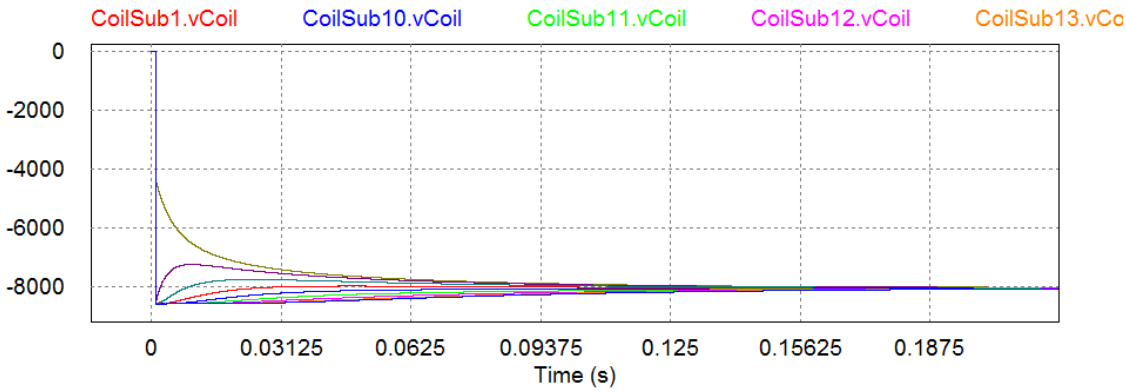

Figure 98 - 18 sectors TOPOLOGY "C" – Op.C. 5 – Vd

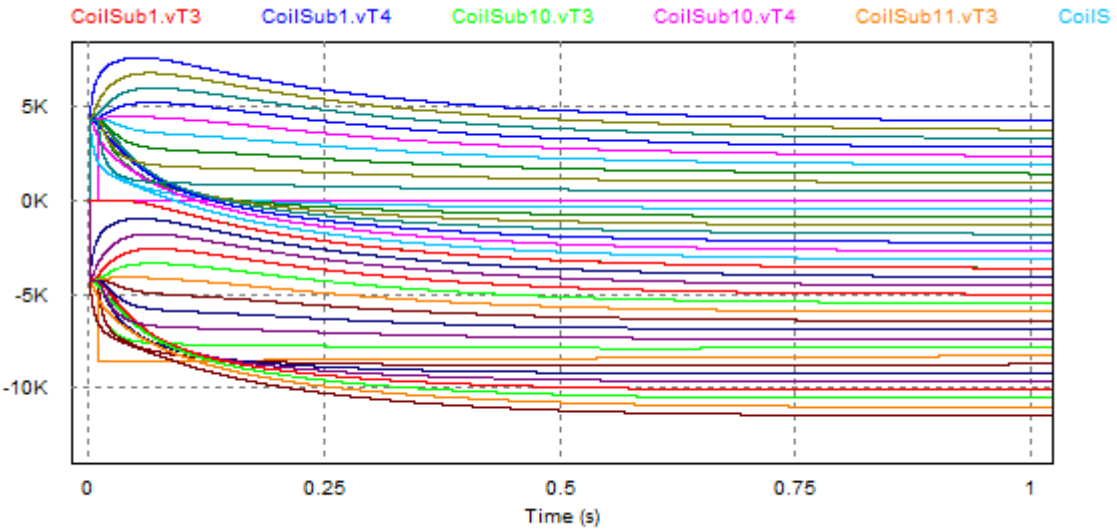

Figure 99 - 18 sectors TOPOLOGY "C" – Op.C. 6 – Vg

After the ground fault C1:T1, C18:T2 and C10:T2 (which is near to the ground fault) go to zero, while all the others reach different values.

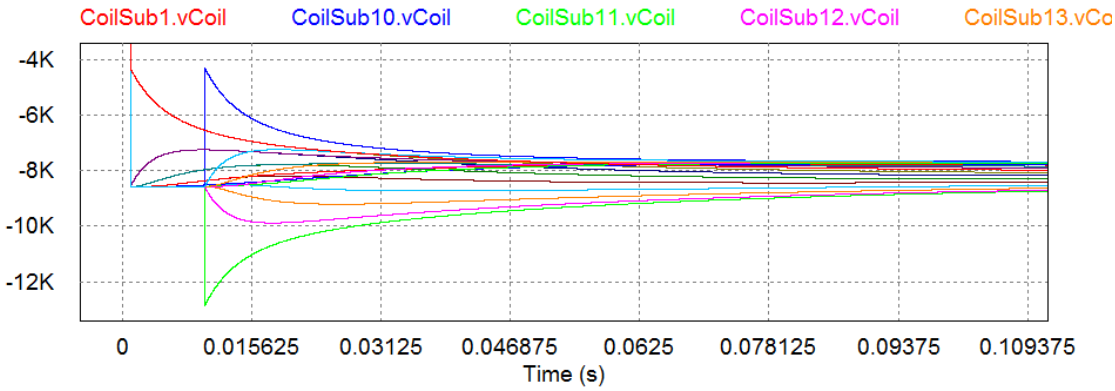

Figure 100 - 18 sectors TOPOLOGY "C" – Op.C. 6 – Vd

C11 reach the highest Vd after the fault.

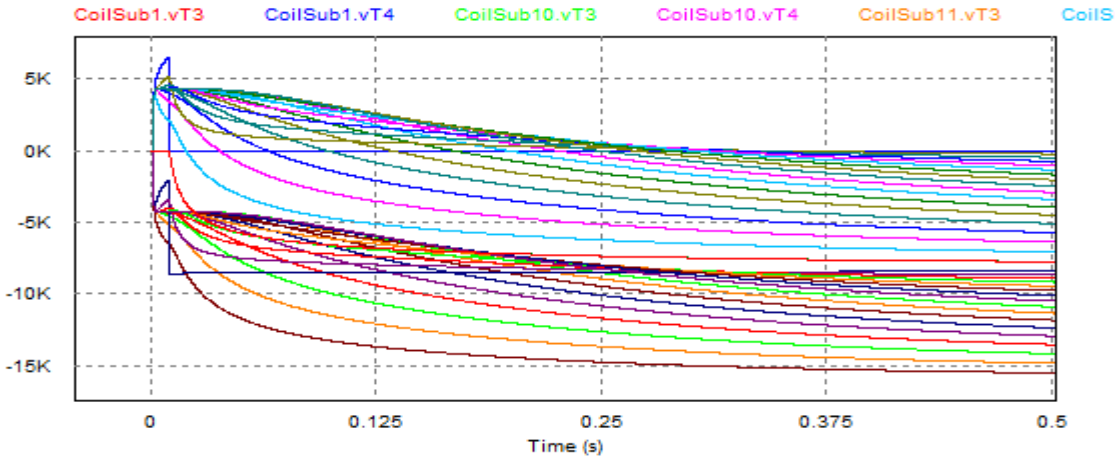

Figure 101 - 18 sectors TOPOLOGY "C" – Op.C. 7 – Vg

The considerations are similar to Op.C. 6, with different values; after the fault C1:T2 goes to zero.

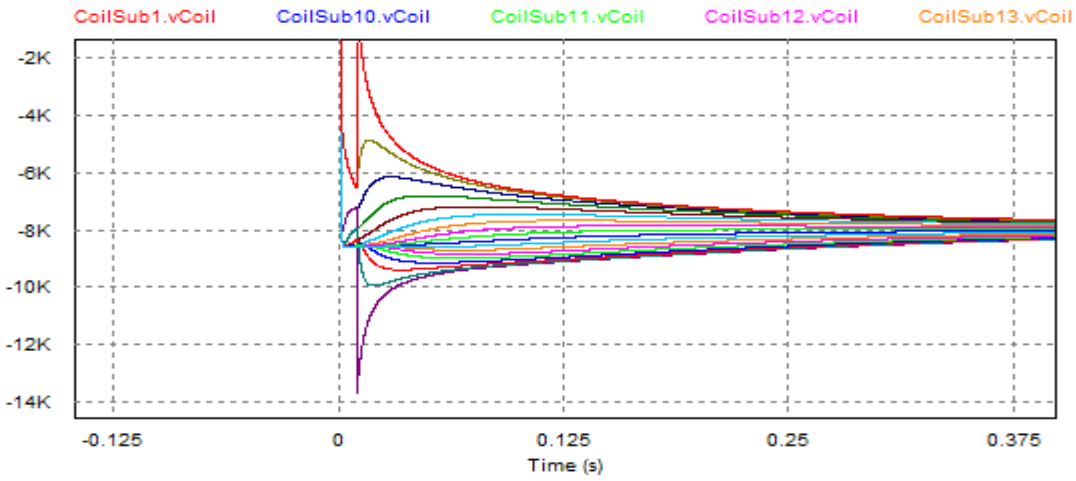

Figure 102 - 18 sectors TOPOLOGY "C" – Op.C. 7– Vd

C2 reaches the highest value.

Op.C.	Vg peak module [kV]	Time (Vg peak) [s]	Location (Vg peak)
1	4.290	0.0010	each coil
2	8.577	0.0101	C2:T1
3	8.022	0.2380	C1:T2
4	6.633	0.0110	C2:T2
5	8.022	0.2387	C1:T2
6	11.452	0.8985	C18:T1
7	15.668	0.7923	C18:T1

Table 19 - Vg, times to be reached and location for 18 sectors TOPOLOGY "C"

Op.C.	Vd peak module [kV]	Time (Vd peak) [s]	Location (Vd peak)
1	8.580	0.0010	each coil
2	12.859	0.0100	C2
3	8.580	0.0010	Each one except C1 and C18
4	10.917	0.0110	C1
5	8.580	0.0010	Each one except C1 and C18
6	12.859	0.0100	C11
7	13.774	0.0100	C2

Table 20 - Vd, times to be reached and location for 18 sectors TOPOLOGY "C"

I^2t analysis

Considering the JT-60SA earthing topology, the results are pretty the same respect to the ITER configuration, with a minimal variation of the values; in fact the earthing system does not influence the I^2t.

4.4.4 18 sectors TOPOLOGY “D”

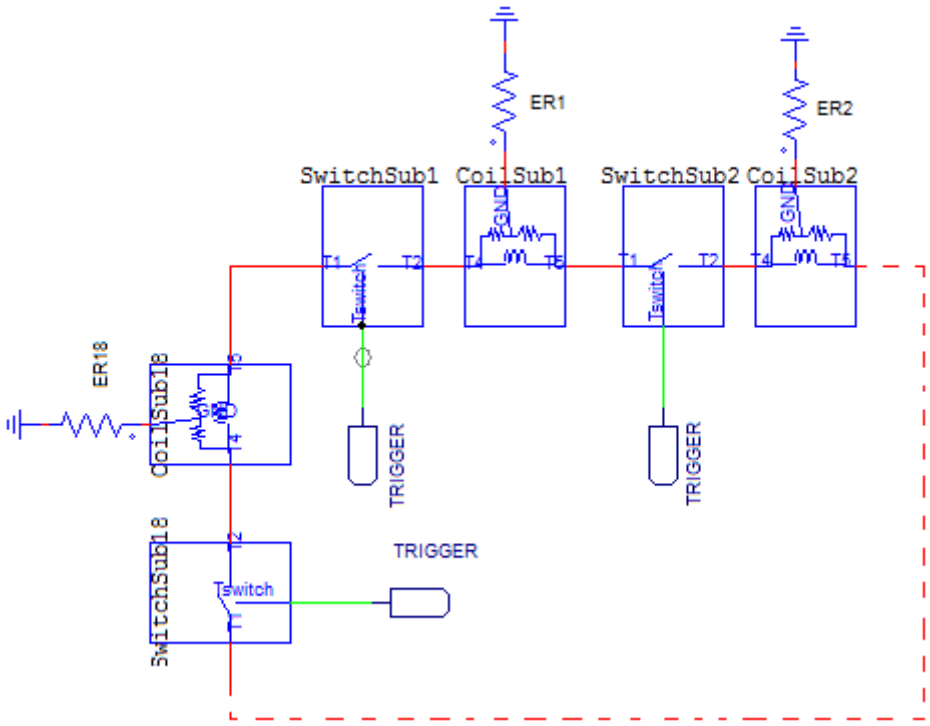

Figure 103 - 18 sectors TOPOLOGY "D"

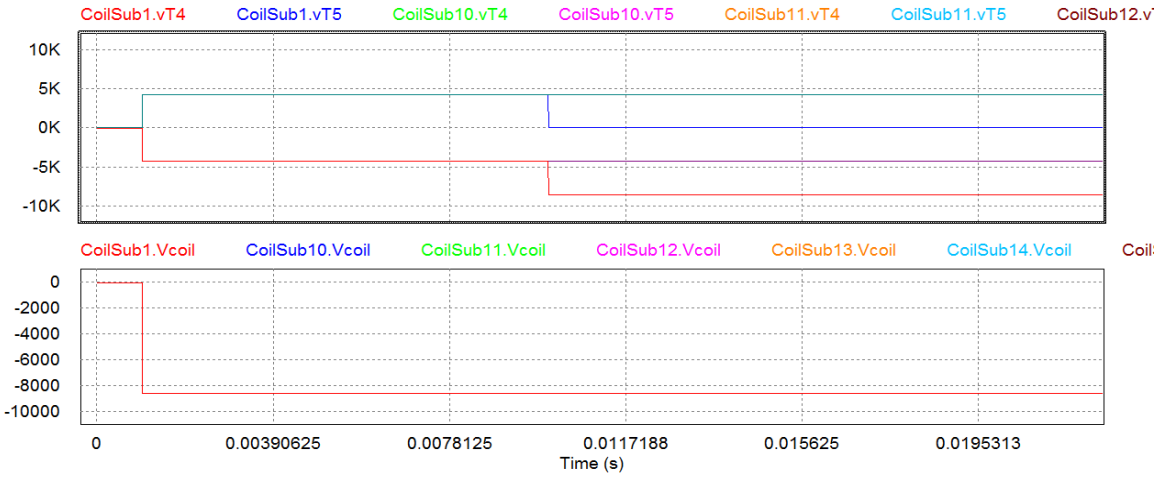

Figure 104 - 18 sectors TOPOLOGY “D” – Op.C. 2 – Vg and Vd

C1:T2 goes to zero after the fault, C1:T1 reaches the highest value, while all the others reach the nominal Vg.
The Vd trends for TOPOLOGY “D” are always the same.

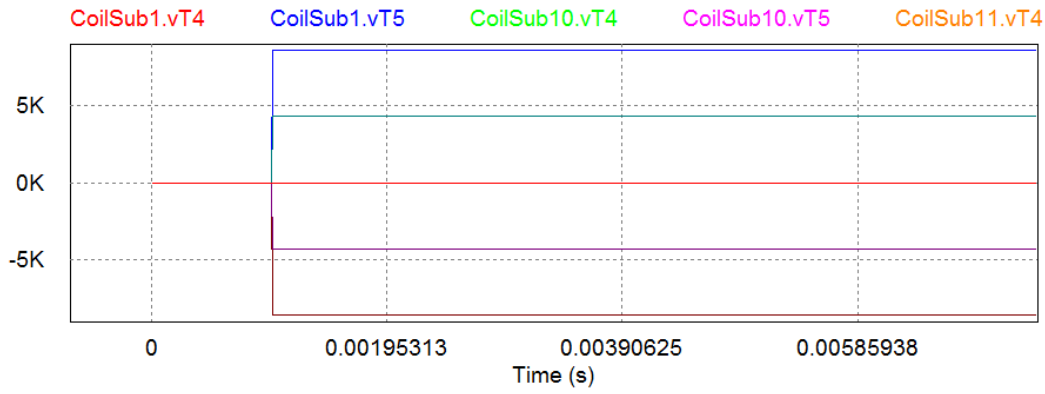

Figure 105 - 18 sectors TOPOLOGY "D" – Op.C. 3 – Vg

Except for C1:T2 and C18:T1, all the other terminals go to their nominal Vg.

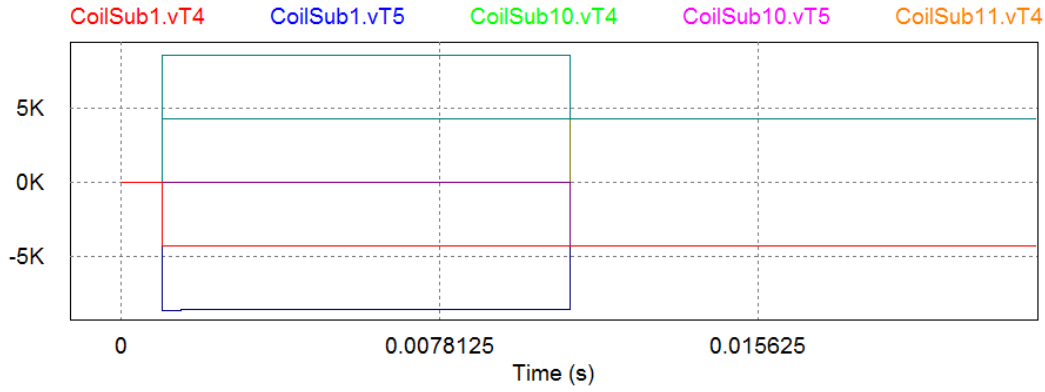

Figure 106 - 18 sectors TOPOLOGY "D" – Op.C. 4 – Vg

During the first 11 [ms] the trends are the same as seen for Op.C.3, and next each terminal reach the nominal Vg.

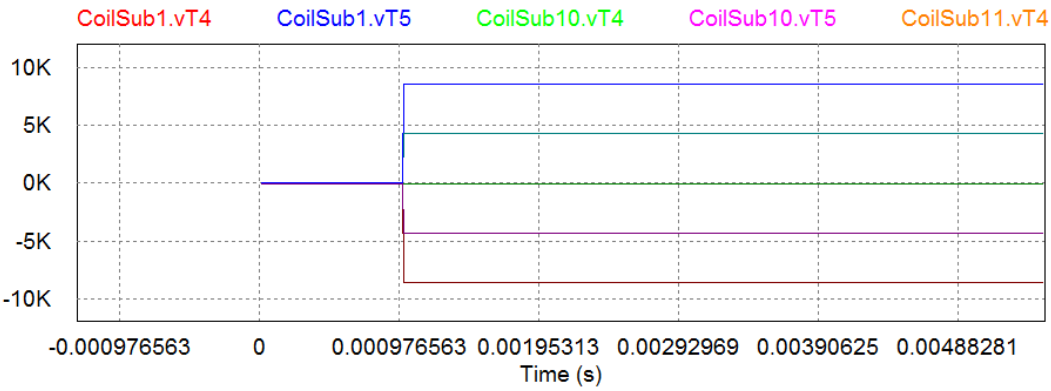

Figure 107 - 18 sectors TOPOLOGY "D" – Op.C. 5 – Vg

The trends are similar to Op.C. 3.

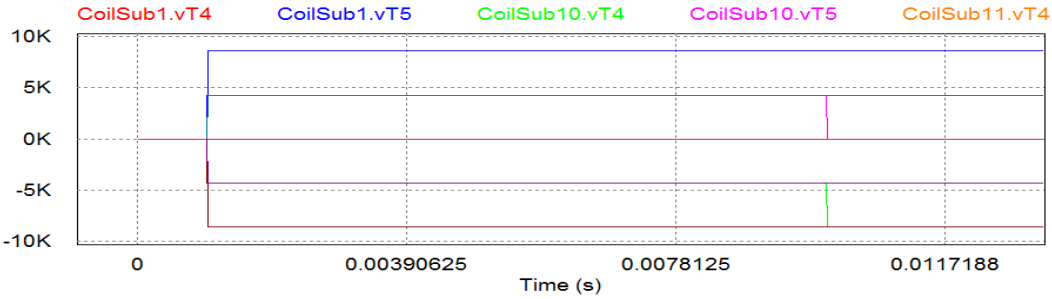

Figure 108 - 18 sectors TOPOLOGY "D" – Op.C. 6 – Vg

C1:T1 remains at zero, while after the ground fault all the other terminals reach the nominal Vg, except for C1:T2 and C18:T1.

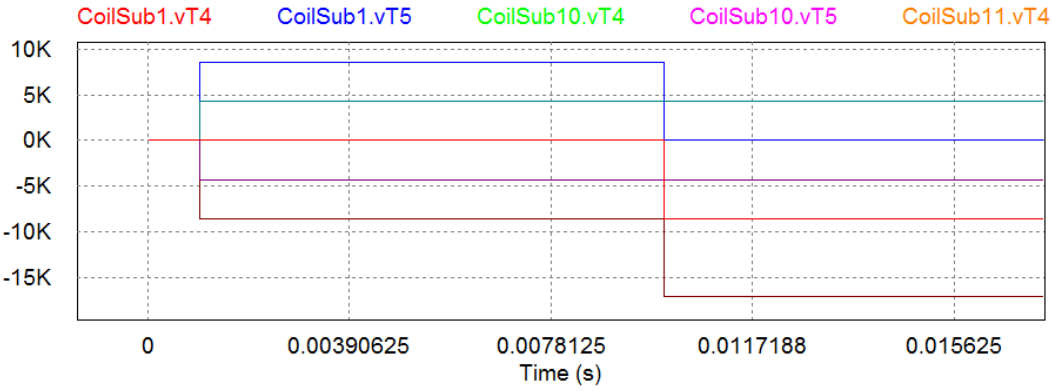

Figure 109 - 18 sectors TOPOLOGY "D" – Op.C. 7 – Vg

After the fault each terminal reach the nominal Vg, except for C1:T2 which goes to zero and C18:T1 which reaches the highest value.

Op.C.	Vg peak module [kV]	Time (Vg peak) [s]	Location (Vg peak)
1	4,300	0,0010	each one
2	8,500	0,0100	C1:T1
3	8,579	0,0010	C1:T2, C18:T1
4	8,579	0,0010	C1:T1, C2:T2
5	8.580	0,0010	C1:T2, C18:T1
6	8,579	0,0010	C1:T2, C18:T1
7	17,149	0,0100	C18:T1

Table 21 - Vg, times to be reached and location for 18 sectors TOPOLOGY "D"

Op.C.	Vg peak module [kV]	Time (Vg peak) [s]	Location (Vg peak)
1	8,580	0,0010	each one
2	8,580	0,0010	each one
3	8,580	0,0010	each one
4	8,580	0,0010	each one
5	8,580	0,0010	each one
6	8,580	0,0010	each one
7	8,580	0,0010	each one

Table 22 - Vd, times to be reached and location for 18 sectors TOPOLOGY "D"

I^2t analysis

Considering the JT-60SA earthing topology, the results are pretty the same respect to the ITER configuration, with a minimal variation of the values; in fact the earthing system does not influence the I^2t.

4.4.5 9 sectors TOPOLOGY “A”

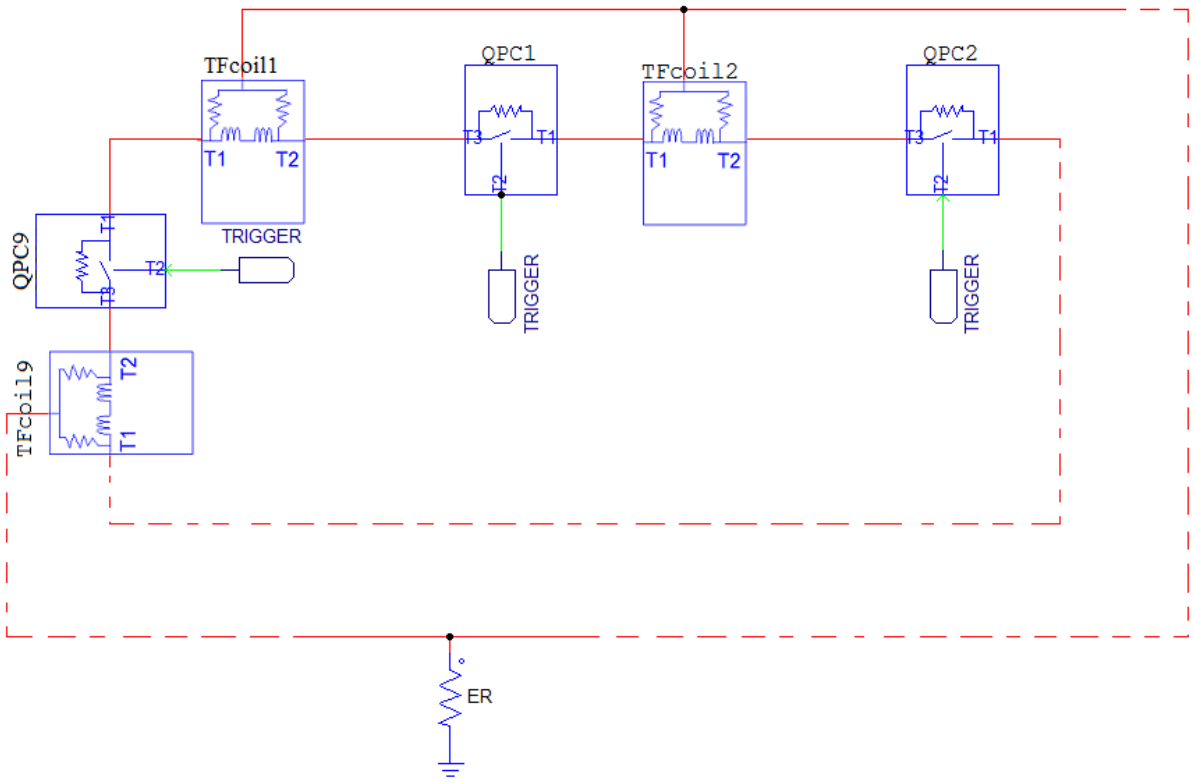

Figure 110 - 9 sectors TOPOLOGY "A"

The trends and the considerations for each topology are similar to the cases of 18 sectors, except to the fact that with 9 sectors the voltage values are double than in the case of 18 sectors.

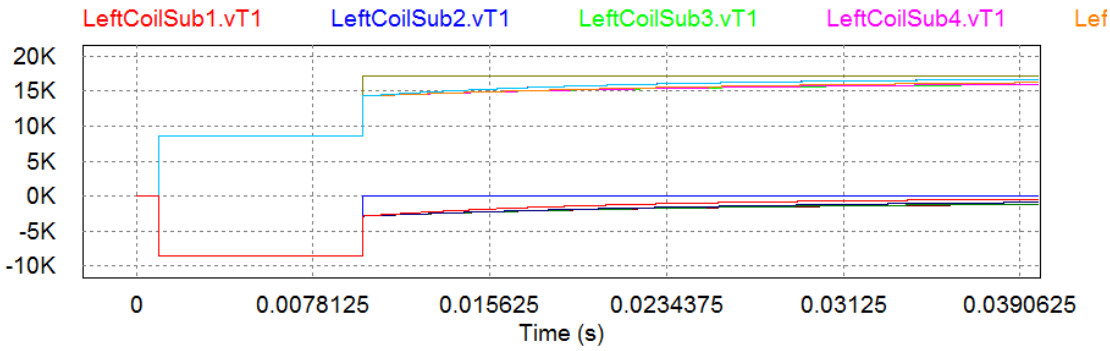

Figure 111 - 9 sectors TOPOLOGY “A” – Op.C. 2 – Vg

The voltage on C2:T1 goes to zero after the ground fault; the maximum value is reached on C1:T2; in short times all the terminals “1” voltages of the coils go to zero, while the others follow the trend of C1:T2.

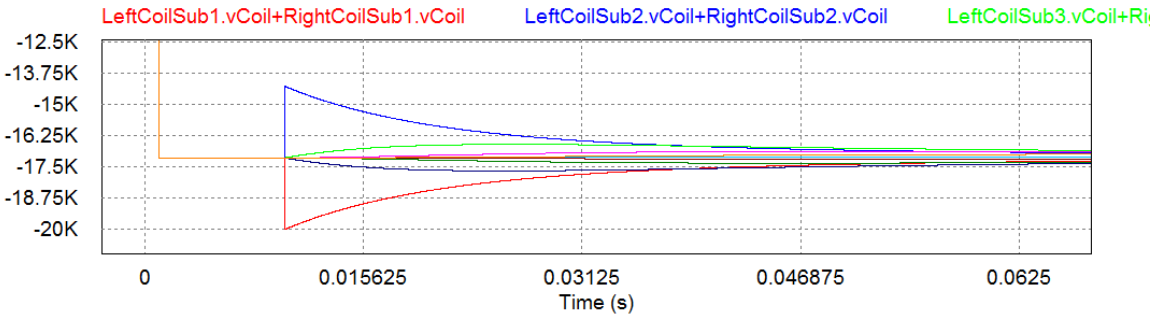

Figure 112 - 9 sectors TOPOLOGY "A" – Op.C. 2 – 2Vd

After the fault the highest value is reached by C1, but in short times all the coils tend to the before-fault Vd.

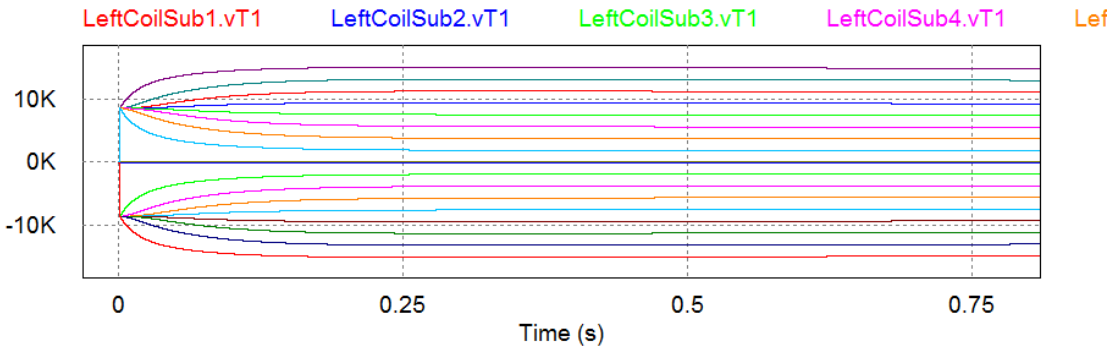

Figure 113 - 9 sectors TOPOLOGY "A" – Op.C. 3 – Vg

After the fault C1:T2 and C2:T1 go to zero, while all the other voltages reach different values for each coil, where the most stressed are C1:T1 and C2:T2.

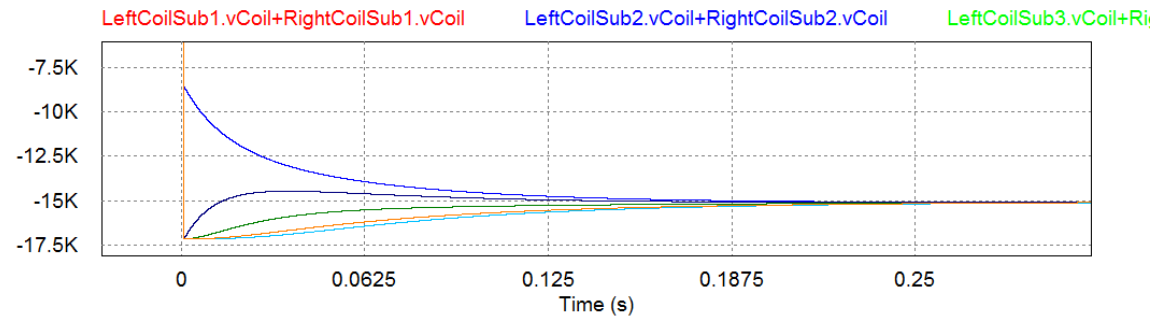

Figure 114 - 9 sectors TOPOLOGY "A" – Op.C. 3 – 2Vd

Each coil is subjected to a different voltage value, but in short times all of them tend to the nominal Vd.

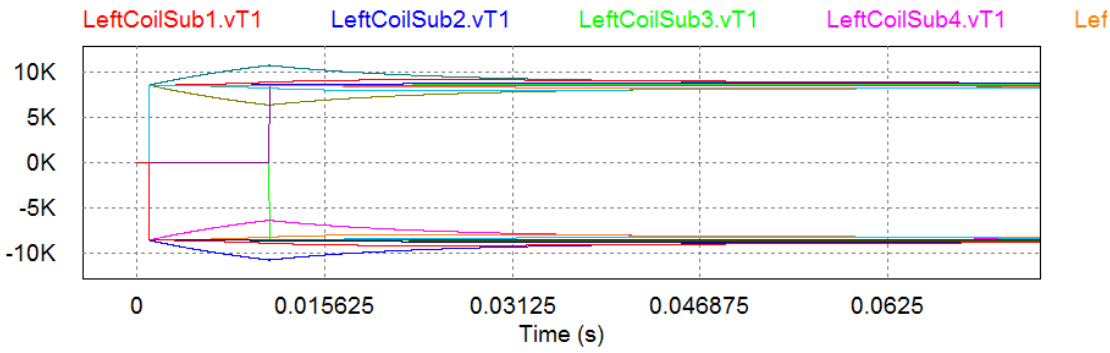

Figure 115 - 9 sectors TOPOLOGY "A" – Op.C. 4 – Vg

During the first 11 [ms] the trends are the same of Op.C.3, but when the delayed QPC intervene all the voltage rapidly reach the nominal Vg.

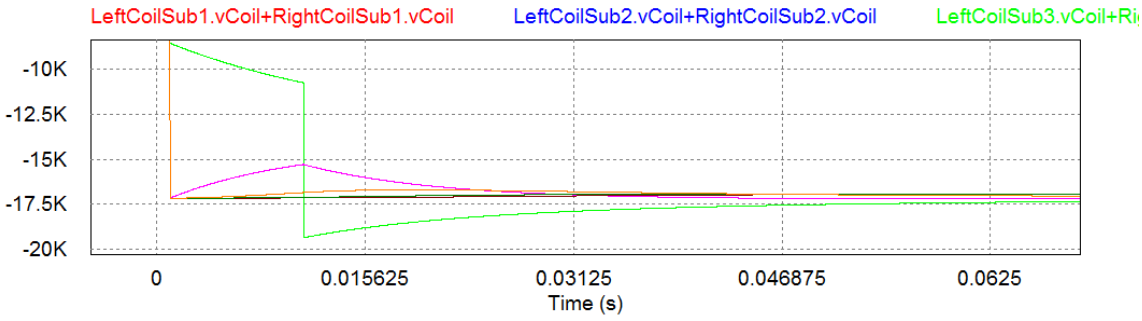

Figure 116 - 9 sectors TOPOLOGY "A" – Op.C. 4 – 2Vd

Same as said for Vg; notice that after the delayed QPC intervention C2 and C3 reach the highest Vd value.

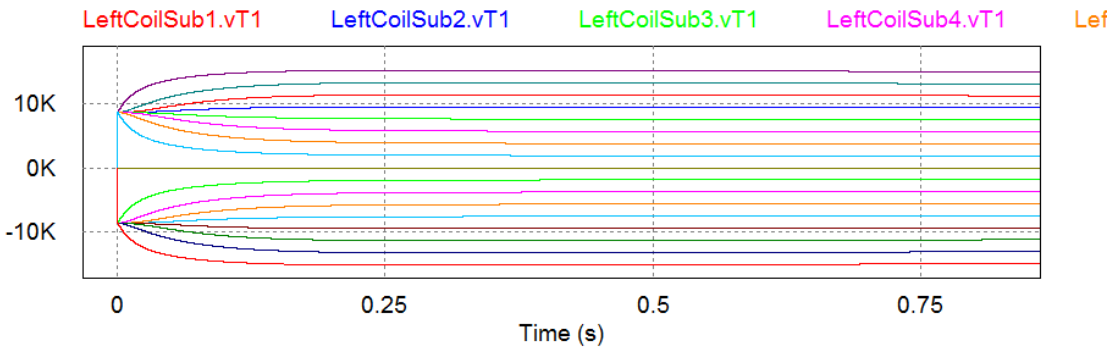

Figure 117 - 9 sectors TOPOLOGY "A" – Op.C. 5 – Vg

The trends for Op.C. 5 are pretty similar to Op.C.3.

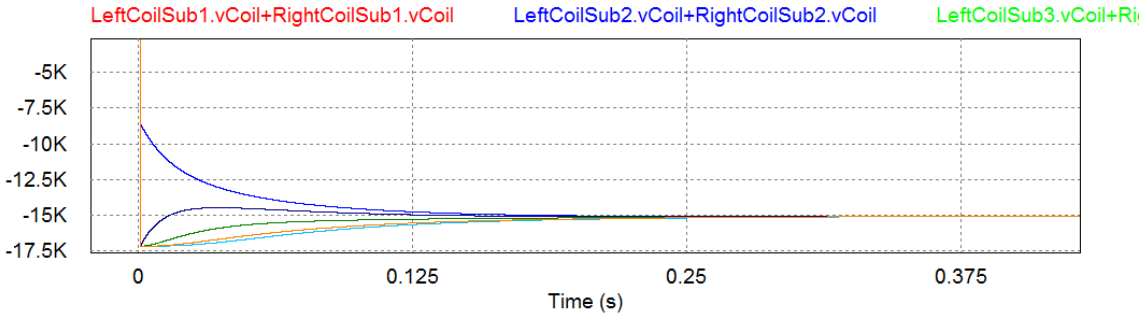

Figure 118 - 9 sectors TOPOLOGY "A" – Op.C. 5 – 2Vd

Same as said for Vg.

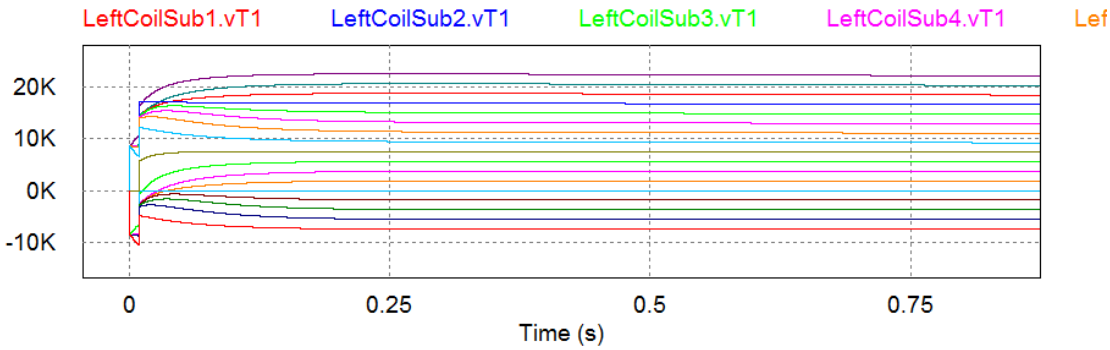

Figure 119 - 9 sectors TOPOLOGY "A" – Op.C. 6 – Vg

Initially the trends are the same as seen for Op.C.3, but after 10 [ms] the effect of the opposite ground fault is evident.

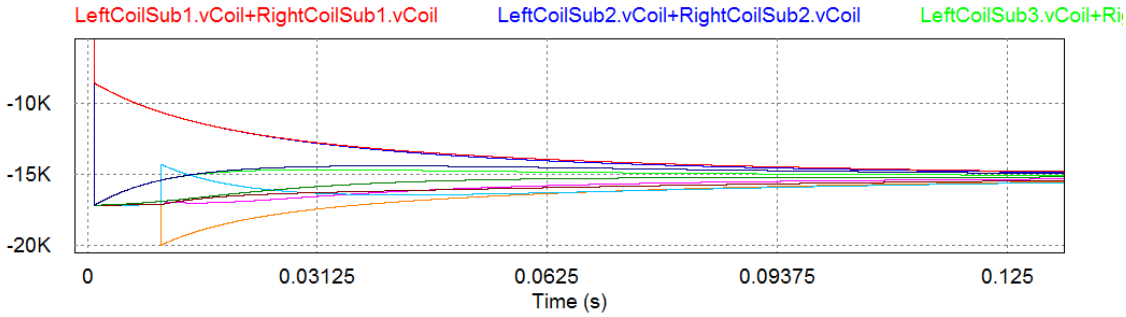

Figure 120 - 9 sectors TOPOLOGY "A" – Op.C. 6 – 2Vd

Same as said for Vg.

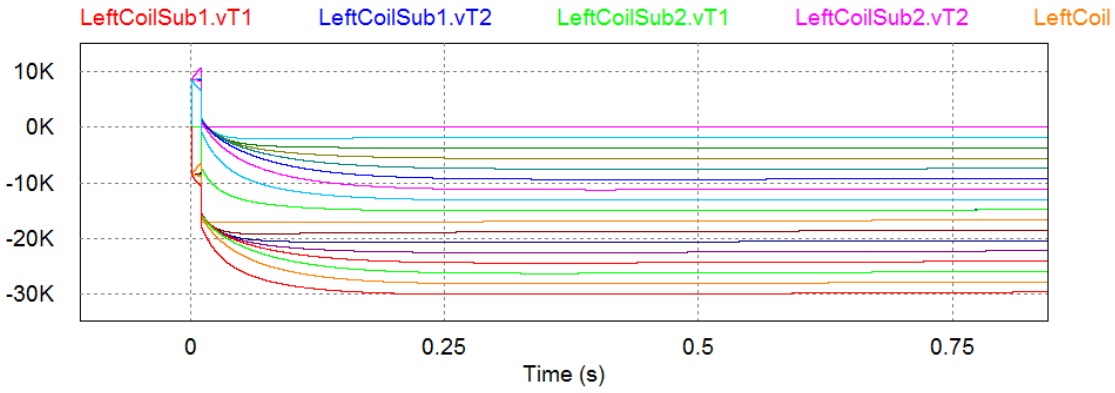

Figure 121 - 9 sectors TOPOLOGY "A" – Op.C. 7 – Vg

In this case there are the same considerations seen for Op.C.6, except for the different and higher voltage values that have been reached; during the first phase C2:T1 stays at zero, but after the ground fault it is C2:T2 which goes to zero.

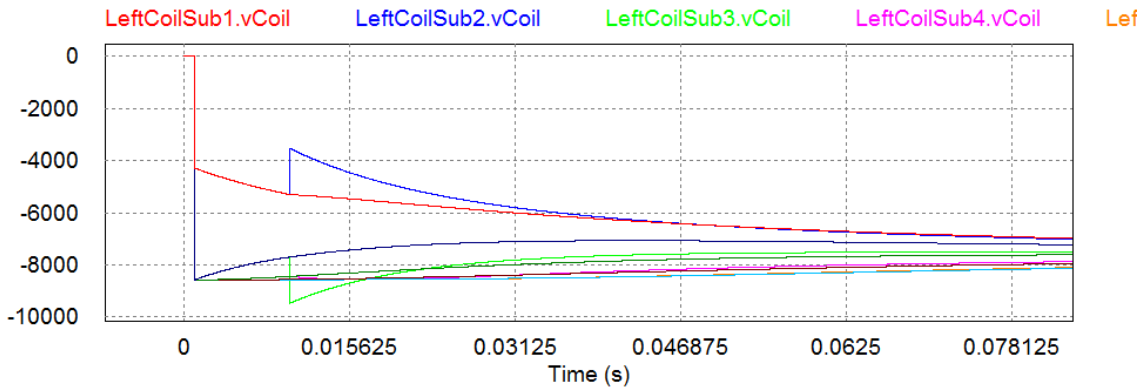

Figure 122 - 9 sectors TOPOLOGY "A" – Op.C. 7 – Vd

C3 reaches the highest Vd.

Op.C.	Vg peak module [kV]	Time (Vg peak) [s]	Location (Vg peak)
1	8.578	0.0010	Each coil
2	17.148	0.0100	C1:T2
3	15.083	0.2882	C1:T1, C2:T2
4	10.772	0.0110	C2:T2, C3:T1
5	15.083	0.2882	C2:T2, C1:T1
6	22.645	0.2526	C2:T2
7	30.137	0.3165	C1:T1

Table 23 - Vg, times to be reached and location for 9 sectors TOPOLOGY "A"

Op.C.	Vd peak module [kV]	Time (Vd peak) [s]	Location (Vd peak)
1	8.578	0.0010	Each coil
2	10.002	0.0100	C1
3	8.578	0.0010	each one except C1 and C2
4	9.673	0.0110	nearest two coils
5	8.576	0.0010	each one except the nearest coil
6	9.988	0.0100	coils nearest to the fault
7	9.468	0.0100	C3

Table 24 - Vd, times to be reached and location for 9 sectors TOPOLOGY "A"

I^2t analysis

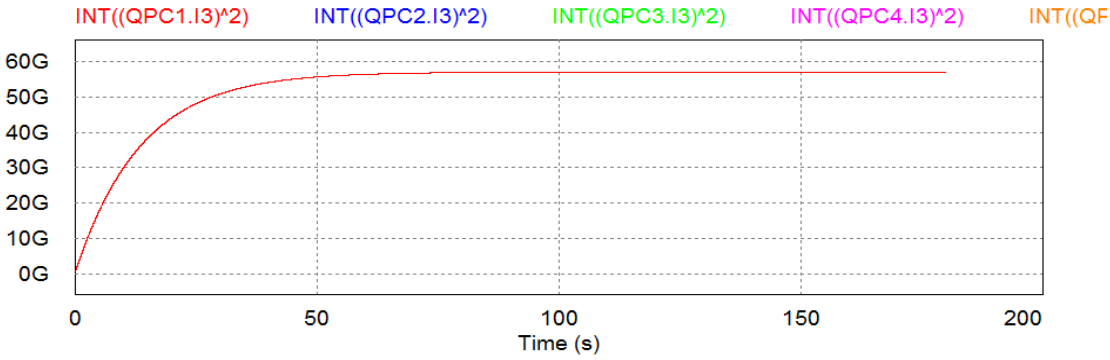

Figure 123 - I2t, TOPOLOGY "A"

Op.C.	Regime value [A^2s]	Tq [s]	Iop [kA]	I^2t [A^2s]
1	$57.11*10^9$	1	65	$61.3*10^9$
2	$57.11*10^9$	1	65	$61.3*10^9$
3	$64.34*10^9$	1	65	$68.6*10^9$
4	$57.11*10^9$	1	65	$61.3*10^9$
5	$64.34*10^9$	1	65	$68.6*10^9$
6	$64.34*10^9$	1	65	$68.6*10^9$
7	$64.34*10^9$	1	65	$68.6*10^9$

Figure 124 - I2t for TOPOLOGY "A"

4.4.6 9 sectors TOPOLOGY “B”

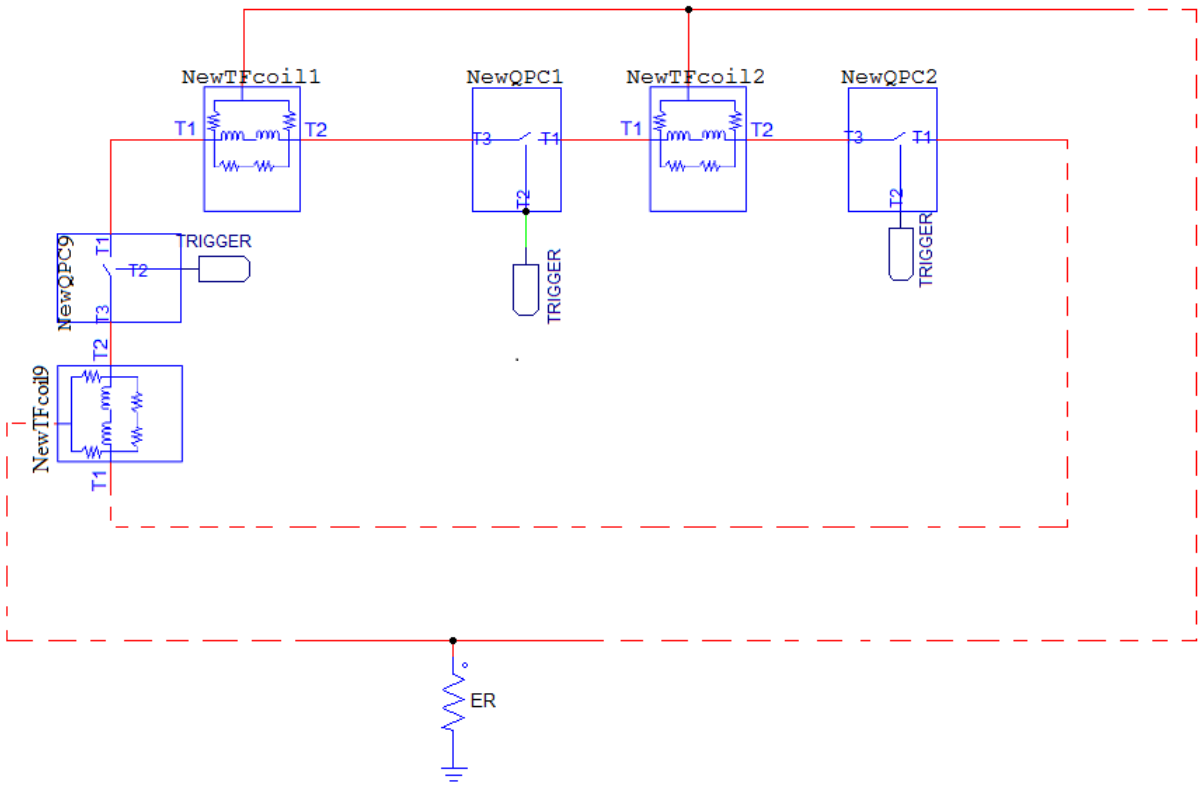

Figure 125 - 9 sectors TOPOLOGY "B"

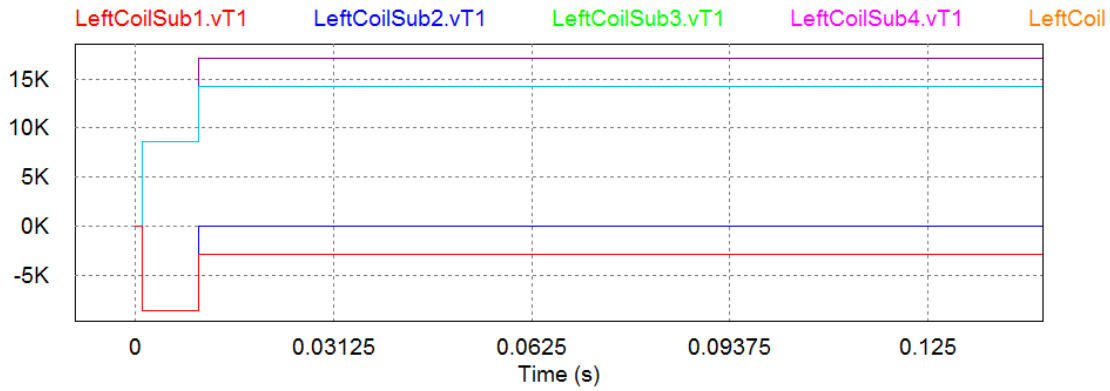

Figure 126 - 9 sectors TOPOLOGY "B" – Op.C. 2 – Vg

The voltage on C2:T1 goes to zero after the ground fault; the maximum value is reached on C2:T2. Except for these two terminals, for all the others half reaches a value which is a bit lower than C2:T2, and the other half reach a value a little higher than zero in module.

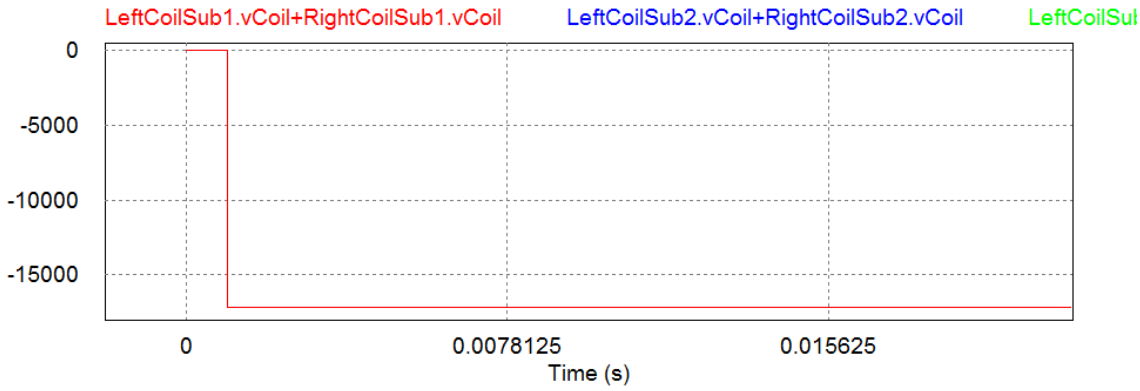

Figure 127 - 9 sectors TOPOLOGY "B" – Op.C. 2 – 2Vd

The Vd trend is always the same in each case of TOPOLOGY "B".

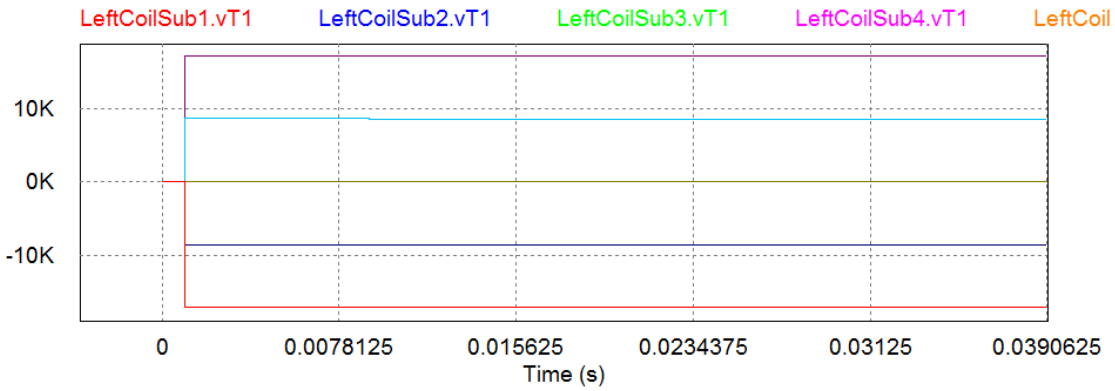

Figure 128 - 9 sectors TOPOLOGY "B" – Op.C. 3 – Vg

C1:T2 and C2:T1 remain at zero after the non-intervention of QPC1. The most stressed are C1:T1 and C2:T2.

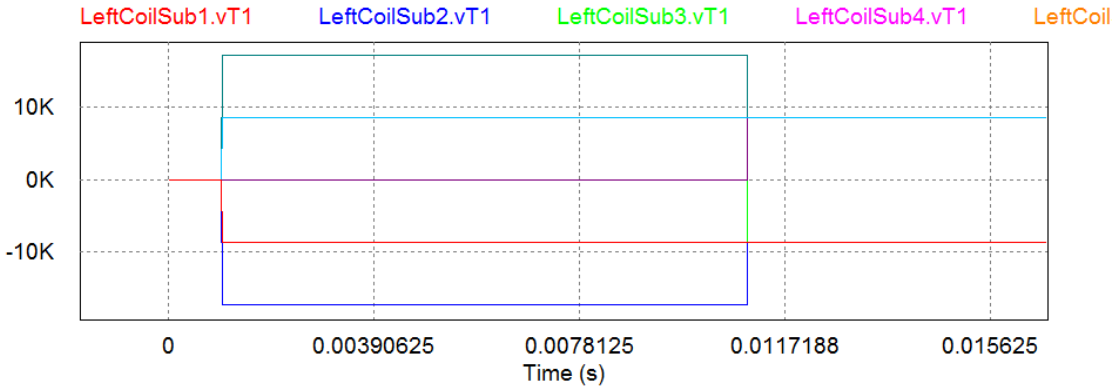

Figure 129 - 9 sectors TOPOLOGY "B" – Op.C. 4 – Vg

During the first 11 [ms] the trends are the same of Op.C.3, but when the delayed QPC intervene all the voltage rapidly reach the nominal Vg.

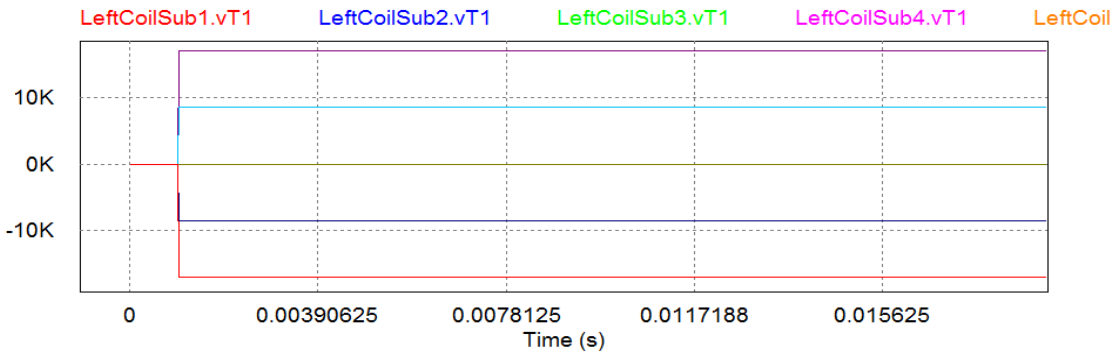

Figure 130 - 9 sectors TOPOLOGY "B" – Op.C. 5 – Vg

Pretty similar to Op.C.3.

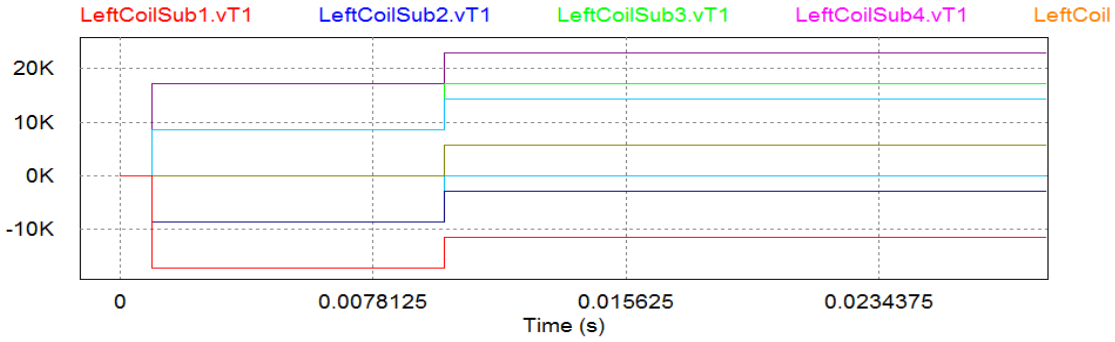

Figure 131 - 9 sectors TOPOLOGY "B" – Op.C. 6 – Vg

Initially the trends are the same as seen for Op.C.3, but after 10 [ms] the effect of the opposite ground fault is evident.

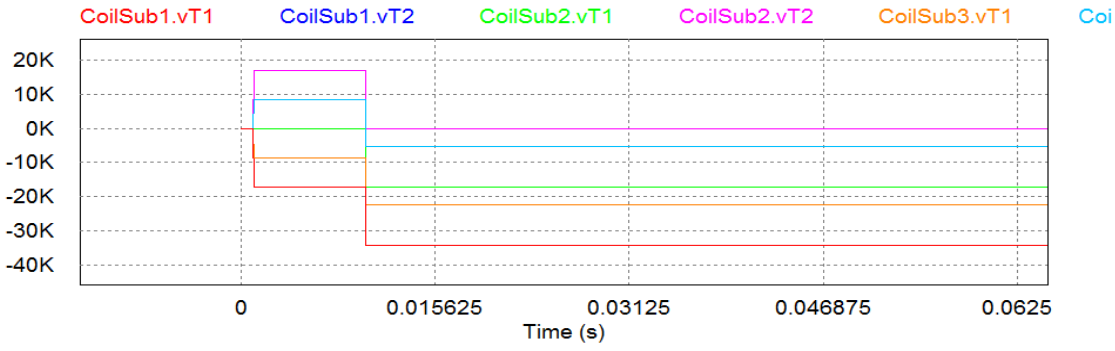

Figure 132 - 9 sectors TOPOLOGY "B" – Op.C. 7 – Vg

The highest value is reached on C1.

Op.C.	Vg peak module [kV]	Time (Vg peak) [s]	Location (Vg peak)
1	8.578	0.0010	Each coil
2	17.148	0.0101	C2:T2
3	17.151	0.0010	C2:T2, C1:T1
4	17.151	0.0010	C3:T2, C2:T1
5	17.151	0.0010	C2:T2, C1:T1
6	22.861	0.0100	C2:T2
7	34.283	0.0010	C1:T1

Table 25 - Vg, times to be reached and location for 9 sectors TOPOLOGY "B"

Op.C.	Vd peak module[kV]	Time (Vd peak) [s]	Location (Vd peak)
1	8.578	0.0010	each coil
2	8.578	0.0010	each coil
3	8.578	0.0010	each coil
4	8.578	0.0010	each coil
5	8.578	0.0010	each coil
6	8.578	0.0010	each coil
6	8.578	0.0010	each coil

Table 26 - Vd, times to be reached and location for 9 sectors TOPOLOGY "B"

I^2t analysis

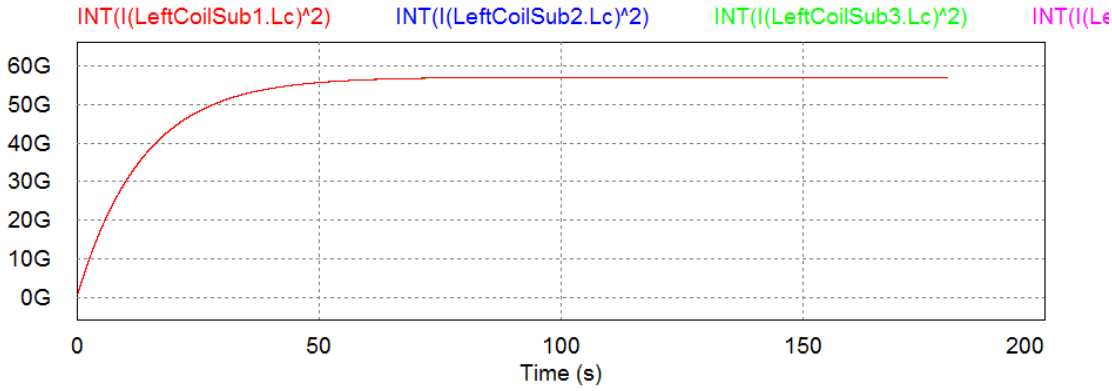

Figure 133 - I2t, TOPOLOGY "B"

Op.C.	Regime value [A^2s]	Tq [s]	Iop [kA]	I^2t [A^2s]
1	$57.11*10^9$	1	65	$61.3*10^9$
2	$57.11*10^9$	1	65	$61.3*10^9$
3	$57.11*10^9$	1	65	$61.3*10^9$
4	$57.11*10^9$	1	65	$61.3*10^9$
5	$57.11*10^9$	1	65	$61.3*10^9$
6	$57.11*10^9$	1	65	$61.3*10^9$
7	$57.11*10^9$	1	65	$61.3*10^9$

Table 27 - I2t for TOPOLOGY "B"

4.4.7 9 sectors TOPOLOGY “C”

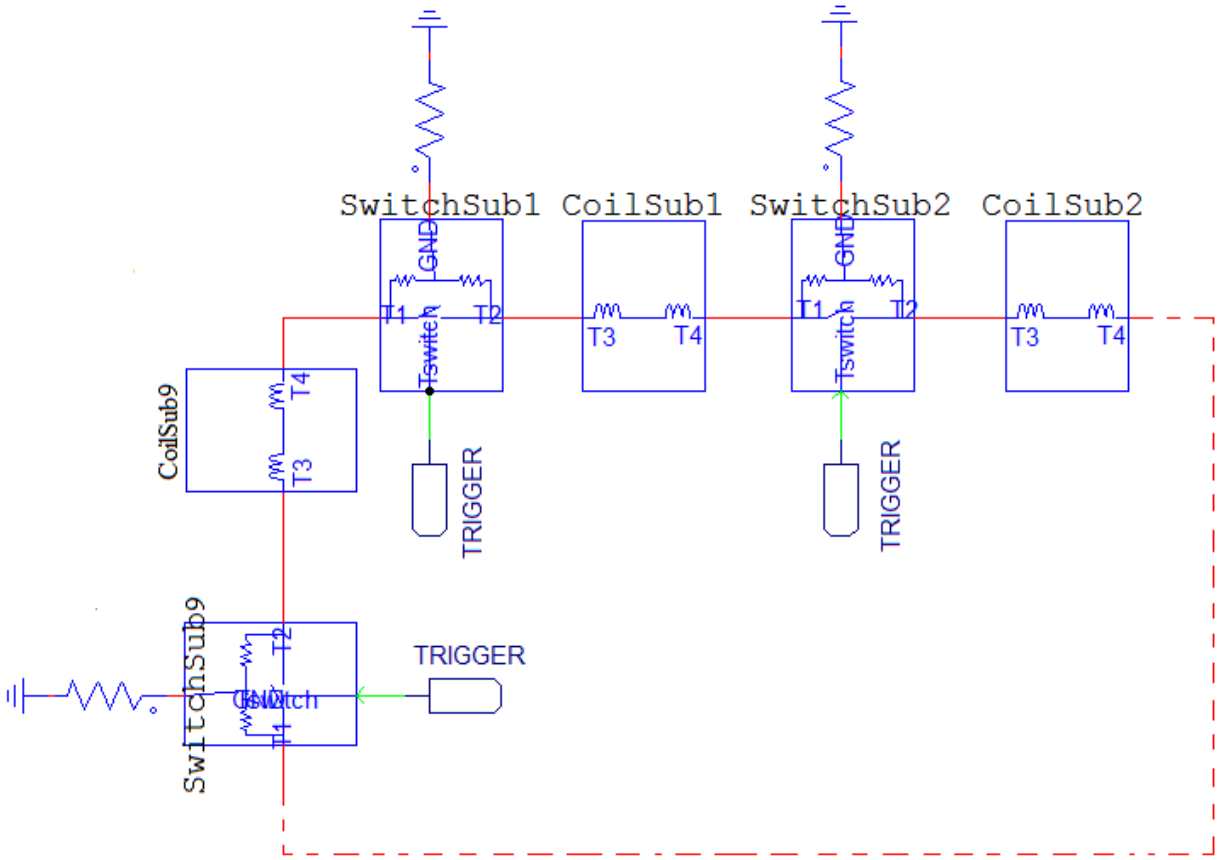

Figure 134 - 9 sectors TOPOLOGY "C"

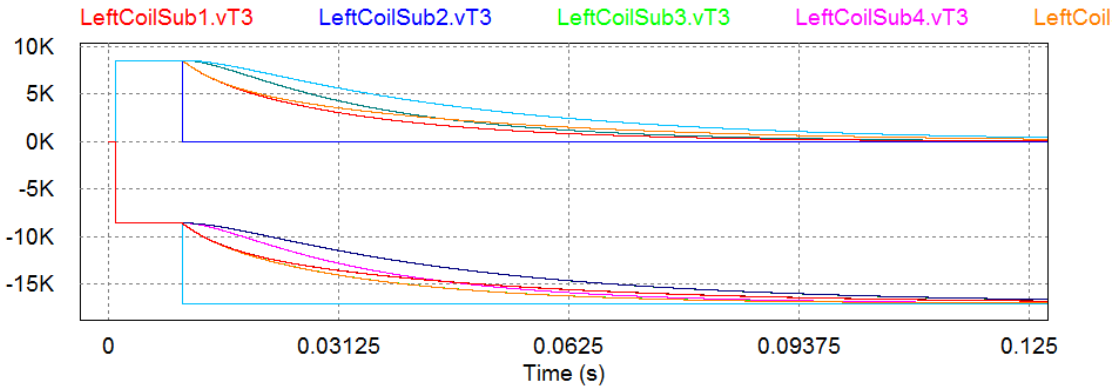

Figure 135 - 9 sectors TOPOLOGY “C” – Op.C. 2 – Vg

C1:T2 goes to zero after the fault, while half of the other terminals goes to zero after the initial peak, and the other half rapidly reach the highest value that have been reached on C2:T1.

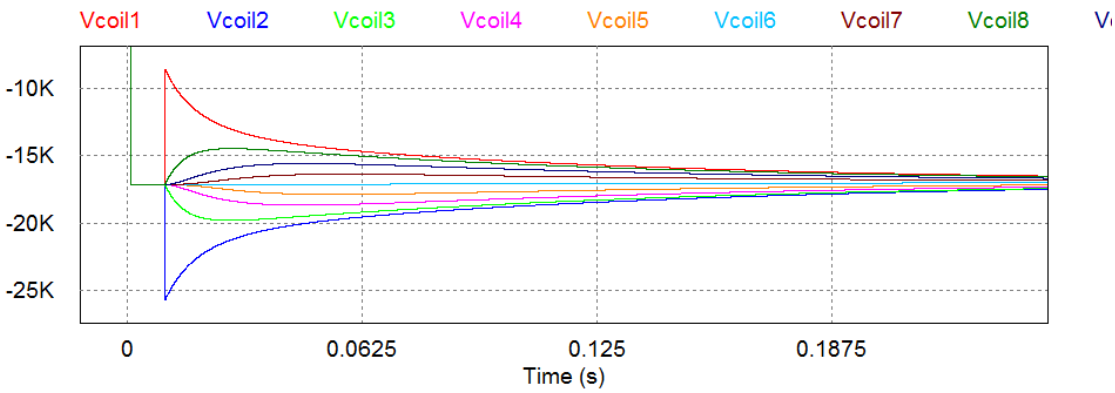

Figure 136 - 9 sectors TOPOLOGY "C" – Op.C. 2 – 2Vd

C2 reaches the highest Vd, but all the coils reach in short times the nominal Vd.

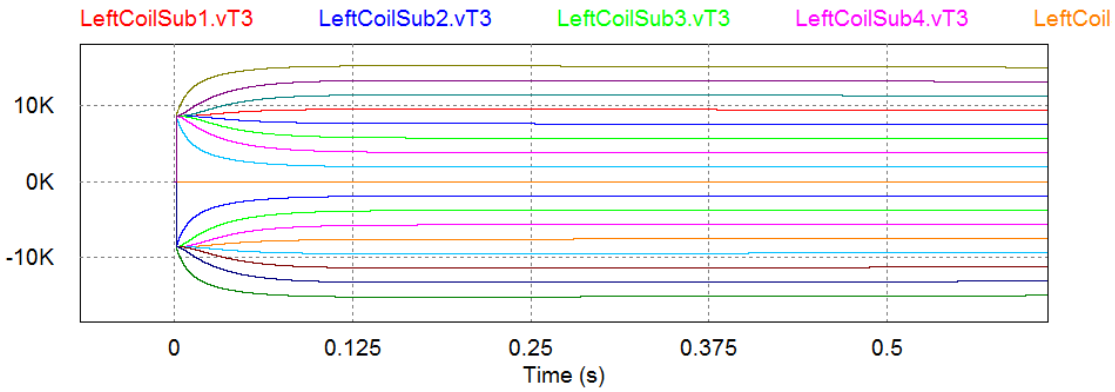

Figure 137 - 9 sectors TOPOLOGY "C" – Op.C. 3 – Vg

C1:T1 and C9:T2 stay at zero, while all the other terminals reach different Vgs.

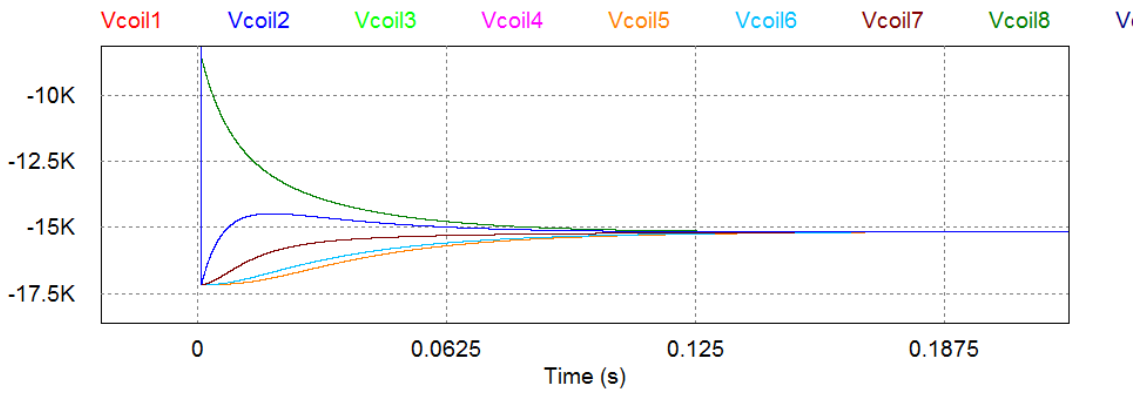

Figure 138 - 9 sectors TOPOLOGY "C" – Op.C. 3 – 2Vd

Each coil reaches a different Vd value, but in short times they reach the nominal Vd.

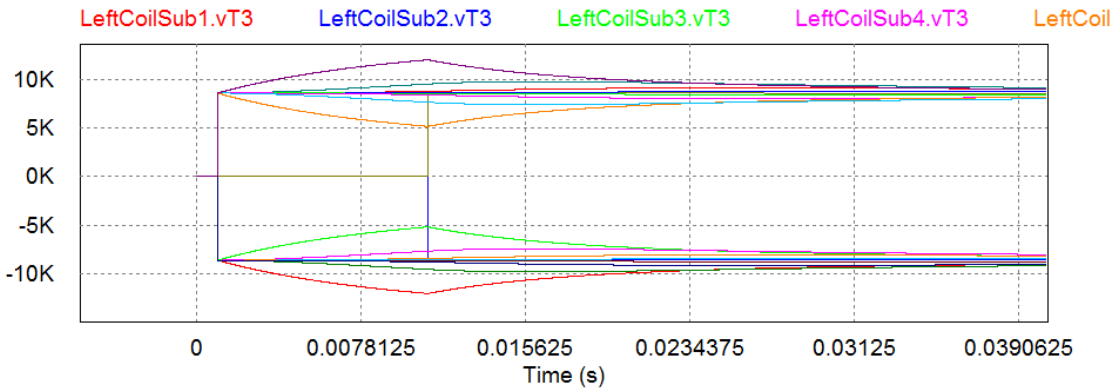

Figure 139 - 9 sectors TOPOLOGY "C" – Op.C. 4 – Vg

During the first 11 [ms] the trends are the same of Op.C.3, but when the delayed QPC intervene all the voltage rapidly reach the nominal Vg.

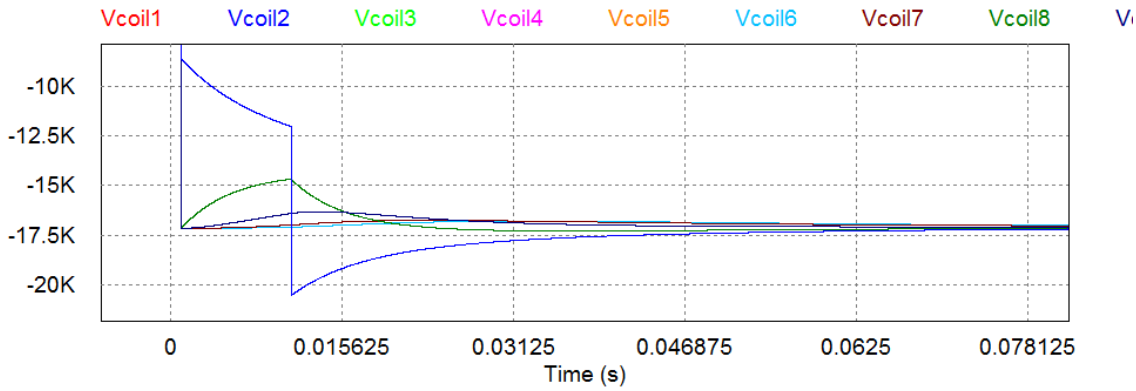

Figure 140 - 9 sectors TOPOLOGY "C" – Op.C. 4 – 2Vd

After the delayed intervention C1 reach the highest value.

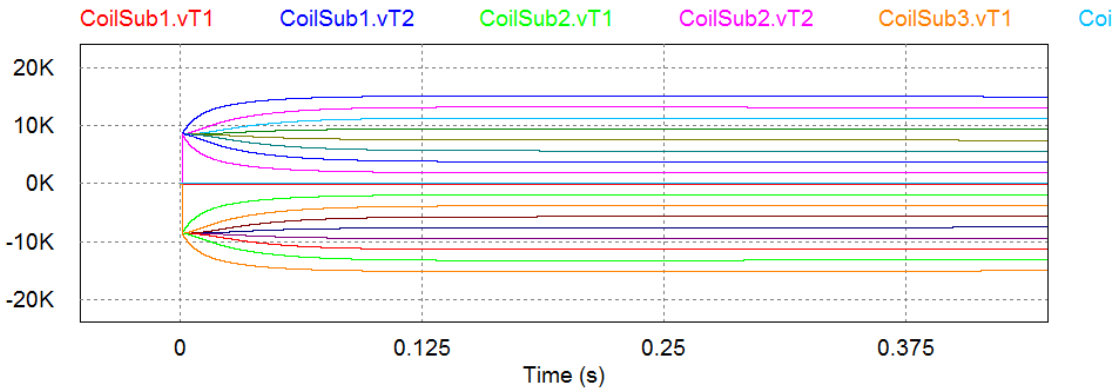

Figure 141 - 9 sectors TOPOLOGY "C" – Op.C. 5 – Vg

C1:T1 and C9:T2 remain at zero, while all the other terminals reach different values.

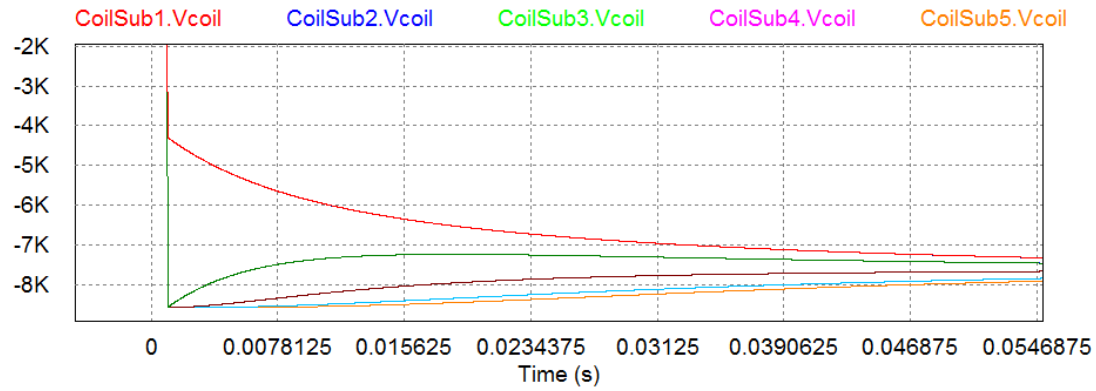

Figure 142 - 9 sectors TOPOLOGY "C" – Op.C. 5 – Vd

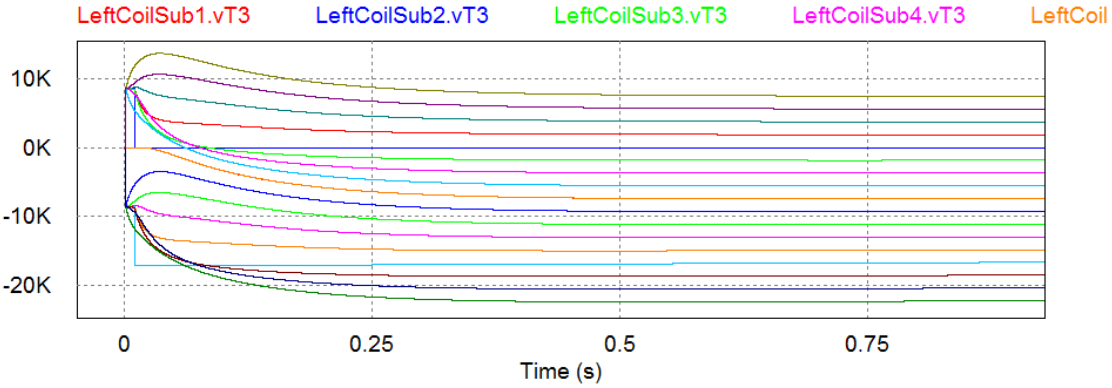

Figure 143 - 9 sectors TOPOLOGY "C" – Op.C. 6 – Vg

After the ground fault C1:T1, C9:T2 and C5:T2 (which is near to the ground fault) go to zero, while all the others reach different values.

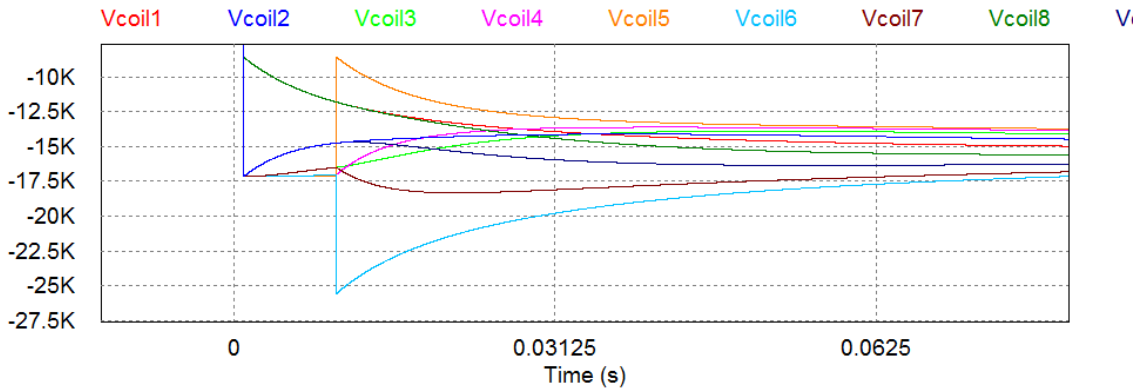

Figure 144 - 9 sectors TOPOLOGY "C" – Op.C. 6 – 2Vd

After the ground fault C1:T1, C9:T2 and C5:T2 (which is near to the ground fault) go to zero, while all the others reach different values.

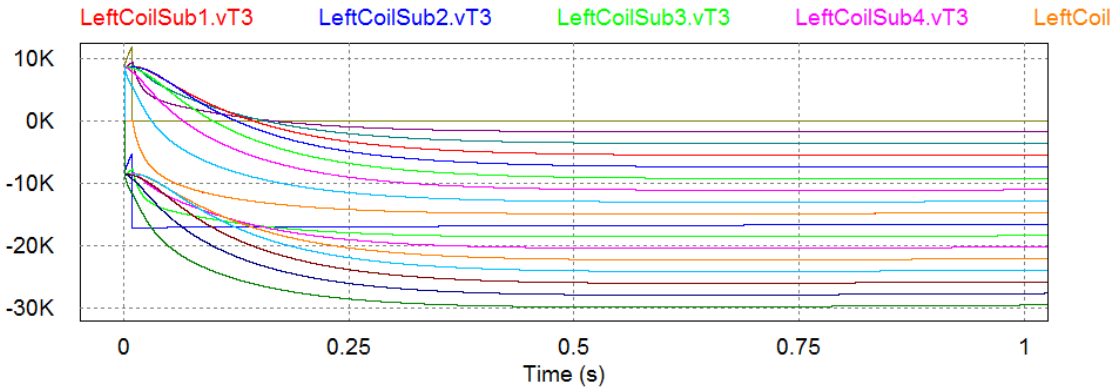

Figure 145 - 9 sectors TOPOLOGY "C" – Op.C. 7 – Vg

The considerations are similar to Op.C. 6, with different values; after the fault C1:T2 goes to zero.

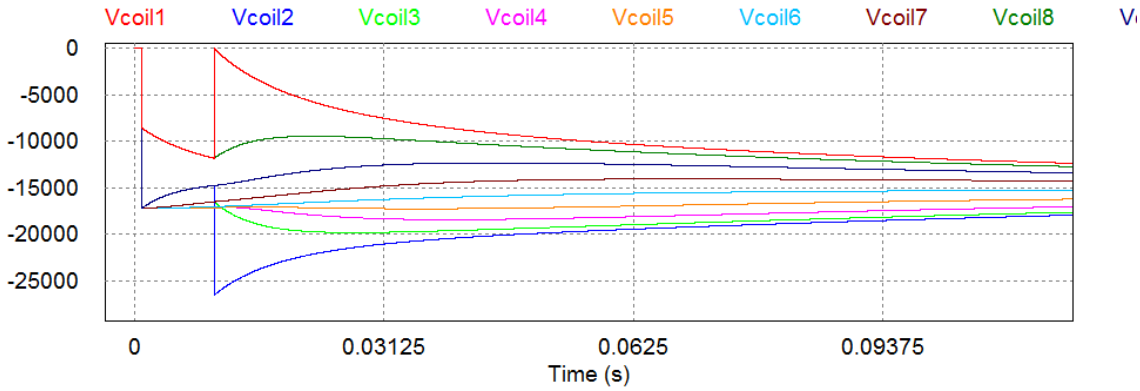

Figure 146 - 9 sectors TOPOLOGY "C" – Op.C. 7 – 2Vd

C2 reaches the highest value.

Op.C.	Vg peak module [kV]	Time (Vg peak) [s]	Location (Vg peak)
1	8.580	0.00101	Each coil
2	17.152	0.01001	C2:T1
3	15.157	0.1827	C1:T2
4	11.997	0.011	C2:T2
5	15.160	0.1657	C1:T2, C9:T1
6	22.382	0.5404	C9:T1
7	29.844	0.4976	C9:T1

Table 28 - Vg, times to be reached and location for 9 sectors TOPOLOGY "C"

Op.C.	Vd peak module[kV]	Time (Vd peak) [s]	Location (Vd peak)
1	8.560	0.00101	each coil
2	12.861	0.01001	C2
3	8.580	0.00101	Each one except C1 and C9
4	10.285	0.01101	C1
5	8.580	0.00101	Each one except C1 and C9
6	12.786	0.01001	C6
7	13.268	0.01001	C2

Table 29 - Vd, times to be reached and location for 9 sectors TOPOLOGY "C"

I^2t analysis

Considering the JT-60SA earthing topology, the results are pretty the same respect to the ITER configuration, with a minimal variation of the values; in fact the earthing system does not influence the I^2t.

4.4.8 9 sectors TOPOLOGY “D”

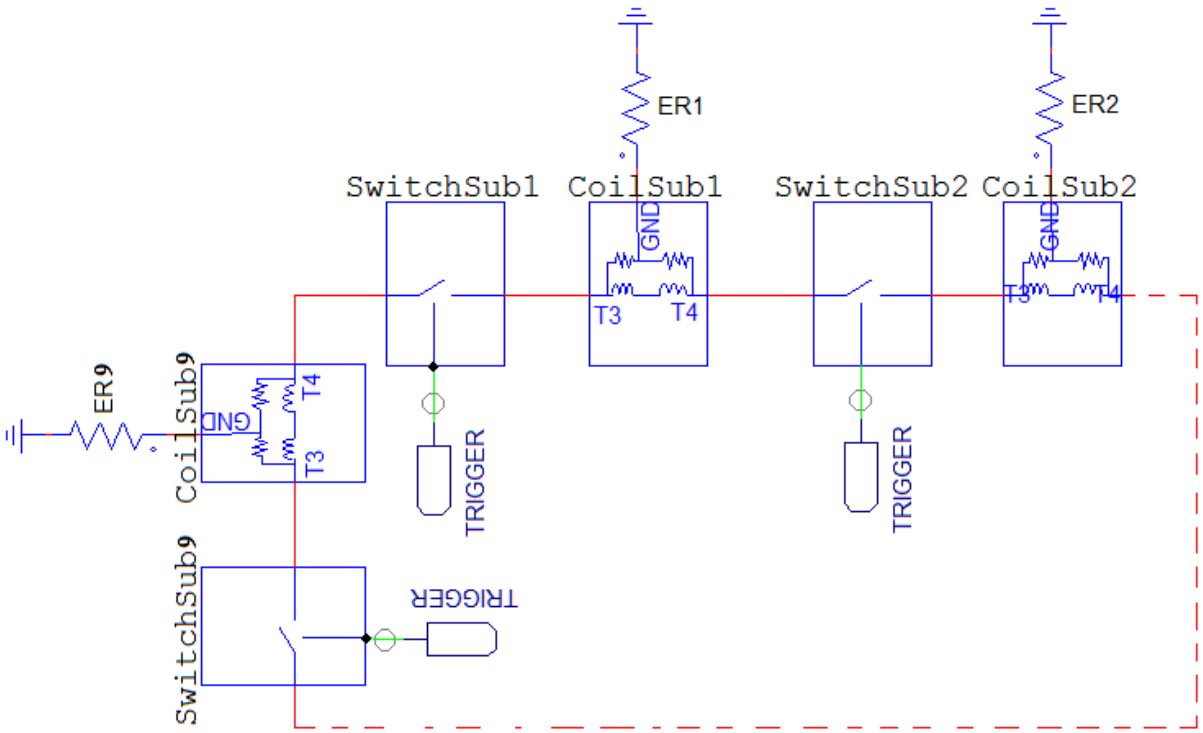

Figure 147 - 9 sectors TOPOLOGY "D"

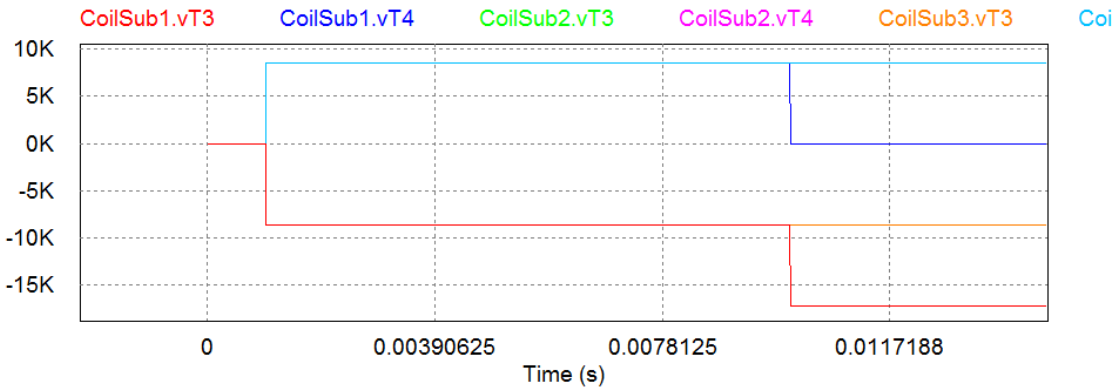

Figure 148 - 9 sectors TOPOLOGY “D” – Op.C. 2 – Vg

C1:T2 goes to zero after the fault, C1:T1 reaches the highest value, while all the others reach the nominal Vg.

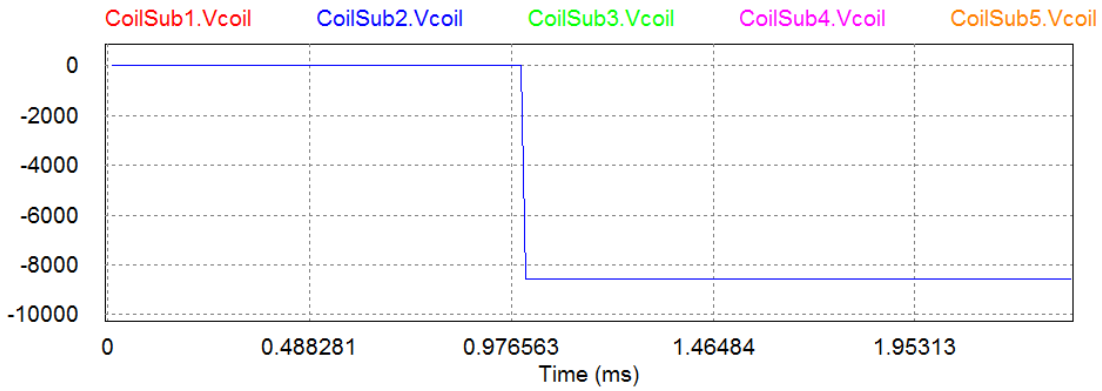

Figure 149 - 9 sectors TOPOLOGY "D" – Op.C. 2 – Vd

The Vd trends for TOPOLOGY "D" are always the same.

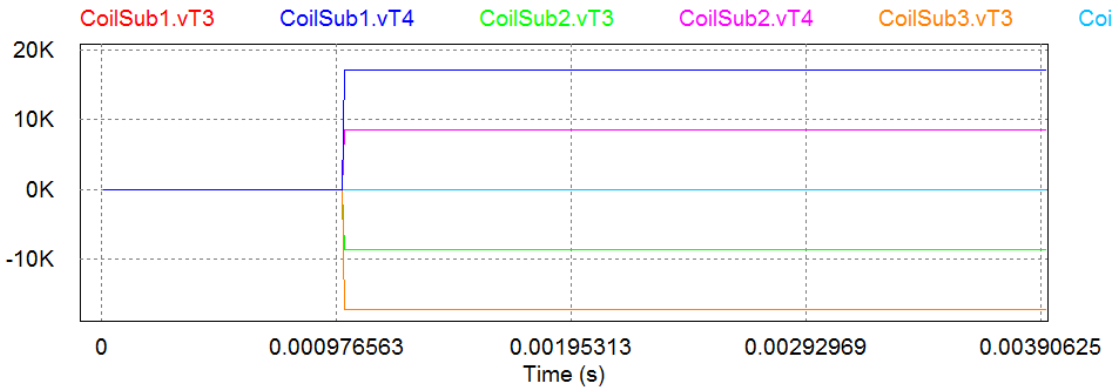

Figure 150 - 9 sectors TOPOLOGY "D" – Op.C. 3 – Vg

Except for C1:T2 and C9:T1, all the other terminals go to their nominal Vg.

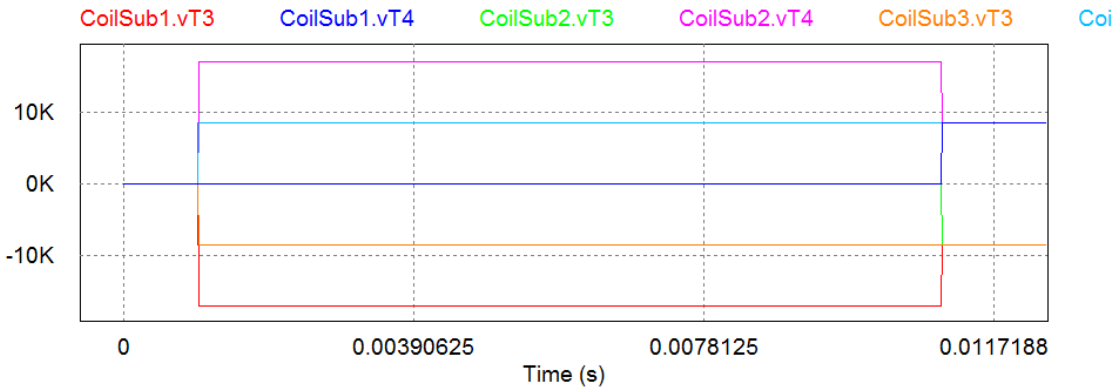

Figure 151 - 9 sectors TOPOLOGY "D" – Op.C. 4 – Vg

During the first 11 [ms] the trends are the same as seen for Op.C.3, and next each terminal reach the nominal Vg.

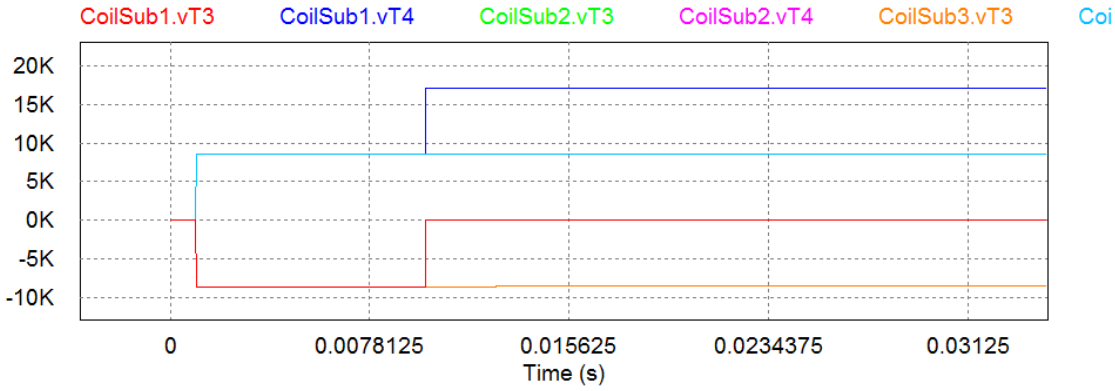

Figure 152 - 9 sectors TOPOLOGY "D" – Op.C. 5 – Vg

The trends are similar to Op.C. 3.

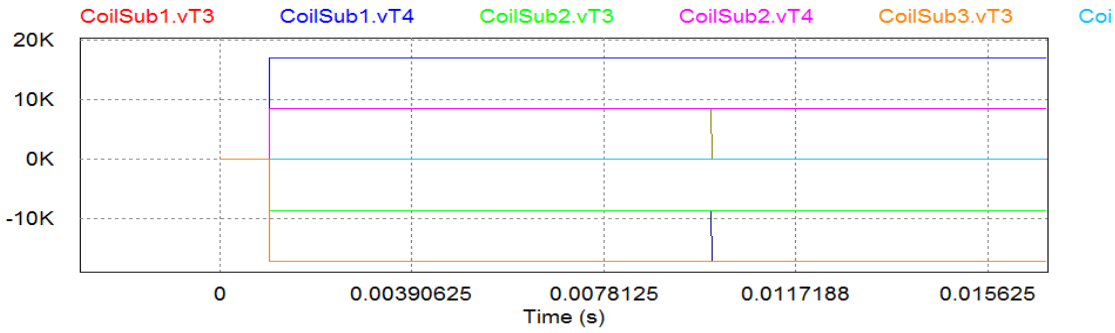

Figure 153 - 9 sectors TOPOLOGY "D" – Op.C. 6 – Vg

C1:T1 remains at zero, while after the ground fault all the other terminals reach the nominal Vg, except for C1:T2 and C9:T1.

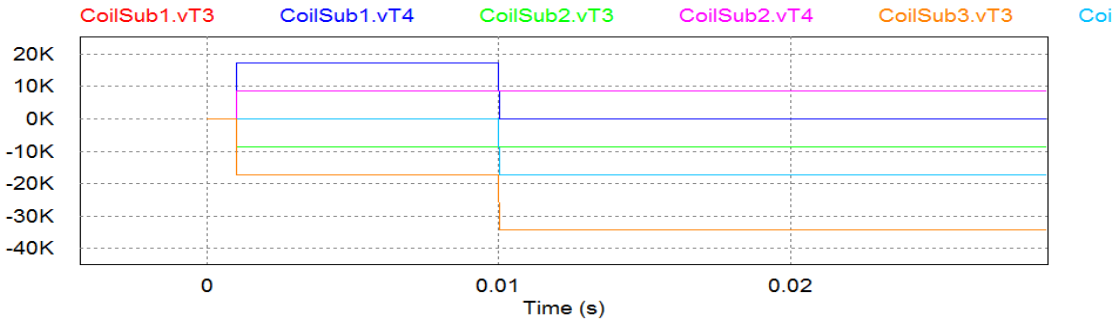

Figure 154 - 9 sectors TOPOLOGY "D" – Op.C. 7 – Vg

After the fault each terminal reach the nominal Vg, except for C1:T2 which goes to zero and C9:T1 which reaches the highest value.

Op.C.	Vg peak module [kV]	Time (Vg peak) [s]	Location (Vg peak)
1	8.580	0.00101	each one
2	17.152	0.01001	C1:T1
3	17.158	0.00101	C1:T2, C9:T1
4	17.158	0.00101	C1:T1, C2:T2
5	17.152	0.00101	C1:T2
6	17.158	0.00101	C1:T2, C9:T1
7	34.286	0.01001	C9:T1

Table 30 - Vg, times to be reached and location for 9 sectors TOPOLOGY "D"

Op.C.	Vd peak module[kV]	Time (Vd peak) [s]	Location (Vd peak)
1	8.580	0.00101	each one
2	8.580	0.00101	each one
3	8.580	0.00101	each one
4	8.580	0.00101	each one
6	8.580	0.00101	each one
7	8.580	0.00101	each one

Table 31 - Vd, times to be reached and location for 9 sectors TOPOLOGY "D"

I^2t analysis

Considering the JT-60SA earthing topology, the results are pretty the same respect to the ITER configuration, with a minimal variation of the values; in fact the earthing system does not influence the I^2t.

4.5 Comparison

Having finally on hand all the data, it's possible to globally compare all the topologies considered in the analysis. Table 32 and Table 33 are divided per Dump Resistor topology and Earthing Resistor topology, taking into account all the events previously considered, focusing on the voltage between terminals and ground (Vg), the voltage across the coil (Vd), the I^2t and the probability of the event. We need to specify which are the admissible Op.C.s, in order to choose the best circuit topology to work on. First of all, from the specifics, the maximum Vg value for Op.C.1 is set to 5 [kV], and in the same condition the maximum Vd is set to 10 [kV]; instead for fault conditions the maximum Vg value is 28 [kV].

REFERENCE DATA: PROCESS

				EARTH RESISTOR TOPOLOGY (18 SECTORS, NO SNUBBERS)								
				ITER LIKE			JT60-SA LIKE					
		ID	EVENT	Vg max [kV]	Vd max [kV]	I^2t [A^2s]	Vg max [kV]	Vd max [kV]	I^2t [A^2s]	Probability	Admissibility (ITER-like)	Admissibility (JT60-SA like)
DUMP RESISTOR TOPOLOGY	PARALLEL TO CB	1	QPC intervention	4.289	8.579	$61.3*10^9$	4.290	8.580	$61.3*10^9$	1	YES	YES
		2	Ground fault	8.575	10.003	$61.3*10^9$	8.577	12.859	$61.3*10^9$	0.5	YES	YES
		3	One QPC does not work	7.963	8.579	$64.8*10^9$	8.022	8.580	$64.8*10^9$	(*)	NO Fault i^2t > nominal i^2t	NO Fault i^2t > nominal i^2t
		4	One 10ms delayed QPC	5.997	10.280	$61.3*10^9$	6.633	10.917	$61.3*10^9$	(*)	YES	YES
		5	One QPC does not work + near ground fault	7.963	8.579	$64.8*10^9$	8.022	8.580	$64.8*10^9$	$10^{-3}*10^{-2}*0.5*0.1=5*10^{-7}$ (*)	NO Fault i^2t > nominal i^2t	NO Fault i^2t > nominal i^2t
		6	One QPC does not work + opposite ground fault	12.200	10.003	$64.8*10^9$	11.452	12.859	$64.8*10^9$	$10^{-3}*10^{-2}*0.5*0.9=4.5*10^{-6}$ (*)	NO Fault i^2t > nominal i^2t	NO Fault i^2t > nominal i^2t
		7	QPC intervention + QPC 1 does not work + ground fault after subsequent coil	15.917	9.294	$64.8*10^9$	15.668	13.774	$64.8*10^9$	$10^{-3}*10^{-2}*0.5*0.1=5*10^{-7}$ (*)	NO Fault i^2t > nominal i^2t	NO Fault i^2t > nominal i^2t
	PARALLEL TO COIL	1	QPC intervention	4.289	8.579	$57.1*10^9$	4.300	8.580	$57.1*10^9$	1	YES	YES
		2	Ground fault	8.576	8.579	$57.1*10^9$	8.500	8.580	$57.1*10^9$	0.5	YES	YES
		3	One QPC does not work	8.578	8.579	$57.1*10^9$	8.579	8.580	$57.1*10^9$	(*)	YES	YES
		4	One 10ms delayed QPC	8.578	8.579	$57.1*10^9$	8.579	8.580	$57.1*10^9$	(*)	YES	YES
		5	One QPC does not work + near ground fault	8.578	8.579	$57.1*10^9$	8.580	8.580	$57.1*10^9$	$10^{-3}*10^{-2}*0.5*0.1=5*10^{-7}$ (*)	YES	YES
		6	One QPC does not work + opposite ground fault	11.433	8.579	$57.1*10^9$	8.579	8.580	$57.1*10^9$	$10^{-3}*10^{-2}*0.5*0.9=4.5*10^{-6}$ (*)	YES	YES
		7	QPC intervention + QPC 1 does not work + ground fault after subsequent coil	17.141	8.579	$57.1*10^9$	17.149	8.580	$57.1*10^9$	$10^{-3}*10^{-2}*0.5*0.1=5*10^{-7}$ (*)	YES	YES

REFERENCE DATA: PROCESS

				EARTH RESISTOR TOPOLOGY (9 SECTORS, NO SNUBBERS)								
				ITER LIKE			JT60-SA LIKE					
		ID	EVENT	Vg max [kV]	Vd max [kV]	I^2t [A^2s]	Vg max [kV]	Vd max [kV]	I^2t [A^2s]	Probability	Admissibility (ITER-like)	Admissibility (JT60-SA like)
DUMP RESISTOR TOPOLOGY	PARALLEL TO CB	1	QPC intervention	8.578	8.578	$61.3*10^9$	8.580	8.560	$61.3*10^9$	1	YES	YES
		2	Ground fault	17.148	10.002	$61.3*10^9$	17.152	12.861	$61.3*10^9$	0.5	YES	NO
		3	One QPC does not work	15.083	8.578	$68.6*10^9$	15.157	8.580	$68.6*10^9$	(*)	NO Fault i^2t > nominal i^2t	NO Fault i^2t > nominal i^2t
		4	One 10ms delayed QPC	10.772	9.673	$61.3*10^9$	11.997	10.285	$61.3*10^9$	(*)	YES	NO
		5	One QPC does not work + near ground fault	15.083	8.576	$68.6*10^9$	15.160	8.580	$68.6*10^9$	$10^{-3}*10^{-2}*0.5*0.1=5*10^{-7}$ (*)	NO Fault i^2t > nominal i^2t	NO Fault i^2t > nominal i^2t
		6	One QPC does not work + opposite ground fault	22.645	9.988	$68.6*10^9$	22.382	12.786	$68.6*10^9$	$10^{-3}*10^{-2}*0.5*0.9=4.5*10^{-6}$ (*)	NO Fault i^2t > nominal i^2t	NO Fault i^2t > nominal i^2t
		7	QPC intervention + QPC 1 does not work + ground fault after subsequent coil	30.137	9.468	$68.6*10^9$	29.844	13.268	$68.6*10^9$	$10^{-3}*10^{-2}*0.5*0.1=5*10^{-7}$ (*)	NO Fault i^2t > nominal i^2t Vg > Vg max	NO Fault i^2t > nominal i^2t Vg > Vg max
	PARALLEL TO COIL	1	QPC intervention	8.578	8.578	$57.1*10^9$	8.580	8.580	$57.1*10^9$	1	YES	YES
		2	Ground fault	17.148	8.578	$57.1*10^9$	17.152	8.580	$57.1*10^9$	0.5	YES	YES
		3	One QPC does not work	17.151	8.578	$57.1*10^9$	17.158	8.580	$57.1*10^9$	(*)	YES	YES
		4	One 10ms delayed QPC	17.151	8.578	$57.1*10^9$	17.158	8.580	$57.1*10^9$	(*)	YES	YES
		5	One QPC does not work + near ground fault	17.151	8.578	$57.1*10^9$	17.152	8.580	$57.1*10^9$	$10^{-3}*10^{-2}*0.5*0.1=5*10^{-7}$ (*)	YES	YES
		6	One QPC does not work + opposite ground fault	22.861	8.578	$57.1*10^9$	17.158	8.580	$57.1*10^9$	$10^{-3}*10^{-2}*0.5*0.9=4.5*10^{-6}$ (*)	YES	YES
		7	QPC intervention + QPC 1 does not work + ground fault after subsequent coil	34.283	8.578	$57.1*10^9$	34.286	8.580	$57.1*10^9$	$10^{-3}*10^{-2}*0.5*0.1=5*10^{-7}$ (*)	NO Vg > Vg max	NO Vg > Vg max

Table 33 - 9 sectors comparison

Op. C.	Highest Vg	Highest Vd	Lowest Vg	Lowest Vd
1	Same values	Same values	Same values	Same values
2	Same values	C	Same values	B,D
3	B,D	Same values	A,C	Same values
4	B,C,D	A,C	A	B,D
5	B,C,D	Same values	A	Same values
6	A,B,C	A,C	D	B,D
7	B,D	C	A,C	B,D

Table 34 - Highest Vg and Vd of the four topologies in the different operative conditions, 18 sectors

Topology	Highest values records	Lowest values records
A	3	4
B	5	4
C	8	1
D	4	5

Table 35 – Voltage records, 18 sectors

Op. C.	Highest Vg	Highest Vd	Lowest Vg	Lowest Vd
1	Same values	Same values	Same values	Same values
2	Same values	A,C	Same values	B,D
3	B,D	Same values	A,C	Same values
4	B,C,D	A,C	A	B,D
5	B,D	Same values	A,C	Same values
6	A,B,C	A,C	D	B,D
7	A,B,D	A,C	C	B,D

Table 36 - Highest Vg and Vd of the four topologies in the different operative conditions, 9 sectors

Topology	Highest values records	Lowest values records
A	6	3
B	5	4
C	6	3
D	4	5

Table 37 – Voltage records, 9 sectors

Topology	Highest	Lowest
A	10	7
B	10	8
C	14	4
D	8	10

Table 38 – Voltage records summary

Considering that the most probable fault is the Operative Condition 2, the B and D configurations obtained the lowest voltage peak values, so they are the best solutions, also because in each operative condition the i^2t is satisfied, differently from topologies A and C. The worst results have been obtained from the C configuration.
By the way the actual purpose for DEMO seems to be the 18 sectors configuration, and with this choice the best topologies seem to be B and D.

For these reasons for the next analysis there will be considered the 18 sectors B and the 18 sectors C topologies as the best and worst ones.

Probability (*)

We refer all the probabilities to the QPC intervention probability value, set to 1; it's possible to evaluate the ground fault probability to 0.5, because it's the most likely Op.C., due to operational and human errors, while all the other faults don't include human errors.

Now for Op.C. 3 and 4 we need to consider some aspects:

- We can adopt a bypass switch together with the circuit breaker, so we can suppose a probability of 10^{-3} for the circuit breaker due to a statistical data collection on RFX, and in the same way 10^{-2} from ITER analysis on the pyrobreaker; in the end the resulting probability for Op.C. 3 is $10^{-3}*10^{-2} = 10^{-5}$, and for event 4 is 10^{-2}

- Alternately we only use the CB without the BS, so the resulting probability is 10^{-3}, while Op.C. 4 does not make sense, because there is no pyrobreaker; eventually we can suppose a delay due to a glitter, but it usually occurs in less than 10ms, so all the values of voltages and i^2t are surely lower.

For Op.C. 5 we put $10^{-3}*10^{-2}$ for the not-working-QPC as said before, or eventually just 10^{-3} with no BS, 0.5 due to the ground fault probability and 0.1 to take into account of the nearest event, which is less likely than in any other random place, and it's also the less dangerous fault, as we can see from the data.
Instead for Op.C. 6 we put $10^{-3}*10^{-2}*0.5$ like before, but we also add a 0.9 factor which is bigger than 0.1 because the opposite ground fault is the most dangerous overvoltage condition for the circuit. For Op.C. 7 are still valid the considerations that have been done for Op.C. 5.

Admissibility

Some of the simulated Op.C.s are not admissible for the coils, because the i^2t and/or the voltage values are greater than the maximum values. In particular the limit value for i^2t is the nominal value, i.e. the value obtained with the QPC intervention without faults (Op.C.1), while the limit value Vg max is given by the coil insulation design and is fixed to 28 [kV] (see Table 5).
According to these considerations, if the admissible voltage values are not increased or if new strategies are not adopted in order to reduce the initial voltage due to the QPC intervention, the 18 sectors solution is the only possibility because for each 9-sectors topology there is at least one non admissible Op.C. (see Table 33), and the only possible choices are the topologies C and D with 18 sectors, as shown in Table 32; in fact for DEMO the studies are actually focusing on the 18 sectors configuration.

Anyway there is another possible choice, which is the adoption of variable resistors already in use in ITER, JT-60SA and W7X. With positive coefficient resistors it is possible to reach low voltages during the first phase of the QPC intervention according to V = RI; after that phase the R value increases thanks to the increasing of the temperature due to Joule effect, but the current value is lower than in the first phase (Figure 155).

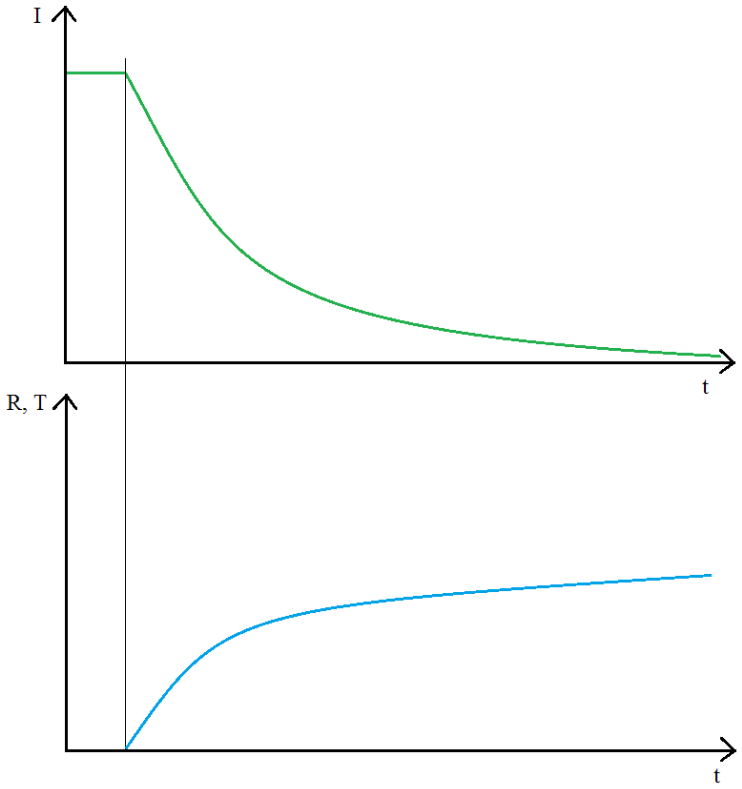

Figure 155 - Discharge process with variable resistors

It has been demonstrated on ITER that using variable resistors the voltage values are 61% with respect to the case with fixed resistors, with an equivalent time constant of 11 [s]. Supposing that the highest voltage peaks are only the 61% of the highest values shown in Table 33, the 9-sectors configuration would now be a considerable choice for DEMO.

4.6 Effect of snubbers

Until now different circuit topologies have been simulated, varying the earth resistor and the dump resistor connections, pointing out in the first steps which are the most stressed solutions from the voltage point of view.

Now it would be interesting to analyse the effect of the insertion of snubbers or clamps in terms of Vg and Vd peaks; in fact the use of snubbers and clamp is very likely. Actually the value of the capacitance (and the eventual resistor) is not known for DEMO, so it will be sized to guarantee that the maximum admitted voltage values at the terminals and inside the coil will not be exceeded.
The purpose is to verify that the obtained results without the snubbers are similar to the values given by the snubber configuration, so that the without-snubbers model is still valid.

As snubber, it was adopted a 2 [mF] capacitance, put parallel to the CB; the analysis will be done on 18 sectors topology B and 18 sectors topology C, because in the first case resulted the lowest voltage peaks, and in the second case the highest.

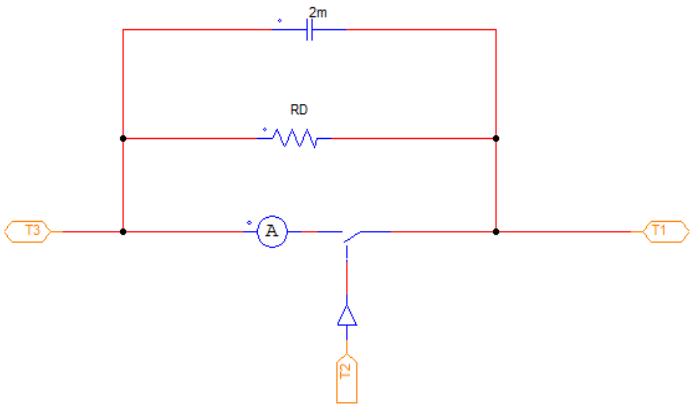

Figure 156 - Circuit breaker subcircuit with snubber (clamp)

4.6.1 18 sectors TOPOLOGY "B"

For this topology there will be studied only the cases in which there are the lowest and the highest voltage peaks, that are Op.C. 1 and 7.

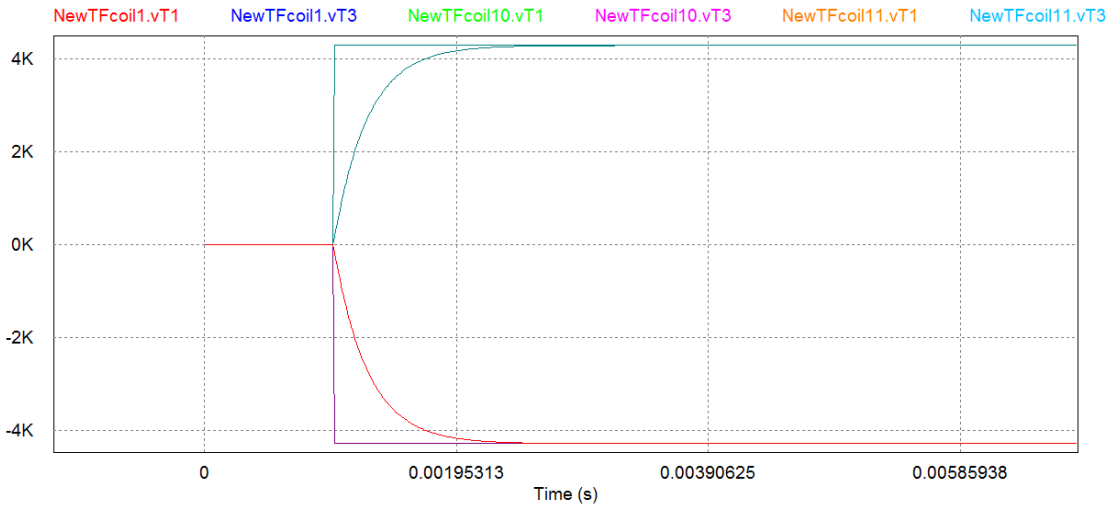

Figure 157 - 18 sectors TOPOLOGY "B" – Op.C. 1 - with and without snubbers Vg

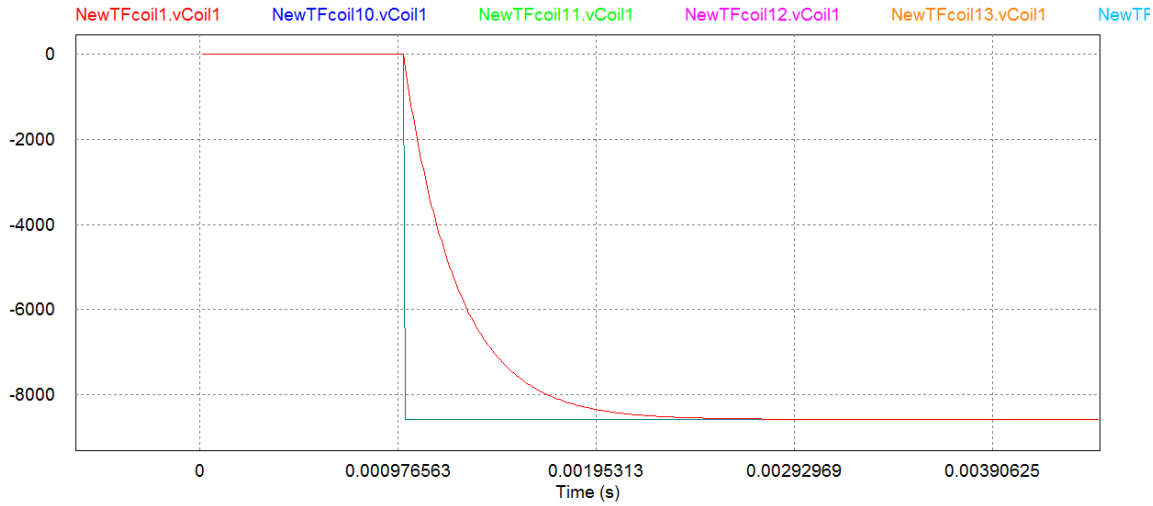

Figure 158 - 18 sectors TOPOLOGY "B" – Op.C. 1 - with and without snubbers Vd

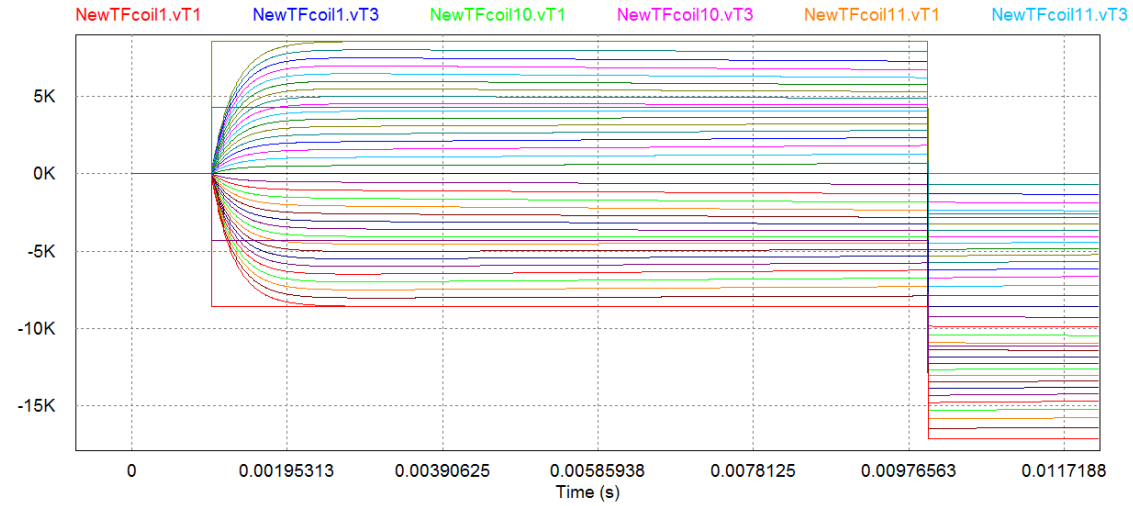

Figure 159 - 18 sectors TOPOLOGY "B" – Op.C. 7 - with and without snubbers Vg

The Vd trend for Op.C. 7 is the same as seen in Figure 158.

The voltage peak values does not change with the presence of snubbers, but after the QPC interventions the voltage transients are smoother than in the configurations without them .

4.6.2 18 sectors TOPOLOGY "C"

Also for this topology there will be studied only the cases in which there are the lowest and the highest voltage peaks, that are Op.C. 1 and 7 also in this case.

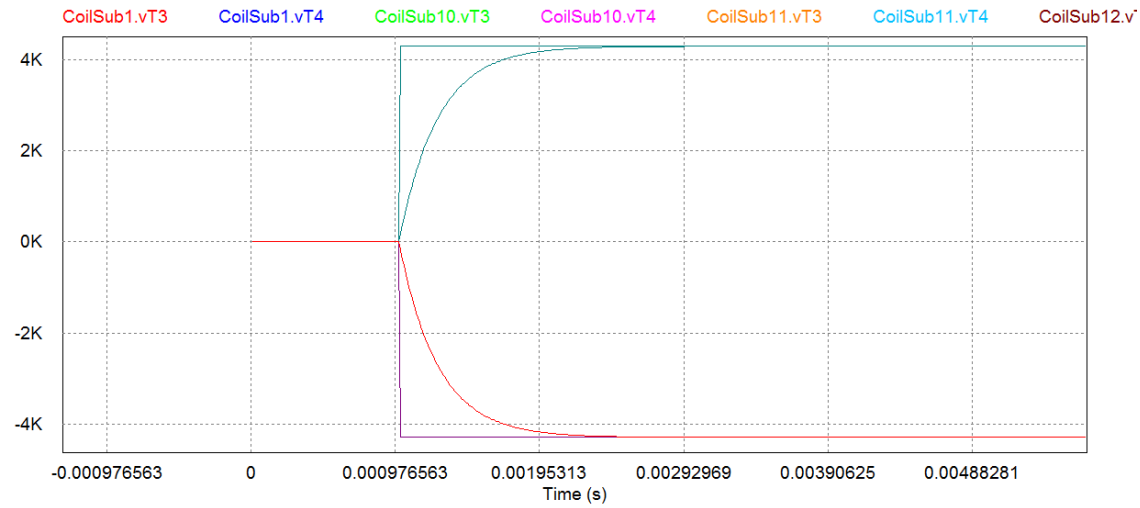

Figure 160 - 18 sectors TOPOLOGY "C" – Op.C. 1 - with and without snubbers Vg

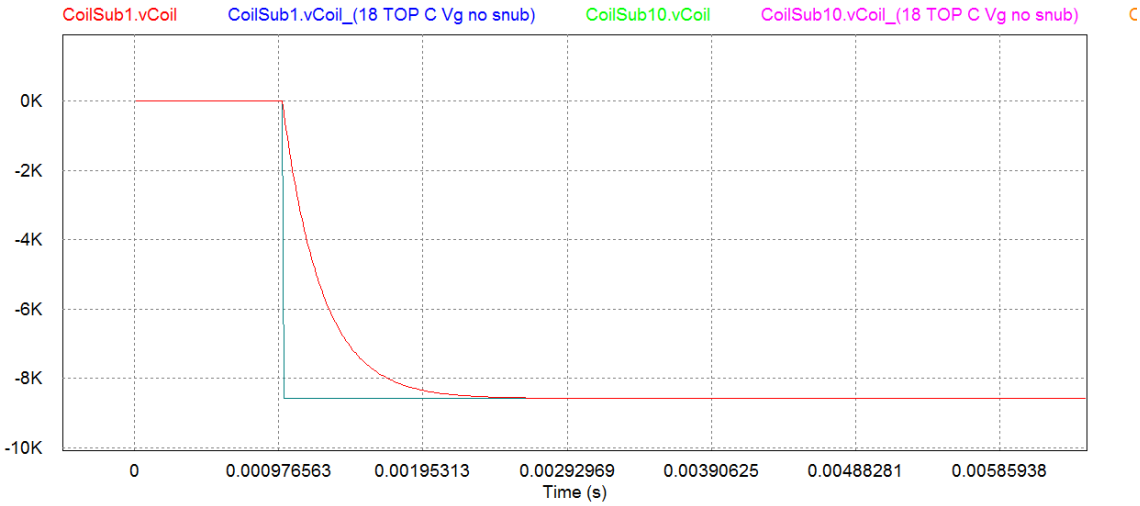

Figure 161 - 18 sectors TOPOLOGY "C" – Op.C. 1 - with and without snubbers Vd

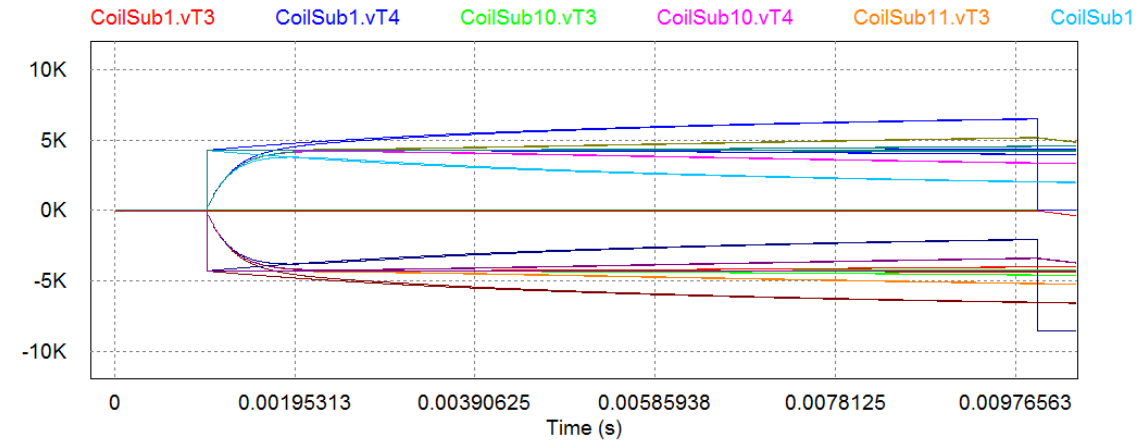

Figure 162 - 18 sectors TOPOLOGY "C" – Op.C. 7 - with and without snubbers Vg

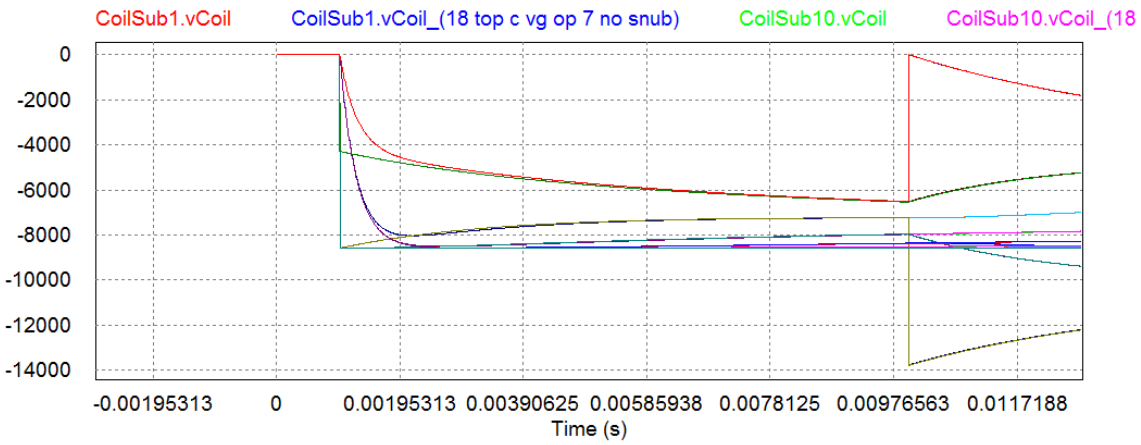

Figure 163 - 18 sectors TOPOLOGY "C" – Op.C. 7 - with and without snubbers Vd

Same as in the previous analysis, the voltage peak values does not change with the presence of snubbers, but after the QPC interventions the voltage transients are smoother than in the configurations without them .

Conclusions

It has been verified that the obtained results without the snubbers are similar to the values given by the snubber configuration, so the without-snubbers model is still valid.

The snubbers are useful for the CB because it is a preferential path for voltage and current high derivatives, which if bigger than the maximum project values could damage the components of the CB; snubbers are also useful to avoid resonances inside the coils, because strong voltage impulses could bring higher voltage values than the maximum allowed for the turns of the coils.

4.7 The delay fault - Op.C. 4:

The importance of a more detailed analysis of this type of fault lies in the fact that 10 ms is also the intervention time of the Pyrobreaker, which intervention must guarantee the circuit safety, and for this reason this fault is perfectly assimilable to it. In 4.5 it was shown that the DR-parallel-to-coil configuration does not need a Bypass Switch, and for this reason now only the DR-parallel-to-CB configuration will be analysed.

Snubber C = 2 [mF] put parallel to the circuit breaker; reference circuit: 18 sectors TOPOLOGY “B”.

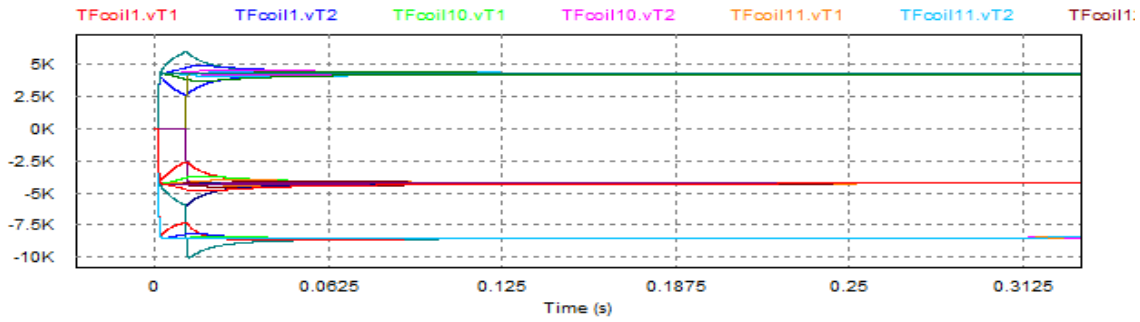

Figure 164 – With snubbers – Vg and Vd

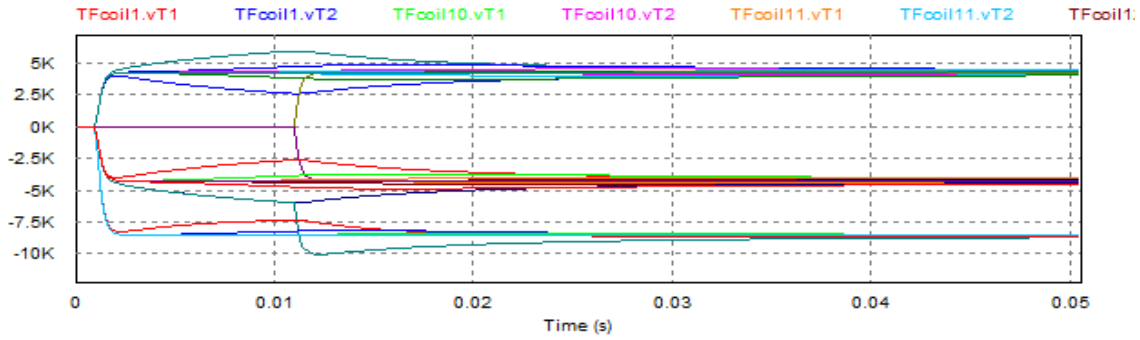

Figure 165 – With snubbers, 0.05 seconds time scale – Vg and Vd

The QPC intervention occurs at 1 [ms]; the delayed QPC starts at 11 [ms], as we can see from the graphs.
Without snubbers, the "delayed" terminals would reach the voltage value of the other terminals in short time (less than 100 [ms]):

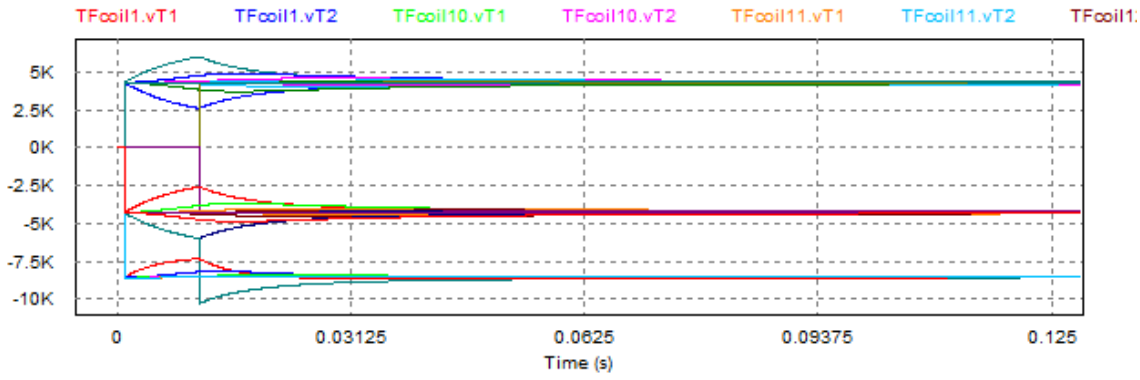

Figure 166 - Without snubbers, delayed QPC intervention – Vg and Vd

With snubbers, this evolution time is much longer (at least 400 [ms]; Figure 166). But also increasing the value of the snubber, the time needed for this evolution is not much different; only the way to reach it will change. For example, with a 200 [mF] snubber:

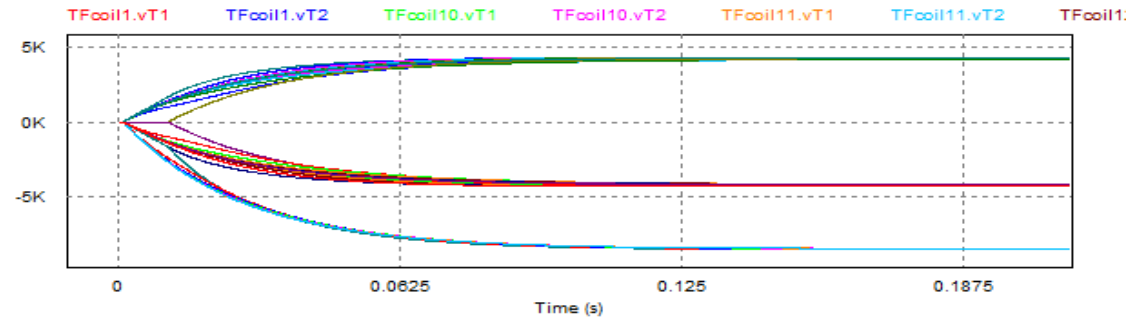

Figure 167 - 200 [mF] snubbers, Vg and Vd evolutions

As shown here, essentially the peaks are cancelled.
If we consider the presence of a resistor inside the snubber, the peak and "regime" values are still the same; with a 1 [Ω] resistor:

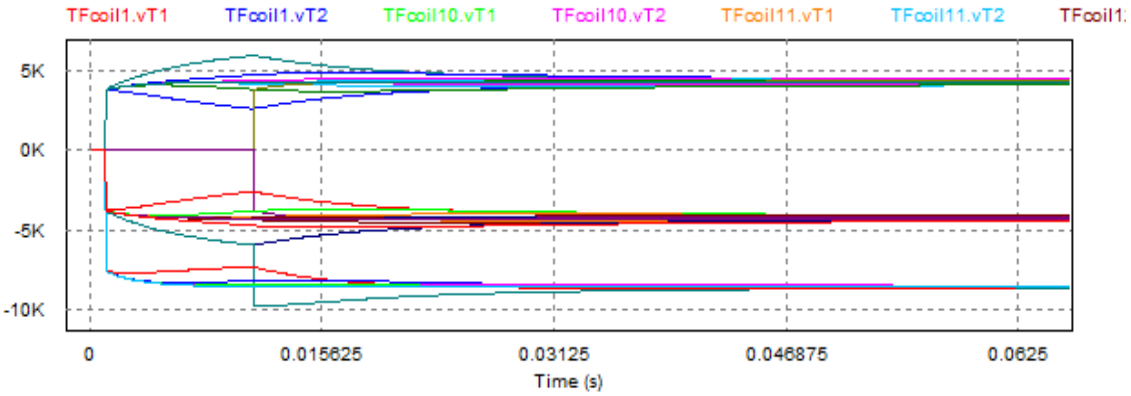

Figure 168 - 2 [mF] clamp + 1 [Ω] resistor, Vg and Vd evolutions

Also even if applying a 100 [Ω] resistor, the graphs are still the same as in the case without resistors; this aspect would be totally different if we considered the DR-parallel-to-coil configuration, but as explained the Pyrobreaker is not needed in that configuration.

5 Conclusions

The objective of this thesis was to study different possible topologies for the toroidal circuit of DEMO, in order to find the best compromise with respect to many different design constraints, such as the discharge time constant of the superconductive coil in order to observe a certain i^2t value, which is an important energetic parameter of the circuit, and the maximum voltage that can be applied to the coils, according to their insulation features.
The toroidal circuit of DEMO is composed of 18 coils that can be grouped in sectors; I analysed in particular four distinct topologies characterised by different protection system topologies and by different earthing connections, and the results of the study highlighted that there are two topologies among the others that led to lower stress in terms of voltage to the ground and in terms of voltage between the terminals of the coils. Furthermore the study focused on a critic and comparative evaluation of the possibility to maintain the 18 sectors configuration for the coils or to group them in 9 sectors composed by two coils and one protection system; this last solution can allow cost and size saving but causes a higher voltage across the coil.
The results of the 9 sectors solution present not negligible overvoltages, but it seems to be reasonably feasible because the study is not conservative; in fact I did not take into account the possibility to adopt variable resistors, which are realised with special materials that allow to exploit the variation of the resistance value with the temperature, leading to lower voltage peaks on the coils.
The analysis produced useful results for the evaluation of the toroidal circuit topology that can represent the best compromise among cost, losses and voltage stresses for the coil insulation.
The results that I have obtained from the analysis allow to evaluate in terms of design the best compromise among a higher number of Quench Protection Circuits, leading to higher costs, losses and obstruction, and the solicitation of the insulation of the coils.

Pictures index

References

CHAPTER 1

[1] public.wmo.int/en/media/press-release/globally-averaged-co2-levels-reach-400-parts-million-2015

[2] World Commission on Environment and Development (WCED), "*Brundtland Commission*", 1987

[3] Francesco Gnesotto, "*La fusione termonucleare controllata*", Consorzio RFX – Padova, 2016

[4] Mitsuru Kikuchi, Karl Lackner, Minh Quang Tran, "*Fusion Physics*", International Atomic Energy Agency, 2012

[5] "*A roadmap to the realisation of fusion energy*", EFDA – Fusion Electricity, November 2012

[6] C. Cesarsky, Ph. Garderet, J. Sanchez et al., "*Strategic orientation of the Fusion Programme - Report of a group of experts assisting the European Commission to elaborate a roadmap for the fusion programme in Horizon 2020 – the Framework Programme for Research and Innovation*" CCE-FU 53/3c

[7] P. Batistoni, S. Clement Lorenzo, K. Kurzydlowski et al., "*Report of the AHG on DEMO activities*" CCE-FU 49/6.7

[8] https://en.wikipedia.org/wiki/Superconductivity

[9] M.N. Wilson, "*Superconducting magnets*", Clarendon Press, 1987

[10] AmaliaBallarino, PierreBauer, Yanfang Bi et al., Design of the HTS Current Leads for ITER, 12 Sept. 2011

[11] Pierluigi Bruzzone, "*Superconducting magnets*", EPFL-Swiss Plasma Center

CHAPTER 3

[12] Ned Mohan, Tore M. Undeland, William P. Robbins "*Elettronica di potenza. Convertitori e applicazioni*", HOEPLI, 2005

[13] A. Ferro "*Guided example of simulation of a thyristor bridge and relevant control with PSIM*", 11-22 Oct. 2010

[14] Roberto Benato, Lorenzo Fellin "*Impianti Elettrici*", UTET, 2011

[15] Massimo Guarnieri "*Elementi di Elettrotecnica Circuitale*", Progetto, 2010

[16] Mauro Andriollo, Giovanni Martinelli, Augusto Morini "*I Trasformatori. Teoria ed esercizi*", Cortina, 2010

[17] A. Maistrello, A. Benn, N. Dumas, J. Jader Framarin, A. Kunze "*GOTP Response to MAST-U TF PSU Tender*", 2nd CCFE GOTP course, 27 Jan. 2012

[18] Jürg Waldmeyer, Björn Backlund "*Design of RC snubbers for phase control applications*", ABB

CHAPTER 4

[19] Alberto Maistrello, Elena Gaio "*Input Data for TF QPS design*", 29 Jan. 2016

[20] Alberto Maistrello, Elena Gaio "*Studies on the TF circuit of DEMO*", 29 Jan. 2016